Design Optimisation of Practical Variable Stiffness and Thickness Laminates

Peeters, Daniel

Important note
To cite this publication, please use the final published version (if applicable).
Please check the document version above.

Design Optimisation of Practical Variable Stiffness and Thickness Laminates

Design Optimisation of Practical Variable Stiffness and Thickness Laminates

Proefschrift

ter verkrijging van de graad van doctor

aan de Technische Universiteit Delft,

op gezag van de Rector Magnificus prof. ir. K. C. A. M. Luyben,

voorzitter van het College voor Promoties,

in het openbaar te verdedigen op dinsdag 31 januari 2017 om 10:00 uur

door

Daniël Maria Jozef PEETERS

Ingenieur Luchtvaart en Ruimtevaart

geboren te Turnhout, België.

This dissertation has been approved by the promotors:

Promotor: Prof. dr. C. Bisagni
Copromotor: Dr. M.M. Abdalla

Composition of the doctoral committee:

Rector Magnificus,	chairman	
Prof. dr. C. Bisagni,	promotor	Delft University of Technology
Dr. M.M. Abdalla,	copromotor	Delft University of Technology

Independent members:

Prof. dr. F. van Keulen	Delft University of Technology
Prof. dr. P. Weaver	University of Limerick
Prof. dr. V. Toropov	Queen Mary University London
Dr. M. Bruyneel	University of Liège
Dr. A.W. Blom-Schieber	Boeing
Prof. dr. ir. R. Benedictus	Technische Universiteit Delft, reservelid

CANAL Project Partners:

An electronic version of this dissertation is available at
`http://repository.tudelft.nl/`.

ACKNOWLEDGEMENTS

While this thesis is the result of four years work, it symbolises the end of a journey that started over 9 years ago when I came to study in Delft. During the last four years, I gained a lot scientific knowledge, but also on a personal basis I will remember these years. It has not always been a fun time, but a lot of people helped to make it as fun as possible on the hard moments when my research was not going as good as I hoped, and even more enjoyable during the moments my research did give go as planned. For this, I have a lot of persons to thank, and while trying to be complete in this part, the chance that I forgot to mention someone is real, forgive me for this.

The first person I would like to thank is my supervisor Dr. Mostafa Abdalla. He was not just the supervisor during my PhD, but also during my Master thesis, and without his enthusiasm during my Master thesis, I probably would have never pursued a PhD. During the 4,5 years we worked together he provided a seemingly endless flow of ideas and suggestions for my work. This technical inspiration was combined with a large number of non-technical discussions about pretty much anything, and a steady flow of sketches with typically British humour. My PhD would not have been of the quality it is now without Mostafa. I would also like to thank Prof. Chiara Bisagni for taking the role of promotor halfway through my PhD research, and providing me with the opportunity to get some teaching experience. It has always been a dream of me to become a teacher, and thanks to her I got this opportunity.

Also the other staff members of the section of Aerospace Structures and Computational Mechanics made sure my time as PhD student was enjoyable. I will not mention all of them here, for I can never do right to all discussions, advice, and insight. A special thanks goes to Laura for helping with a lot of paper work and pointing me in the right direction with practical questions a lot of times. A special thanks to Roeland as well for making sure there was a Belgian touch to my PhD. Even though Delft is not far from Belgium, it was always nice to discuss the typical Belgian issues.

Next, my thank goes to all fellow PhDs, and post-docs, who joined me on and before/after conferences, or just made for a good laugh and discussion in Delft. Lunch would not have been the same without them: a moment where you could

SUMMARY

The use of composite materials in airplanes has been increasing over the last decades. This is mainly due to the high strength-to-weight and stiffness-to-weight ratio and the ability to tailor composite materials. By changing the stacking sequence, the mechanical properties of the resulting laminate can be altered significantly. This implies that the designer has a lot of freedom to tailor the material to the structure it will be used in. This in turn leads to weight savings, attracting industry's attention.

For historical reasons, the fibre angles used are often restricted to $0°$, $\pm45°$ and $90°$, referred to as conventional laminates in this work. The first composite materials were manufactured using hand lay-up, which caused these limitations. A lot of experience with conventional laminates was accumulated over the years, and a lot of tests were performed. Hence, as manufacturing methods progressed and these limitations were no longer necessary, designers still had more confidence in conventional laminates than in non-conventional ones. The vast amount of experience with conventional laminates is captured in design guidelines, which give rules of thumb of good composite laminate design.

With the rise of fibre placement machines, both the accuracy with which fibres are laid down and the production rate significantly increased. Fibre placement machines offer a lot of extra possibilities: not only can any ply angle be placed, the fibres can even be steered. By steering the fibres, the mechanical properties of the material are made spatially varying while maintaining material continuity, hence these laminates are called variable stiffness laminates. This enlarges the design space considerably. Next to the extra possibilities, extra constraints appear as well: for example, the steering radius cannot be too small. Hence, new optimisation algorithms need to be developed.

An optimisation strategy that has been proven to be computationally efficient is a three-step optimisation approach originally proposed by IJsselmuiden. In step one, the stiffness distribution is optimised, where lamination parameters are used to describe the stiffness. In step two the stacking sequence at each node of a finite element model is retrieved. In step three, the fibre paths are constructed using a streamline analogy.

The three-step optimisation approach is an efficient optimisation approach, but

certain limitations still exist that will be handled in this thesis. For example, in step one, the stiffness distribution is optimised, but even more efficient structures can be obtained by optimising the place where material is and the material properties concurrently. This is achieved in this thesis by combining topology optimisation with lamination parameter optimisation. To obtain a clear topology description, implicit and explicit penalisation are compared with each other. They are found to lead to similar results, but since explicit penalisation guarantees a clear topology description it is the preferred method. Numerical results show that efficient structures can be obtained this way.

In step two, the focus is laid on manufacturability of the optimised design by implementing a steering constraint. When the steering radius is too small, the fibres will wrinkle and lose (part of) their load-carrying capability. Rather than an average (i.e., global) steering constraint that was implemented before, a local one (i.e., per element) is formulated in this work to assure the steering radius is never too small such that the optimised design can be manufactured using fibre placement machines without fibre wrinkling occurring. Since the number of constraints is significantly increased, from one constraint per layer to one constraint per element per layer, a purpose-built optimisation algorithm is necessary to handle these constraints in an efficient manner. A predictor-corrector interior-point optimisation algorithm is implemented to achieve this. Numerical results show that by loosening the steering constraint, the performance of the optimised design in terms of the fibre angles is approximating the optimal performance found in terms of the stiffness, implying that the optimisation is giving good results.

Since a lot of experience is included in the design guidelines, they are 'translated' to constraints that are added to the optimisation formulation in this work. By implementing the design guidelines in the optimisation, the feasibility of the optimised design is increased. This may be a first (small) step towards certification of non-conventional laminates. Numerical results show that by taking the 10% rule into account, about half of the performance increase over conventional laminates is lost, but still a significant performance increase is found. Hence, by sacrificing part of the performance improvement, industrial feasibility is increased.

Another way of obtaining laminates with varying mechanical properties is by changing the number of layers from one point to the next by dropping plies. This possibility was not included in the original three-step optimisation approach, but is included in this thesis by performing a layer-by-layer topology optimisation. Next to the ply drop location, the ply drop order is optimised as well. The result can either be traditional straight-fibre plies with ply drops, called variable thickness laminates, or steered fibres can be combined with ply drops, leading to variable stiffness, variable thickness laminates.

An efficient optimisation algorithm, requiring a low number of finite element analyses, able to generate variable stiffness laminates, variable thickness laminates, and the combination of both has been developed. For variable stiffness laminates

extra constraints have been implemented to ensure manufacturability and feasibility. Numerical tests have shown that considerable improvements in structural performance are possible by varying the fibre angle and/or thickness spatially.

SAMENVATTING

Het gebruik van composieten materialen in vliegtuigen is de laatste tientallen jaren sterk toegenomen. Dit komt voornamelijk door de hoge specifieke stijfheid en sterkte en de mogelijkheid om de materiaal-eigenschappen te veranderen. De eigenschappen van het laminaat kunnen aanzienlijk veranderd worden door het veranderen van de volgorde en de hoeken van de verschillende lagen. Dit geeft de ontwerper veel vrijheid om het materiaal aan te passen aan de structuur waarin het gebruikt zal worden. Dit resulteert op zijn beurt in een gewichtsbesparing, wat de aandacht van de industrie trekt.

Om historische redenen zijn de hoeken waarin de vezels liggen vaak beperkt tot $0°$, $±45°$and $90°$, waarnaar in dit werk verwezen wordt als conventionele laminaten. De eerste composieten materialen werden met de hand gemaakt, met deze beperkingen tot gevolg. Met deze conventionele laminaten is in de loop der jaren veel ervaring opgedaan, en veel testen zijn hiermee gedaan. Daardoor hebben ontwerpers toch nog steeds meer vertrouwen in conventionele laminaten dan in niet-conventionele, ook al zijn de processen om composieten te maken ondertussen geavanceerder, waardoor de limieten op de hoeken niet langer nodig zijn. De ervaring die tijdens de jaren is opgebouwd met conventionele laminaten is samengevat in ontwerp richtlijnen, die vuistregels geven over wat een goed composiet laminaat is.

Door de opkomst van productiemachines zijn zowel de nauwkeurigheid waarmee de vezels worden neergelegd en de productiviteit aanzienlijk verhoogd. Productiemachines geven veel extra mogelijkheden: naast de mogelijkheid om de vezels onder eender welke hoek te plaatsen, kunnen de vezels ook gestuurd worden. Door de vezels te sturen, veranderen de materiaaleigenschappen van punt tot punt terwijl de continuïteit van het materiaal bewaard wordt. Daarom worden deze laminaten 'variabele stijfheid laminaten' genoemd. Hierdoor wordt het ontwerpgebied aanzienlijk groter. Naast de extra mogelijkheden zijn er ook extra voorwaarden: bijvoorbeeld, de straal waarmee de vezels worden gestuurd moet groot genoeg zijn. Hiervoor moeten nieuwe optimalisatie-algoritmes ontwikkeld worden.

Een optimalisatie-strategie die al bewezen heeft efficiënt te zijn op het gebied van rekenwerk is een drie-staps optimalisatie-algoritme, voor de eerste keer voorgesteld door IJsselmuiden. In stap één wordt de stijfheidsverdeling, beschreven door de

laminatie-parameters, geoptimaliseerd. In stap twee wordt de verdeling gevonden van de hoeken waaronder de vezels liggen. In stap drie worden de vezelbanen bepaald door gebruik te maken van een stroomlijn analogie.

De drie-staps optimalisatie is een efficiënt optimalisatie-algoritme, maar er zijn nog steeds bepaalde beperkingen die in deze thesis werden aangepakt. Bijvoorbeeld, in stap één is de stijfheidsverdeling geoptimaliseerd, maar nog efficiëntere structuren kunnen worden gevonden door tegelijk de plaats van het materiaal, en de materiaaleigenschappen te optimaliseren. Dit is in deze thesis gedaan door topologie en laminatie-parameter optimalisatie te combineren. Om een duidelijke beschrijving van de topologie te verkrijgen is een impliciete aanpak vergeleken met een expliciete. Beide geven vergelijkbare resultaten, maar omdat de expliciete aanpak een duidelijke topologie-beschrijving verzekert, wordt de voorkeur aan deze aanpak gegeven. Numerieke resultaten laten zien dat op deze manier efficiënte structuren kunnen worden bekomen.

In stap twee ligt de focus op de produceerbaarheid van het geoptimaliseerde ontwerp door een voorwaarde op de minimale straal waarmee de vezels worden gestuurd te implementeren. Als deze straal te klein is, zullen de vezels kreuken en (een deel) van hun capaciteit om krachten te dragen verliezen. In plaats van de gemiddelde (ook wel globale genoemd) straal te beperken, zoals vroeger gedaan is, wordt in dit werk de voorwaarde lokaal (per element) geïmplementeerd om zeker te zijn dat de straal nergens te klein is en het geoptimaliseerde ontwerp gemaakt kan worden met machines zonder dat de vezels kreuken. Omdat het aantal voorwaarden aanzienlijk toeneemt, van één per laag naar één per laag per element, is een specifiek ontworpen optimalisatie-algoritme nodig om al deze voorwaarden op een efficiënte manier mee te nemen. Een predictor-corrector algoritme is geïmplementeerd om dit de bereiken. Numerieke resultaten laten zien dat als de voorwaarden op de straal waarmee de vezels worden neergelegd wordt gematigd, de prestatie van het geoptimaliseerde ontwerp in termen van de hoeken waaronder de vezels liggen, de prestatie van het beste ontwerp in termen van de laminatie-parameters benadert. Dit impliceert dat de optimalisatie goede resultaten geeft.

Aangezien er veel ervaring in de ontwerprichtlijnen is gevat, zijn ze in dit werk 'vertaald' naar voorwaarden die zijn toegevoegd in de optimalisatie-formulering. Door deze ontwerprichtlijnen te implementeren in de optimalisatie, is de haalbaarheid van de geoptimaliseerde laminaten groter. Dit zou een eerste (kleine) stap naar certificatie van niet-conventionele laminaten kunnen zijn. Numerieke resultaten laten zien dat door het meenemen van de 10% regel, ongeveer de helft van de prestatie-toename in vergelijking met conventionele laminaten verloren gaat, maar de toename is nog steeds significant. Kortom, door een deel van de prestatietoename te op te offeren, wordt de industriële haalbaarheid groter.

Een andere manier om laminaten met variabele materiaaleigenschappen te verkrijgen, is het veranderen van het aantal lagen van de ene naar de andere plaats door lagen te laten vallen. Dit was niet mogelijk in de originele drie-staps optimalisa-

tie, maar is mogelijk in deze thesis door een laag-per-laag topologie optimalisatie te doen. Naast de plaats waar lagen wegvallen, wordt ook de volgorde waarin lagen wegvallen geoptimaliseerd. Het resultaat kan ofwel een traditioneel ontwerp zijn met niet-gestuurde vezels en lagen die wegvallen, variabele dikte laminaten genoemd, ofwel gestuurde vezelpaden gecombineerd met lagen die wegvallen, dit wordt variabele stijfheid, variabele dikte laminaten genoemd.

Er is een efficiënt optimalisatie-algoritme ontwikkeld, dat weinig eindige elementen analyses nodig heeft, en in staat is om variabele stijfheid laminaten, variabele dikte laminaten en de combinatie van beide te verkrijgen. Voor variabele stijfheid laminaten zijn extra voorwaarden geïmplementeerd om produceerbaarheid en haalbaarheid te garanderen. Numerieke testen hebben aangetoond dat aanzienlijke verbeteringen in structurele prestaties mogelijk zijn door de hoeken waaronder de vezels liggen en het aan aantal lagen te wijzigen.

NOMENCLATURE

ROMAN SYMBOLS

A	Area
a	Mode shape
a	Inverse of the in-plane stiffness matrix
A	In-plane stiffness matrix
b	External force
B	Coupling matrix
B	Strain-displacement matrix
C	Compliance
d	Damping function
d	Distance
d	Ply drop order
D	Out-of-plane stiffness matrix
$\mathcal{D}$	Feasible region
e	Objective-constraint vector
E	Young's modulus
f	Function
f	Structural response
f	Force vector
g	Grey area
g	Gradient
G	Shear modulus
h	Thickness of the laminate
H	Approximation of the Hessian
$\mathbf{H}_d$	Regularisation matrix
i	Improvement
J	Jacobian
k	Current iterate
K	Stiffness matrix
l	Length
L	Laplacian matrix
L	Linking matrix

$\mathcal{L}$	Lagrangian
m	$\cos(\theta)$
m	Modification function
M	Moment vector
n	$\sin(\theta)$
n	Direction normal to the streamline
n	Number of layers
N	Number of nodes
N	Shape function
N	Normal force vector
p	Ply count percentage
p	Penalisation power
Q	Stiffness Matrix
r	Failure index
r	Steering radius
s	Direction of the streamline
s	Number of plies in the symmetric part
s	Slack variables
t	Thickness
U	Material invariants
U	Strain energy
u	Displacement vector
V	In-plane lamination parameter
V	Volume
w	Weight factor
w	Width
W	Out-of-plane lamination parameter
x	x-coordinate
x	design vector
y	y-coordinate
z	Through-the-thickness coordinate
z	Objective

GREEK SYMBOLS

α	Scaling factor
β	Optimum after LP optimisation
γ	Shear strain
γ	Eigenvalue
Γ	Boundary
δ	Step size

Δ	Change
$\boldsymbol{\Gamma}$	Matrices containing material invariants
ϵ	Normal strain
ϵ	Scaling factor
ζ	Damping factor
η	Coefficient of mutual influence
η	Maximum fraction to be used
θ	Fibre angle
κ	Curvature
κ	Machine accuracy
κ	Relaxation factor
λ	Scaling factor
λ	Buckling factor
$\boldsymbol{\lambda}$	Vector containing the Lagrangian multipliers
μ	Homotopy factor
ν	Poisson ratio
ρ	Density
σ	Normal stress
ς	Steering
τ	Normal logarithm of the thickness
τ	Shear stress
$\boldsymbol{\Phi}$	Sensitivity with respect to the stiffness
Ψ	Stream function
$\boldsymbol{\Psi}$	Sensitivity with respect to the inverse stiffness
Ω	Area

SUB/SUPERSCRITPS

0	Nominal solution
0	Value at the reference plane
0	Value at the approximation point
1	Normal to fibre direction
2	Perpendicular to fibre direction
6	Shear stress in plane of fibres
I	First level
II	Second level
*	Outcome of optimisation
*	Threshold value
ˆ	Approximation
$\underline{x}$	lower bound
$\overline{x}$	upper bound

+	Positive semi-definite part
-	Non-positive semi-definite part
all	Allowable
b	Bending
c	Centre
c	Constraint/objective
d	dual
e	Edge
e	Element
g	Geometric
i	Ply number
i	Node number
in	Inflow
k	Gauss point
l	Lower bound
m	Membrane
p	Primal
s	Steering
u	Upper bound

ABBREVIATIONS

N	Yet another statement
AFP	Automatic fibre placement
APPLY	Advanced placed ply
BCP	Bi-value coding parametrization
CFRP	Continuous fibre reinforced plastics
CD	Coordinate Descent
CL	Conventional laminate
CMTS	Continuous multi-tow shearing
ConLin	Convex linearisation
CSL	Constant stiffness laminate
CTS	Continuous tow shearing
DMO	Discrete material optimisation
DMTO	Discrete material and thickness optimisation
FEA	Finite element analysis
GA	Genetic algorithm
LP	Lamination Parameter
NCL	Non-conventional laminate
NURBS	Non-uniform rational B-splines
QI	Quasi-isotropic

SFP	Shape function with penalisation
SIMP	Solid isotropic material penalisation
SST	Stacking sequence table
TFP	Tailored fibre placement
VSL	Variable stiffness laminate
VSVTL	Variable stiffness variable thickness laminate
VTL	Variable thickness laminate

CONTENTS

Voilà.
Antigone, written by Sophocles

1

INTRODUCTION

1.1 ADVANTAGES OF COMPOSITE MATERIALS

A composite material is a material that is a combination of two or more materials. The properties of the composite, if it to be of practical use, should be better suited to the application in mind than any of the consitituents. The use of composites is a fairly ancient idea: during the times of the Pharaohs, chopped straws were used to reinforce bricks. Another example are the Japanese Samurai warriors using laminated metals in the forging of their swords [158].

Multiple types of composites have been developed in the modern technological era. Composites may be characterised according to the geometric arrangement of the constituents. Laminated composites consist of layers of different materials. Particulate composites are composed of particles of one or more materials dispersed within a matrix. Finally, in fibrous composites microscopically thin fibres are dispersed within a matrix. These fibres can either be short and scattered throughout the matrix, or they can be continuous having a clearly defined direction over the structure [158]. The sort of composites considered in this work are a combination of laminated composites and continuous fibre reinforced plastics (CFRP): continuous fibres, for example carbon or glass, are embedded in a resin matrix, and multiple layers, with the fibres possibly oriented in different directions, are stacked to obtain a composite laminate, as is shown in Figure 1.1.
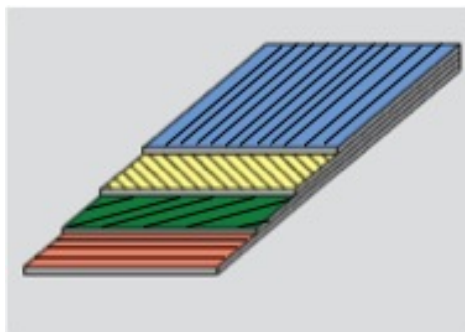
Figure 1.1: Example of a composite consisting of 4 plies.

Composite laminates are often used in the aerospace industry because of their high stiffness-to-weight and strength-to-weight ratios. The percentage of composite materials in aircraft has gradually increased since their first introduction. Composites went through the same implementation cycle as most new materials: first they were only used on secondary structures, then on small scale structures, and by now they are the most-used material in the latest aircraft such as the B-787 and A-350[75]. In terms of weight, these aircrafts are made of over 50% composite material[1,2], as is shown in Figure 1.2.
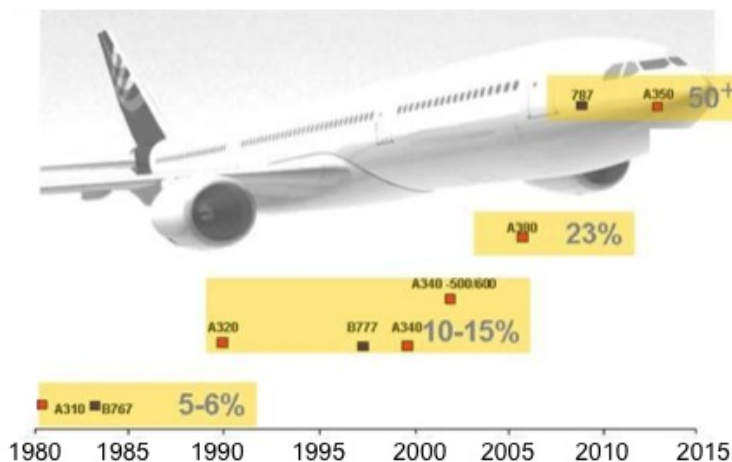
Figure 1.2: Increase of composites in commercial aerospace[3].

A great advantage of composites is the ease with which the material properties can

1

be tailored for particular applications. The mechanical properties of the laminate are dependent on the orientation of the fibres in the different layers. Hence, by changing the orientation of the layers, the mechanical properties of the laminate can be changed. This is a powerful mechanism for optimally tailoring the material to its service conditions that is not available for example for metals.

A comparison of composite materials to steel or aluminium reveals the reasons why composites are increasingly used in aerospace structures. The weight per volume is in general lower; certainly compared to steel, the weight decrease is large. Partly due to the relatively low density, the specific stiffness and specific strength are higher than for steel and aluminium. Furthermore, the thermal expansion coefficient is much lower, though not negligible; the difference is some orders of magnitude. Finally, the resistance to fatigue of composite materials is expected to be better[139].

Comparing the cost of aluminium versus composites is not as straightforward. In terms of raw material cost, composites are more expensive than aluminium. On the other hand the amount of scrap material when using composites is generally less than when using aluminium. Furthermore, the price of composite parts is continually decreasing in part due to increased demand and in part due to accumulated experience in economically producing them. Next to the material cost and amount of scrap material, the cost of manufacturing and maintaining the product needs to be considered as well. Depending on the complexity of the shape, composite materials are usually cheaper to manufacture and maintain: a composite design generally consists of less parts, and thus requires less joining points. For example, for a spar, a lot of material will be milled away from aluminium, making for much extra material and processing cost, while a composite spar is built up, leading to a fraction of the scrap material. Furthermore, the composite spar is likely lighter, leading to lower operating cost of the airplane. The initial investment needs to be taken into account as well: a fibre placement machine is very expensive compared to the tools necessary to process aluminium.

Concluding, in terms of cost, the initial cost of composites is certainly higher than aluminium. But when considering the cost over the entire lifetime, composites can be comparable, and can even be lower in cost depending on the structure[72].

1.2 MANUFACTURING OF COMPOSITES IN AEROSPACE INDUSTRY

When composites were first introduced, the most common manufacturing technique was hand lay-up, which is time consuming and has a limited accuracy. Usually only a limited set of fibre angles was used in hand lay-up typically 0°, 90°, and ±45° plies. While hand lay-up may not be the most accurate or fastest

1

manufacturing method, it did allow composite structures to be produced and their advantages to be demonstrated without the need for the huge initial investment costs associated with automated manufacturing. As the volume of composite production grew, automated manufacturing methods were extensively developed. It is not possible within this short section to give justice to this area of extensive technological innovation. Instead, attention is limited to one of the most versatile general purpose techniques: automated fibre placement.

Nowadays, for accurate and relatively fast lay-up of composite laminates on complex shapes, automatic fibre placement (AFP) machines are the tools of choice. These machines lay down a strip of composite material with each pass. The general working principle can be seen in Figure 1.3. As can be seen in this figure, the composite material is kept on a big supply roll of material in the form of tapes. This material passes by two rolls, which can normally be moved in vertical direction to remove any tension from the material, without any slacking occurring, before the material is laid down on the mould. While the material is guided from the supply roll along the rolls, it is cooled to decrease it tackiness, to make sure it does not stick to the rollers. At the moment the material is laid down, it is heated to increase its tackiness, so that is sticks, better, to the mould. The placement head applies pressure on the material to make sure it sticks to the mould or the previously laid down layers, and to remove as much entrapped air as possible. The placement head is kept perpendicular to the direction of the fibres during the complete process[129]. A working AFP machine can be seen in Figure 1.4.
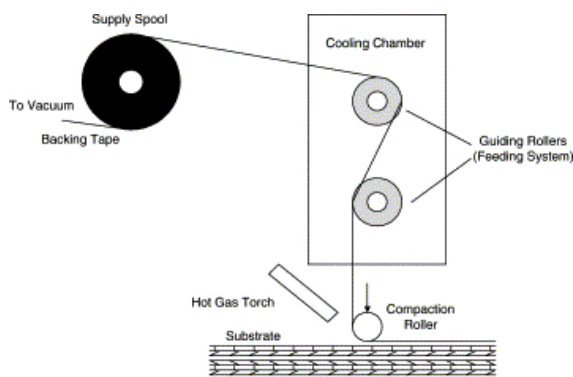
Figure 1.3: Schematic view of the AFP process[129].

Using AFP the production rate is increased compared to hand layup: an increase from just under 1 kg/hour to 5 kg/hour is reported. At the same time, the labour cost is reduced by up to 86%[37]. Furthermore, the accuracy of AFP is higher than using hand lay-up, in general a deviation of 2° at most is observed. Usually, a small gap is left between parallel courses of $0.5 - 1$ mm to account
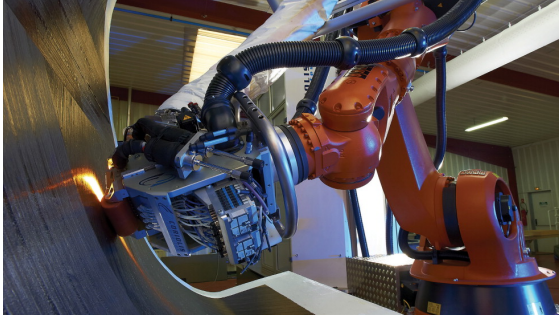
Figure 1.4: Working AFP machine[101].

for tape tolerances and avoid overlapping courses[95]. A final advantage of AFP compared to hand lay-up is that the larger the structure, the more economical the manufacturing becomes, while a larger structure with hand lay-up increases manufacturing complexity[37].

At the edges of a part, some scrap material will always be present since the edge of a course is not necessarily aligned with the edge of the product to be manufactured. At this point, a choice has to be made: is the course continued until a part of it hits the edge of the structure, called 0% overlap, or is the course continued until the whole course is outside the structure, called 100% overlap? Something in between the two extremes is also possible. This is shown in Figure 1.5.
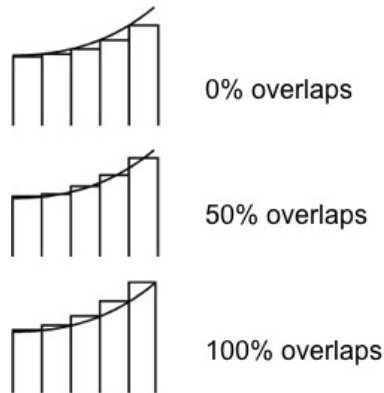
Figure 1.5: Different strategies at the edge of a structure[95].

During one pass of the machine, one course is laid down at a time. To increase production rates, it is best to have as wide a course as possible. However, when

more complex geometries are manufactured, for example a curved panel, the tows may need to be steered. The steering here refers to in-plane curvature of the fibres and not to changes in the fibre angle which may or may not be kept constant. In this case a narrow course is best since there is a difference in length of deposited tape between the inner and outer tow of a course. To avoid having to buy different material widths for different applications, placement heads have been developed that can lay down multiple, up to 32, tows in a single course. This can also be used to reduce the amount of scrap material, related to the overlaps at the edge of the structure: when cutting multiple small tows, the amount of scrap material is much smaller than when cutting one wide tape.

Steering sets constraints on the geometry of the structure or the fibre angle that can be laid down. When the steering radius becomes too small, the tow material will wrinkle on the inside and lose (a large part of) its load-carrying capability. Furthermore, the resulting structure would have poor surface finish. An example of steered fibres can be seen in Figure 1.6.

A typical aluminium wing consists of multiple panels that are connected to each other with a decreasing thickness towards the wing tip. This tapering is introduced to save weight since the loads on the inner part of the wing are much higher. When applying the same principle to composite materials, multiple panels would have to be connected to each other, which is not attractive due to the known difficulties in composite joining. A better option is to have certain plies continuing over the complete structure, and dropping other plies, to generate a similar tapering of thickness as for the aluminium wing, without having to join several panels.

AFP is seen to be a versatile automated manufacturing technique for laminated composites. It allows the production of high quality parts of complex shapes. It has the ability to support complex fibre architectures through the use of steering and thickness variation through the use of ply dropping. These increased abilities open the door for wider opportunities in tailoring composite materials to attain optimal performance.

1.3 NON-CONVENTIONAL LAMINATES: POSSIBILITIES

Since the first composites were, for manufacturing reasons, limited to fibre angles of 0°, 90°, and ±45°, experience, knowledge, and extensive experimental characterisation about these laminates was accumulated over the years. Hence, for a long time, designers kept using this restricted set of fibre angles. Consequently, more tests were performed with these materials, more experience was gained and designers felt even more comfortable with them since they had a much better understanding of their use and of their behaviour in service. That is why these

Figure 1.6: Example of fibres steered using different turning radii [16].

types of laminates are called *conventional laminates* in this work.

With the advent of fibre placement machines, the need for the limited set of fibre angles from a manufacturing point of view disappeared, but it took a while before these possibilities were exploited by designers. Recently, multiple *non-conventional laminates* (NCLs) have been developed. Not all of them will be discussed. Three are discussed in this section, and will be used later on in the thesis as well. Two types of NCL concepts have been developed with a view to increase the post-impact behaviour of composites. The first type is the dispersed laminate concept. In this concept the fibre angle between consecutive plies is forced to differ measurably. The second concept is the advanced placed ply, or APPLY, laminate which mimics the behaviour of woven composites at a fast deposition rate. The third NCL concept is that of variable stiffness laminates which acts at the structural level. In this concept, fibre steering is not only used to follow the complex shape of a curved structure, but also used to optimise the fibre paths so as to achieve a good redistribution of the loads throughout the structure as well. All three concepts are discussed in more detail below.

DISPERSED LAMINATES

In nature it is observed that members that have to withstand repetitive impacts, such as claws, have a helical arrangement of mineralised fibre layers [48]. This can be mimicked by having the same difference in fibre angle between consecutive layers, as shown in Figure 1.7. Doing so has been shown to have a positive effect on post-impact behaviour. The difference in fibre angles improves the post impact behaviour, but the in-plane properties are essentially isotropic, reducing the potential weight savings composites may lead to.

In the dispersed laminate concept, good impact resistance is achieved by maintaining a minimum difference in fibre angles between consecutive plies. This reduces
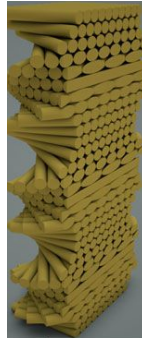
Figure 1.7: Helical dispersing of plies [48].

the interlaminar shear stress by supporting crack fibre bridging and increasing the number of interfaces (i.e., compared to conventional laminates consecutive plies no longer have the same orientation). Hence, to improve post-impact behaviour, dispersed laminates have a significant difference in ply angle between consecutive layers to improve impact resistance [94]. This has been shown to improve the post-impact behaviour of composites by Lopes et al. [91,124].

APPLY LAMINATES

The characteristics of woven plies can be mimicked using the APPLY principle: when laying down 2 layers, first half of the fibres in one direction is laid down, always leaving a gap of exactly one bandwidth. Next the fibres in the other direction are laid down, and the gaps are filled in step three and four. This is shown in Figure 1.8 [105]. APPLY combines the advantages of the characteristics of woven plies with fast and accurate manufacturing using fibre placement machines.

By interweaving the plies using the APPLY principle, delamination is stopped at the edges of the unit cell. The interface between the two plies where the delamination occurred suddenly stops. A unit cell is defined as the area where the stacking sequence is the same. The APPLY principle will lead to different stacking sequences: on some parts it is $[\theta_1/\theta_2]$, in the next unit cell it is $[\theta_2/\theta_1]$. Furthermore, the interwoven plies can be seen as one thick layer, being stiff in two rather than one direction. Interweaving plies is easiest when the difference between the plies is 90°, as shown in Figure 1.8. However, as long as a minimum difference between plies is adhered to, they can be interwoven using the APPLY principle.
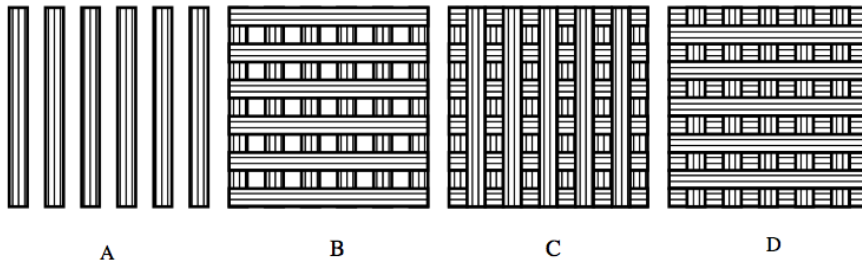
Figure 1.8: Schematic overview of the manufacturing using the APPLY principle [105].

STEERED LAMINATES

It was mentioned in the previous section on complex structures, steering has to be used to keep the fibre angle constant over the structure. However, steering can also be used to vary the fibre angle over the structure, while maintaining a continuous fibre path. When steering changes the fibre angle, and thus the stiffness, these composites are called variable stiffness laminates (VSL). These composite laminates have been shown to have greatly improved performance over their conventional counterparts for the same structural weight. This has attracted attention from both academia and industry, and multiple projects have been undertaken to design and optimise VSL. One example is the European AUTOW (Automated Preform Fabrication by Dry Tow Placement) project [4], where a sine-beam was developed, which can be seen in Figure 1.9. More examples and a literature review can be found in the next chapter.
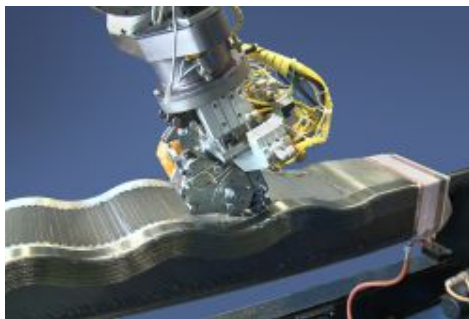
Figure 1.9: Sine-beam built during the AUTOW project [4].

A disadvantage of VSL is that since the fibres are steered, they will always either converge to or diverge from each other, leading to overlaps or gaps in a layer.

When shifting one curved path in a certain direction, the shifting direction is in the same direction over the complete structure, but the axis perpendicular to the course is constantly changing, either gaps or overlaps will appear, as can be seen in Figure 1.10. The third option shown in this figure has no gaps or overlaps since the perpendicular axis is constantly the same, but this implies the tow width is changing, and the roller is not perpendicular to the tow, both of which are impossible using automated fibre placement machines. If the tows would be shifted perpendicular to the local tow direction, to avoid gaps and overlaps, the steering radius is constantly decreasing, as can be seen in Figure 1.11. This may lead to problems with tow wrinkling as discussed in the previous section. Hence, for practical VSL made using AFP, gaps and overlaps are practically inevitable. The resulting thickness variability due to the gaps and overlaps can be clearly seen on the manufactured plates, as can be seen in Figure 1.12[68]. The foregoing discussion applies to simple flat geometries. On complex shapes even conventional laminates require steering with the attendant presence of gaps and overlaps.
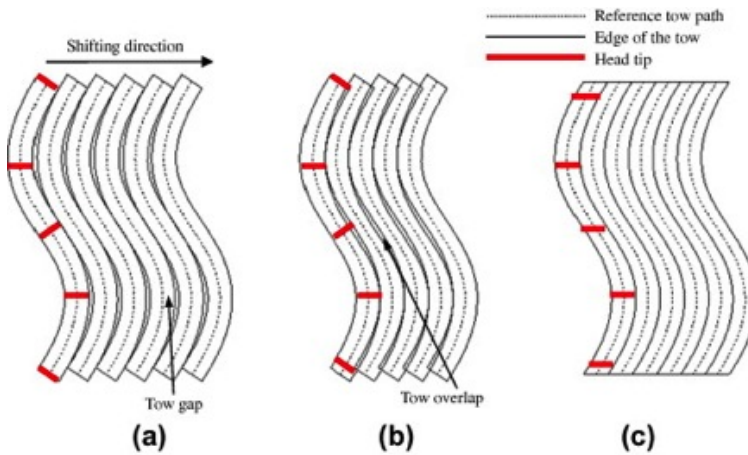
Figure 1.10: Gaps and overlaps appearing when shifting[80].

Figure 1.11: No gaps or overlaps appearing, but steering radius decreasing.
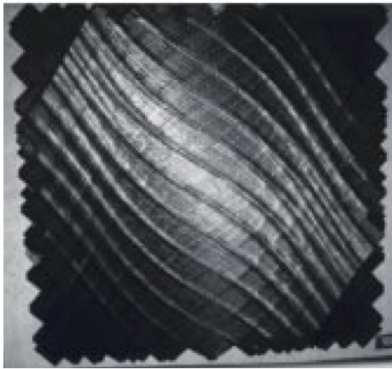
(a) Using overlap strategy.
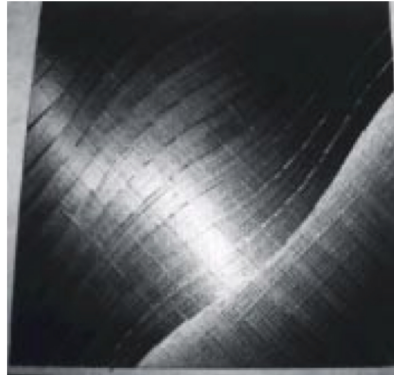
(b) Using gap strategy.

Figure 1.12: Manufactured plates [68].

1.4 GOAL OF THE THESIS

Current optimisation techniques do not take full advantage of the design possibilities opened by automated fibre placement (AFP). Both fibre steering and ply drops can be optimised simultaneously to obtain a laminate that has the best performance-to-weight ratio. The performance can be expressed as lowest compliance, highest buckling load, or lowest maximum stress in the structure. The goal of this thesis is precisely to develop such optimisation algorithms. There are many requirements on the laminate design for it to be manufacturable using AFP. For example, the radius of curvature of the fibre path should not be too small. Moreover there are many design guidelines that were developed for conventional laminates. These need to be somehow *translated* to be applicable for non-conventional laminates before it would be feasible for them to be implemented in an industrial environment.

The outcome of the thesis would be optimisation algorithms for non-conventional laminates that are manufacturable using automated fibre placement and satisfying industrial guidelines.

1.5 OUTLINE OF THE THESIS

The outline of this thesis is as follows: first the current state of the art on variable stiffness composite optimisation is discussed in chapter 2. Next, one of the key decisions in optimisation is discussed in chapter 3: the parametrisation of the

problem. Consequently, based on the optimisation approaches currently used and the chosen parametrisation, the novel optimisation method used in this work is explained in chapter 4. This method is a multi-level optimisation using convex conservative separable approximations, solved using a predictor-corrector interior-point algorithm, implemented specifically for the current work. How the approximations for the different structural responses are found is discussed in chapter 5.

After the general approach, the optimisation of laminates with steered fibres is discussed. Two important characteristics of the optimised design, which are implemented in the current work, are that it should be manufacturable, and practical. A manufacturable design is achieved by posing constraints on the minimum steering radius. These are discussed in chapter 6. Including only manufacturing constraints means the laminate can be laid down by a fibre placement machine, but to have a practical optimum design, design guidelines need to be implemented as well. Their implementation, including an equivalent 10% rule and limits on the angle difference between adjacent plies, is discussed in chapter 7.

Following the laminates with steered fibres, variable thickness laminates, meaning with ply drops, are discussed. In chapter 8, the focus is on topology optimisation of composite laminates, and it is found explicit penalisation is the preferred method to find a clear description of the topology. In chapter 9, variable thickness laminates are optimised by posing it innovatively as a layer-by-layer topology optimisation. By optimising the dropping order and posing this as constraint during the optimisation, a feasible variable thickness laminate is found. Finally, the conclusion and recommendations are given in chapter 10.

2

STATE OF THE ART

Before diving into the details of the work done during this PhD, it is time to look back on the work that has already been done. An overview of the different optimisation approaches that have been developed over the years is given in section 2.1. The focus of this overview is on laminates with non-constant stiffness. This can be achieved by either changing the fibre angle, by steering the fibres, or by changing the local thickness, by dropping plies. Both ways can also be combined: dropping plies and fibre steering at the same time. All three possibilities to generate laminates with varying stiffness properties are discussed, and some optimisation approaches are discussed in more detail. All approaches that are relevant for the current work will be highlighted and some others will also be discussed. But this overview is not meant as a complete review of all types of composite optimisation approaches.

One optimisation approach is discussed in more detail: the three-step optimisation approach originally proposed by IJsselmuiden in his PhD thesis[59]. He proposed to perform an optimisation of the stiffness distribution in terms of the lamination parameters in step one, followed by the retrieval of the fibre angle distribution in step two, and finally generate fibre paths in step three. The stiffness and angle distributions are defined at the nodes of a finite element model. The three-step optimisation approach, explained in section 2.2, will be used in this work.

2.1 OPTIMISATION APPROACHES

Before starting with the literature on optimisation, it is important to define the terminology used for the different laminates in this work. In literature one finds different names for laminates of which the fibre angles are changing over the structure (e.g., curvilinear fibre format, variable angle tow, variable stiffness, or variable-axial composites). In this work, the term 'variable stiffness laminates' (VSL) is used to describe laminates with a constant thickness and a changing fibre angle over the structure. Constant stiffness laminates (CSL) is used to describe laminates with a constant thickness and constant fibre angle over the structure. Another way to change the material properties from one point to another is changing the thickness. The term 'variable thickness laminates' (VTL) is used to describe laminates with constant fibre angle and changing number of layers. The combination, changing fibre angle and number of layers is described using 'variable stiffness variable thickness laminates' (VSVTL). Since the goal of this thesis is to optimise laminates with varying stiffness properties, hence VS, VT, or VSVT laminates, these will be discussed, CSL optimisation is not discussed. The interested reader is referred to a recent review by Ghiasi et al. [45], or by Venkataraman and Haftka [157]. Furthermore, optimisation of composites with varying stiffness properties is an active field of research and new papers are constantly being published. Only the work that was already done during the PhD thesis is discussed, implying the most recent work may be missing in this survey.

2.1.1 VARIABLE STIFFNESS LAMINATES

When using hand lay-up the orientation within a ply had to be constant for manufacturing reasons. With the advent of fibre placement machines this constraint disappeared: plies could be laid down in any direction, and individual tows could be steered. This is often done using automatic fibre placement (AFP) [37,95]. The most important manufacturing constraint using AFP is the minimum turning radius. Depending on the material and placement speed, radii as low as 400 to 1000 mm are typically achievable.

Recently, a new manufacturing method has been proposed that has almost no limit on the turning radius: tailored fibre placement (TFP) [137]. TFP can best be compared to stitching single tows on a shape, which leads to the very tight steering radii. Some structures have been optimised to reduce the stress concentration, and have been manufactured and tested [34,102]. However, since AFP is more common in industry the work in this thesis will focus on AFP.

The first laminates with varying stiffness were manufactured without AFP. Instead of drilling holes (e.g., for rivets) in a plate after it was cured, these holes were moulded in during manufacturing by pushing a pin through the laminate.

This led to a better load-carrying capability for two reasons. One, the fibres, meaning the load paths, were continuous from one side to the other and were not interrupted at the hole. Two, the fibre volume percentage increased locally around the hole [29].

One of the first optimisations using the principle of variable stiffness laminates is performed by Hyer and Lee [58]. They performed a buckling optimisation of a simply-supported plate with a central circular hole loaded in compression. The plate was divided into different patches and each patch was optimised using a gradient-based optimisation. It was shown that updating the sensitivities after a new fibre angle distribution was found leads to better results. An example of the outcome can be seen in Figure 2.1. The principle of VSL is shown in this figure: the load is redistributed away from the unsupported hole towards the supported edges. The tensile load capacity was increased as well, although the plate was optimized for buckling. Observing the outcome, clearly manufacturing this part is not possible while maintaining continuity: the large jumps in fibre angle between the different patches are impossible to lay down. Concluding, this work clearly showed the potential of VSL, but the design obtained was not manufacturable.
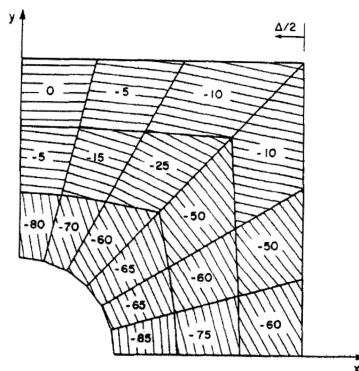
Figure 2.1: Example of the outcome when structure is divided in parts [58].

In a follow-up work [57], plates were manufactured and tested, based on the optimised designs that were adapted to allow manufacturing. The fibre paths were chosen go around the cut-out as can be seen in Figure 2.2. These fibre paths preserved continuity of the fibres going around the cut-out, trying to lead the load away from the cut-out. During testing, it was found that the buckling load increased. However, since the paths at the side were not continuous, the tensile strength was reduced. This is the difference between the design shown in Figure 2.1 and 2.2: in Figure 2.1 the fibre paths at the edge are (almost) parallel to the sides, meaning all fibres are continuous, while this is not possible in the manufactured part. Hence, the idea of leading the load away was shown to work in

practice, but due to manufacturing reasons, the tensile strength decreased.
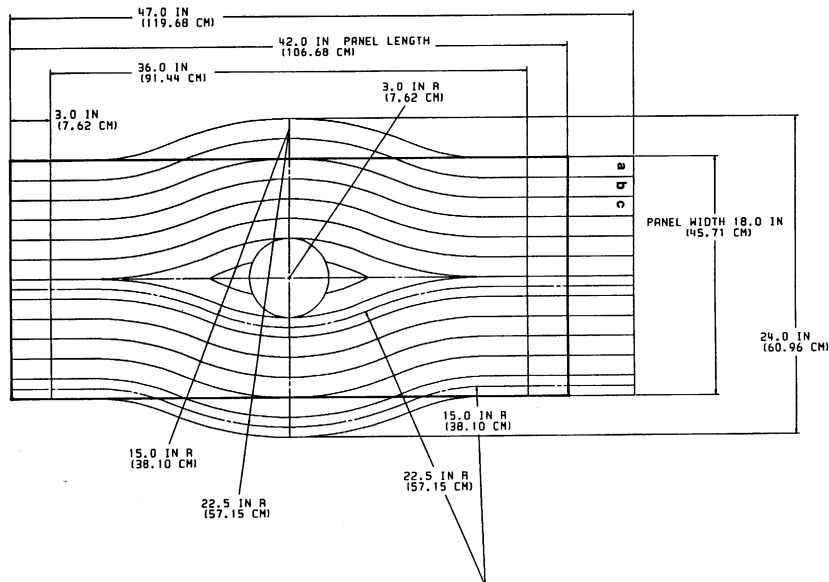
Figure 2.2: Steered paths manufactured by Hyer et al.[57].

Based on the observation that continuity has to be preserved, the idea of using load paths to define the fibres came in existence. A load path in this sense is defined as a path where the load is constant from the point of load application until the point of reaction out of the structure[76,77]. By placing the fibres along this path, continuity is guaranteed. Plates designed using this approach were manufactured and large increases in strength of 60% up to 85% were reported[144]. However, a design thus found is not sure to be manufacturable: the load paths may converge or diverge, leading to (large) gaps or overlaps.

A closely related approach is placing the fibres in the direction of principal stress. Doing so, the shear stress becomes small. This is advantageous since the relatively weak resin has to carry the shear stress, while the fibres carry the normal stress. Since the direction of principal stress changes when the fibre direction is changed, this is an iterative process. Usually only a few iterations are necessary[142]. Another way to explain this principle is that by ignoring the shear stress, the resulting structure can be seen as a Michell structure[103]. When defining another layer orthogonal, the problem of secondary stress, or the load being slightly off from the design load, is shown to have a limited influence[73]. Using tailored fibre placement, the direction of principal stress can always be followed[34,122].

However, when using AFP modifications may be necessary to make sure the path can be followed by the machine. This is most likely to happen at places with stress concentrations. Hence, manufacturability is not guaranteed.

To assure manufacturable fibre paths, the concept of linearly varying fibre angles was proposed. When using linearly varying fibre angles, the fibre paths are parallel to each other in one direction, and changing linearly in the other direction according to[93]

$$\theta(x) = \theta_0 + (\theta_1 + \theta_0)\frac{|x|}{d}, \tag{2.1}$$

where θ_0 is the angle in the middle, θ_1 is the angle at the side, and d is the length from the middle until the side. This is shown graphically in Figure 2.3. The advantage of this parametrisation is that only two angles need to be optimised, and it is easy to ensure the design can be manufactured: by limiting the difference between θ_0 and θ_1, based on the distance d.
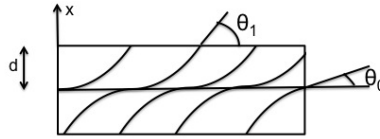
Figure 2.3: Example of linearly varying fibre angle distribution.

Using linearly varying fibre angles, closed-form solutions can be found for the stiffness of the structure, considerably reducing the computational cost[49]. The Rayleigh-Ritz method can be used to find the buckling load numerically. Since only two variables exist, the optimisation could be done in an exploratory way: by changing θ_0 and θ_1 in 10° intervals between 0° and 90°, the complete space can be explored doing 100 calculations. The overall outline of the results is often as shown in Figure 2.4, where the critical buckling load versus in-plane stiffness is shown. As can be seen, using straight fibres meaning CSL, a certain in-plane stiffness corresponds to a certain buckling load, while multiple values for the in-plane stiffness are possible for the same buckling load when using VSL[51]. Furthermore, it is observed that the buckling load can be more than doubled when using VSL compared to CSL. The strength and first-ply failure have also been optimised using the concept of linearly varying fibre angles[92,93]. Hence, this shows once more the potential of VSL to increase performance without adding weight.

When manufacturing the panels, a choice has to be made whether gaps or overlaps
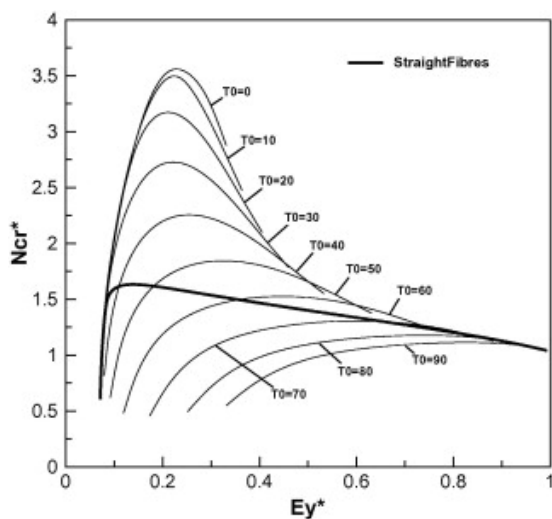
Figure 2.4: Critical buckling load versus in-plane stiffness [93].

are allowed when shifting the tows, as was explained in section 1.3. Both options were manufactured, and as a reference, a CSL was manufactured. All three types of panels were tested for buckling under compression and shear load [68,69]. Under compression, the buckling load of the CSL was predicted quite accurately: the buckling load of panels with gaps was on average about 10% higher than predicted, the buckling load of the panels with overlaps was almost 50% higher than the predicted load. This is the result of a combination of effects: due to curing some pre-stress appears, which has a positive effect on the buckling load. Furthermore, the actual material properties could differ from the assumed properties, and the gaps and overlaps have not been taken into account [68]. The buckling results under shear load were different: the buckling load was predicted accurately for both the panel with gaps and overlaps. The buckling load of the VS panels under shear is lower than that of the CS panels, because they were optimized for buckling under compression. The failure load on the other hand is increasing [69]. These tests clearly show that VSLs lead to an actual increase in performance, not just to a theoretical one.

Next to plates, also stiffened plates have been optimised. In these cases the bay between two stiffeners is optimised and repeated, as has been done by Coburn et al. [31], and Jeliazkov et al. [70]. A genetic algorithm is used to find the best fibre angle distribution. In general, the distribution goes close to 0° at the stiffeners to introduce the load, much like at the edges of a simply-supported panel, and towards ±45° in the middle. The improvement in buckling load was smaller than for plates since the distance over which the angle had to change from θ_0 to θ_1 and

back is smaller, reducing the load redistribution capability.

Cones have been optimised using linearly varying fibre angles as well. The maximum fundamental frequency was optimised with a manufacturing constraint on the radius of curvature. The cone was divided in multiple stages in the direction in which the cone is getting wider, and at the sides of each edge, the angle is defined[17]. The 0° angle on the cone is defined by projecting the axis of rotation onto the surface. A geodesic path, which requires no steering, can be defined by specifying the fibre angle at any point on the cone. The fibre angle along a geodesic path will vary with the axial coordinate, unless the specified fibre angle is 0°. A constant angle path, on the other hand, requires fibre steering. A different method to define the fibre paths is to use a constant curvature path, which is relatively easy to manufacture, but the correct fibre angles have to be retrieved to perform a finite element analysis (FEA). Both can be used during optimisation. All three cases are shown in Figure 2.5.
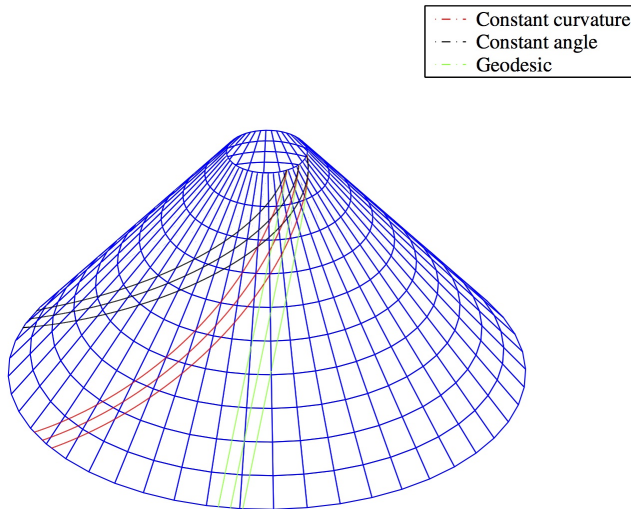
Figure 2.5: Definition of different paths on a cone[19].

Cylinders with varying fibre angles have been optimised and manufactured too[18]. For cylinders, the fibre angle is constant over the length of the cylinder and is varying as a function of the angle in the circumference. Multiple stages are defined to increase the design freedom , and the angle is linearly changing in each stage, as is shown in Figure 2.6. When a cylinder under bending is optimised, the results show that the upper side, which is in tension, is made stiffer to attract more load. A larger part of the load is taken by the part in tension, and a smaller portion is carried in compression, increasing the overall load by up to 17%[18].

2
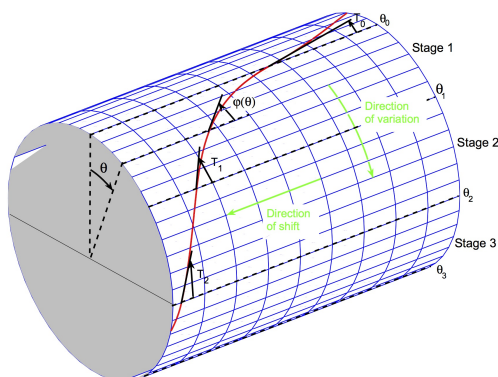
Figure 2.6: Definition of a VSL cylinder [18].

Some VSL cylinders have been built and both a modal and bending test was performed [14]. The results for both the modal and bending tests showed good agreement between FEA and experiments, for both mode shape and modal frequency, as well as for the strain field. It was noted that the load redistribution behaves as expected: the tension side carried a larger part of the load than the compressive side. Furthermore, the maximum strain at the same load was significantly reduced: the compressive strain was 10% lower, the tensile strain even 35% compared to the CSL design. This shows the potential when a strength-critical design is optimised using VSL: using a strain-based failure criterion, this reduction in strain is significant. Hence, these tests again confirmed the possibilities to improve structural performance by using VSLs.

Another set of cylinders was built and a series of tests was done by Wu in cooperation with different co-workers. The same VS cylinders were used for a series of tests [159,163]: first pristine [161], then making cut-outs in them [162], followed by large cut-outs [164]. Two cylinders were manufactured and tested with the same fibre angle distribution. The only difference is that one cylinder is manufactured using an overlap strategy, the other using the gap strategy. The difference in weight, for the pristine cylinders, is 27%. The axial stiffness and buckling load, normalised with respect to the weight, is 28% and 78% higher for the cylinders made using the overlap strategy compared to the cylinders made using the gap-strategy respectively. The experiments agree within 10% with FEA, suggesting that VS cylinders are less sensitive to imperfections than their CS counterparts [161].

The cylinders were not damaged during the buckling test, and another set of tests was done, with a cut-out on one side scaled to represent a passenger door on a

commercial aircraft[162]. Although the cylinders were not designed with cut-outs in mind, the reduction in both axial stiffness and buckling load do not exhibit a large decrease: on average 93% (94 and 91% was measured) of axial stiffness, and 86% (82 and 91% was measured) of buckling load remains compared to the pristine cylinders. This shows the advantage that VS cylinders offer: the influence of cut-outs is small. Furthermore, it is expected that this influence could be further reduced when they are accounted for during design[162]. It has to be noted that the cut-outs were made in the low-stiffness part of the cylinder, which could be part of the reason for the small influence.

The cylinders still did not show any sign of damage, so the size of the cut-out was increased to represent a cargo door on a commercial aircraft. Increasing the size of the cut-out had a limited effect on the performance: on average still 91% (92% and 90% was measured) of axial stiffness and 85% (both 85%) of buckling load was preserved compared to the pristine cylinders. For the tests with cut-outs good agreement was found with the linear bifurcation buckling loads. Since it is known that the buckling load of unstiffened CS cylinders and plates are sensitive to geometric imperfection recently, a numerical study on the influence of imperfections on the performance of VS cylinders has been performed[160]. Results showed what was expected based on the previous results: the imperfections have a limited influence. The reason is that the buckling always occurs in the same region: by varying the fibre angle a large difference in local stiffness is created. Hence, the location of the buckling is not influenced by imperfections. This implies that the load redistribution is hardly influenced by the imperfections, and thus the effect of these imperfections is small[160].

Running an FEA is computationally expensive, even though the description of the fibre angle distribution is easy when using linearly varying fibre angles. To reduce the amount of FEAs necessary during optimisation, Ungwattanapanit and Baier[149] used a global response surface method to perform post-buckling optimisation. Another approach is proposed by Nik et al.[109], who use a surrogate model combined with an evolutionary algorithm to find the Pareto front describing the in-plane stiffness versus buckling load. In a follow-up work, they even consider the effect of gaps and overlaps during the optimisation[111], something that is not taken into account by other approaches even though the resulting thickness distribution is severely influenced, as could be seen in Figure 1.12. A more complete overview of optimisation using metamodels can be found in the work of Nik et al.[110].

Summarising, the principle of linearly varying fibre angles has been shown to be very useful due to the relatively easy implementation of manufacturing constraints. Furthermore, only two angles need to be optimised. Using the linearly varying fibre angles principle, plates and cylinders were manufactured which clearly proved the potential of VSL. However, since the number of design variables is limited, the full potential of VSL to improve performance is not exploited. In

2

certain cases it may be beneficial to have a lot of steering on one place, and less in another. This is not possible using linearly varying fibre angles.

Another approach, which requires more design variables, is parametrising the fibre paths as NURBS (Non-Uniform Rational B-Splines). NURBS describe the fibre path based on the fibre angle distribution at the control points [24,106,107]. An example of the control point definition can be seen in Figure 2.7. As can be seen, the number of control points for a complete wing is small, making this description an attractive candidate for optimisation. Describing the fibre paths using NURBS allows the inclusion of constraints on the minimum steering radius assuring manufacturability [24]. Closely related approaches are using 'standard' splines and optimising the angle distribution of the control points, as has been done by van den Brink et al. [152], or using polynomials and optimise the coefficients, as has been done by Wu et al. [166]. While all these methods lead to exact descriptions of continuous tow paths, the result is still limited by the number of basis functions one takes into account. While it is a nice feature that the fibre paths are described, determining the angle within an element for an FEA is an extra step that needs to be taken. After the FEA, the sensitivity of each control point has to be found if a gradient-based approach is to be used: this requires the opposite scaling: from elements in the FEA to control points.

Control Points

θ_0: -15 -10 -5 0 5 10 15 20 25 30 35 40
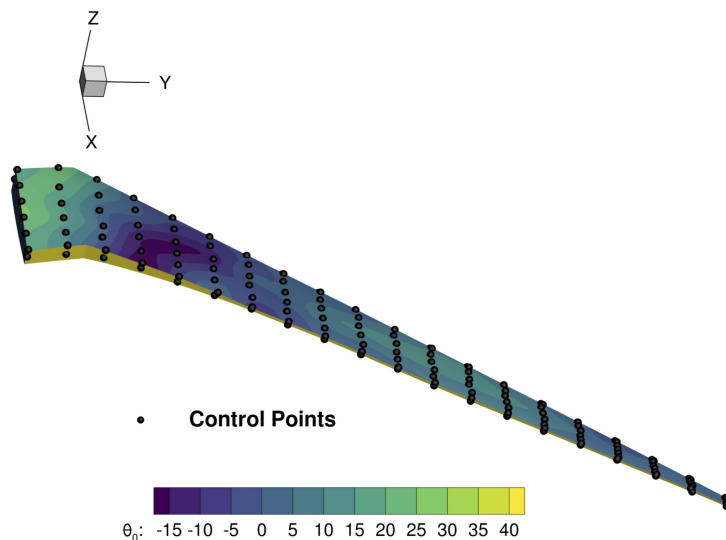
Figure 2.7: Definition of the control points in a wing [24].

The level-set method is usually applied in topology optimisation [153], but has recently been used to optimise laminates as well [23,88]. When using the level-set method in topology optimisation, a certain constant level is used to define the

boundary: everything above is material, everything below is void[153]. When using the level-set method to optimise the fibre paths, a certain constant level is used to define the fibre path. By using multiple levels, multiple fibre paths are found. Since the convergence/divergence of the paths is not constrained, gaps or overlaps will appear, and the steering radius is not constrained, hence manufacturability cannot be guaranteed[23]. Manufacturability has been guaranteed in a recent patent by Boeing[32]. Another way to implement the level-set method was performed optimising just a few parameters describing a reference fibre path, which is consequently shifted in such a way that no gaps or overlaps are created. By this shifting, the steering radius decreases, however, this has been constrained[88]. The level-set method has only recently been applied to the optimisation of variable stiffness laminates, hence not a lot of references are available. The first results suggest that it allows for a general description of the fibre paths, and allowing for a constraint on curvature as well. Furthermore, it does not seem to be prone to get stuck in a local optimum. Hence, it is a method that certainly deserves more research, but is not generally applicable yet.

Concluding the review of optimisation techniques for variable stiffness laminates, it is observed that the earliest methods demonstrate the theoretical advantages of VSLs, but did not lead to manufacturable designs. Using linearly varying fibre angles, manufacturability was no longer an issue, but the design freedom was limited. The combination of manufacturable and more design freedom was achieved using direct description of the fibre paths, where the parametrisation of the fibre paths has an influence on the outcome of the optimisation, and the use of FEAs is not straightforward. The final method discussed was the level-set method, which is still being developed, but looks promising. Concluding, currently no method exists that exploits the full design space of VSL, while guaranteeing a manufacturable design.

2.1.2 VARIABLE THICKNESS LAMINATES

When changing the thickness of an isotropic material like aluminium or steel, a smooth change is often used. One of the plies is dropped when the thickness of a composite laminate changes, meaning the drop-off is not smooth and the thickness is not continuous. Certain plies need to be continuous to ensure manufacturability when changing the thickness, a requirement usually referred to as *blending*. The easiest way to ensure continuity is dropping the plies in a certain order. Dropping plies from the symmetry plane is called inner blending, dropping from the outside is called outer blending[125]. This is shown graphically in Figure 2.8.

One of the most popular approaches to optimise variable thickness laminates is dividing the panel in different patches and optimise the thickness and lay-up of each patch[8,62,84,89,125]. A genetic algorithm is often used for the optimisation. The possible fibre angles are usually limited to $0°$, $\pm 45°$, or $90°$. When optimising

the thickness and stacking sequence per patch, manufacturing issues appear: the layers of the same ply in different patches are not continuous because the fibre angle has changed. To guarantee continuity, a guide laminate can be used, which is the thickest laminate appearing in the structure. From this guide laminate all other laminates are found by dropping certain plies[8,62,84]. This can be done using inner or outer blending, but more complicated drop orders can be used as well[150]. This methodology works well, and is computationally efficient, but the possible ply drop locations are pre-specified by the user by defining the patches. Hence, the final outcome depends on the patches the user defines.

A more advanced approach takes into account that only some plies need to be continuous over the complete structure, while others can end at patch boundaries[71,89,150]. This enlarges the design space considerably, but requires the user to define all plies that have to be continuous between the different patches. Hence, the approach offers more options, but also requires the use to pre-specify more parameters. Some examples of blending patterns are shown in Figure 2.8.

(a) Outer blending.

(b) Inner blending.

(c) General blending.

(d) General blending with restarting.
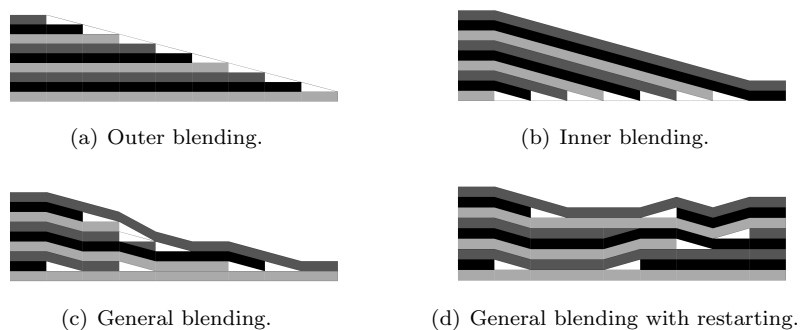
Figure 2.8: Different blending patterns.

Good results have been obtained using a multi-step approach. One two-step approach uses lamination parameters: in the first step the thickness and lamination parameters are optimised, in the second step the stacking sequence is retrieved[62,89]. The retrieval is easier when more layers are to be optimised because the optimiser has a larger design space to match the lamination parameters[89]. Another two-step approach is similar: in the first step, the thickness and ply percentages are optimised. In the second step the blending and manufacturing constraints are satisfied by shuffling the layers[89,131,171]. Disadvantage of these methods is that the constraints on structural performance are not guaranteed to be satisfied because the performance can decrease during the retrieval step.

A single step, bi-level approach that resembles the last two-step approach is to optimise the general thickness of the plies of $0°$, $45°$, $-45°$, and $90°$ in a fixed order where the thickness is a continuous variable. This is done in each patch separately,

with as only constraint that the thickness of 45° and −45° plies have to be the same. During the second level, the exact number of plies of each orientation is found, and they are shuffled to obey manufacturing and blending constraints [170]. By combining the two steps in one, the outcome of each iteration is guaranteed to satisfy the constraints, increasing the computational efficiency of the algorithm.

A method that allows for the optimisation of the order in which the plies are dropped is the stacking sequence tables method, originally proposed by Irisarri et al. [65,104]. The method simultaneously optimises the thickness of each patch, the stacking sequence of the guide laminate and the order in which the plies are dropped. Optimising the drop order gives the optimiser more design freedom. For example, during a buckling optimisation with prescribed drop order, the continuous plies will most likely be ±45°, which are located preferably as far from the symmetry axis as possible. However, if a layer further towards the outside gets dropped before the one closer, it may be advantageous to have the inner layer be ±45° instead of the outer one. When optimising the drop order, the outer layer may be made continuous and the inner one dropped, pushing the ±45° layer to the outside, increasing the performance. This method still works using patches, hence the ply drop boundaries are still prescribed. The method of stacking sequence tables is used in section 9.2, where a more detailed description is provided.

A method where the possible ply drop boundaries are not prescribed is proposed by Delgado [35]. This method iterates between two different optimisations: the fibre angle of each layer is optimised in one optimisation, while the other optimisation determines the shape of each ply, as is shown in Figure 2.9. Each ply is optimised using level-set optimisation. The fibre angles are restricted to the set of 0°, ±45°, and 90°. This methodology has the advantage that the continuity of each ply is guaranteed, but has a restricted set of possible fibre angles.

Concluding, the optimisation of VTLs is clearly a less-researched area than VSL. Most algorithms have two major drawbacks: they are constrained in terms of the number of possible fibre angles and the location where the ply drops can occur: these are usually prescribed to be at patch boundaries, limiting the design space. When using a single-step optimisation, one of these two drawbacks is always present for the methods reviewed. Using a multi-step approach, it is possible to have a more general VTL. This resembles the idea behind the three-step optimisation approach, which is adhered to in this thesis, and is discussed in section 2.2.

2.1.3 VARIABLE STIFFNESS VARIABLE THICKNESS LAMINATES

One of the most researched methods to obtain variable stiffness, variable thickness laminates is the discrete material and topology optimisation (DMTO) by Sørensen et al. [135]. It is based on the discrete material and optimisation method (DMO),

2
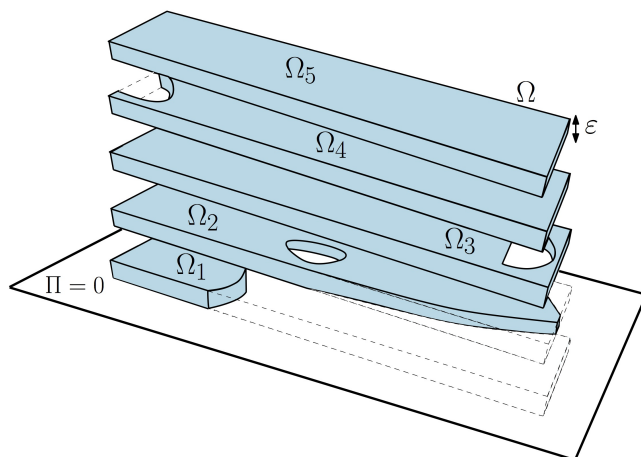
Figure 2.9: Example of the shape optimisation per ply [35].

originally proposed by Stegman and Lund [138]. This method optimises which material is present at any layer at a certain location. The different materials are defined by a 6×6 stiffness matrix that can represent a different fibre angle or a completely different material. Different patches are optimised, that may consist of multiple elements in the FEA. Analogous to the optimisation of variable thickness laminates, the choice of the patches has a significant influence on the final outcome and computational cost. Each patch can have a different material and different orientation, leading to a variable stiffness laminate. The original method was developed for compliance optimisation, but works for buckling [96], or minimisation of sound radiation during vibration [112] as well.

Later on, the possibility of having a void (i.e., no material) as material was included and the method was called DMTO by Sørensen et al. [135]. An example of the outcome can be seen in Figure 2.10. To ensure manufacturability, the plies are always dropped from the outside. This does not mean that the outside of the laminate is not continuous: when manufacturing the inner plies may be dropped to avoid delaminations. Later on, a different constraint was formulated removing the need to always drop from the outside [133]. Other constraints include a limit on the rate of thickness variation and the contiguity [134]. To reduce the size of the patches, thus increasing the possible ply drop locations, while assuring manufacturability, a minimum length is implemented [132]. Since each patch can have a different fibre angle and layers may be dropped between patches, the outcome is a variable stiffness, variable thickness laminate.

A different approach is the shape function with penalisation (SFP) [25]. This method uses the shape functions that are already embedded in the FEA to con-
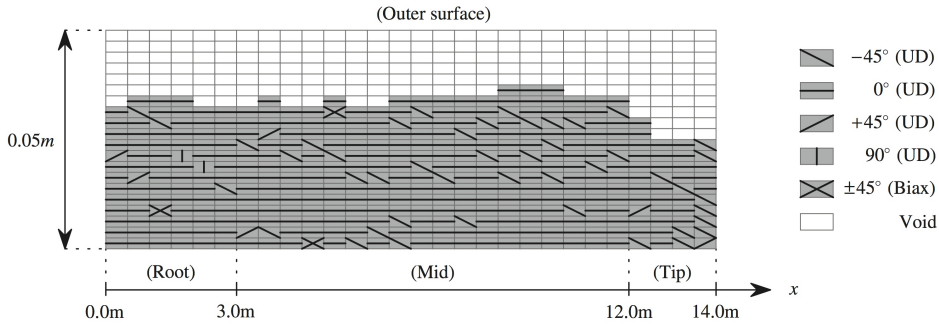
Figure 2.10: Example of the outcome using the DMTO method[135].

siderably reduce the number of design variables. The weighing factors are used to determine the exact material. It is shown to work with multiple possible fibre angles and includes the possibility of dropping plies, hence the parametrisation is almost the same as the DMO method[27]. The idea of SFP is generalised in the Bi-value Coding Parameterization (BCP), which uses values of +1 and −1 for m material phases, which reduces the computational cost when a lot of possible fibre angles are included. Originally, the BCP method was developed for variable stiffness laminates, hence with constant thickness[43]. Afterwards, it was extended to include the possibility of dropping plies, while obeying a volume constraint[44].

A disadvantage of the DMTO, SFP, and BCP method is that the overall problem is not convex. Since convexity is an important characteristic of an optimisation problem, an alternative formulation is proposed by Sørensen and Stolpe that is convex. This implies that the optimum found is guaranteed to be the (near) global optimum. The convergence rate is improved using heuristics[136]. A disadvantage is that the possible material orientations are still limited.

Another approach is introduced by Pedersen, who optimises the density and orientation concurrently[113]. This is done for both isotropic and anisotropic materials. The anisotropic materials are defined as materials with a certain ratio of the stiffness in normal and perpendicular direction, hence the direction cannot be seen as a fibre angle exactly. When this ratio is 1, isotropic materials are obtained. The orientations are decided by the direction of principal stress. To obtain optimised designs, only $10 - 20$ iterations were necessary in this work[113].

A completely different approach is developing a new manufacturing method: continuous tow shearing (CTS), introduced by Kim et al.[80]. CTS leads to variable stiffness variable thickness laminates without any gaps or overlaps. This is achieved by shearing the tows as they are laid down, before curing. This thickens the plate locally because the fibres are packed together, but no gaps or overlaps

2

are created, as can be seen in Figure 2.11. Furthermore the steering radius can be as small as 100 mm[80,82]. The accuracy of the fibre paths was found to be higher using CTS than using AFP, highlighting the potential of the method[82]. The packing of the fibres leads to a special characteristic: the amount of steering is directly proportional to the thickness increase. Contrary to AFP, the structures manufactured using the CTS method can be implemented in an FEA without the need to account for defects introduced by cutting tows[83].
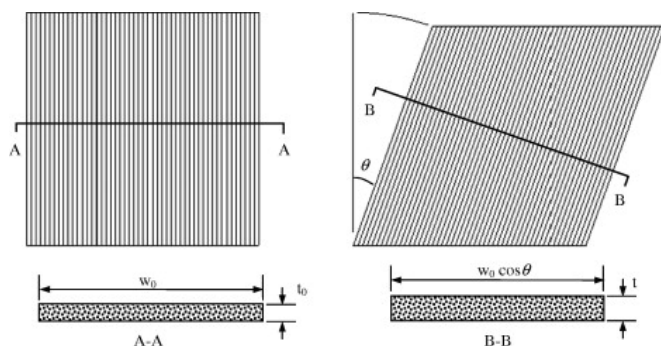
Figure 2.11: Thickness change due to the shearing: left before shearing, right after sharing[80].

When plates manufactured using CTS are cured on a flat surface, next to the thickness change, the neutral surface is also no longer flat. This has an influence on the structural behaviour of the manufactured laminate which should be taken into account during the optimisation of such a laminate, as has been done by Groh and Weaver[47]. When the mass of a plate under uni-axial compression is optimised considering buckling constraints, a reduction of 31% in weight is found. When an additional constraint on the maximum compression strain of 4000 microstrain is added, a reduction in weight of 21% is found[47].

CTS has a very slow deposition rate. In an attempt to increase the deposition rate, Kim et al. proposed continuous multi-tow shearing (CMTS), which uses the same principle, but with multiple tows at the same time[81]. CMTS leads to a faster deposition rate, but the reference and actual path are further apart, which can be due to the large shift required. The minimum steering radius obtained was 300 mm, which is an order of magnitude lower than AFP can achieve with fibres of the same width[173]. So far only prototypes have been used to manufacture relatively small samples using the CTS or CMTS method, hence it is too early to judge the viability of this method, but the slow production rate and link between steering and thickness are currently limiting factors.

Summing up, not a lot of methods leading to VSVTL are developed. The methods identified that aim for manufacturing using AFP all have the major drawback that only a limited set of fibre angles can be used during the optimisation. This has two

important implications: one, the design space of the optimiser is limited, two, it is not clear how the optimised design can be manufactured since sudden changes in fibre angle are present. The method of CTS was also mentioned since it is an interesting manufacturing method, linking the fibre angle and fibre thickness. However, in this thesis, only manufacturing using AFP is considered, for which the limited set of fibre angles still exist.

2.2 THREE-STEP OPTIMISATION APPROACH

From the previous section it is clear that a lot of different optimisation approaches have been developed over the years. Some of them use a multi-step approach which has been shown to increase computational efficiency. A method that has been developed at Delft University of Technology is a three-step optimisation approach[59]. In step one, the stiffness distribution, in terms of lamination parameters, is optimised. During step two the fibre angle distribution of the different layers is retrieved trying to match the stiffness distribution as closely as possible. During step three the fibre paths are found; these can be sent to the fibre placement machine for manufacturing. Each step has its own advantages and disadvantages, which will be discussed in the following sections. The advantage of the three-step optimisation approach is that the optimisation is done in terms of the lamination parameters during step one. Step two and three are retrieval steps: no FEA is done during these steps, the only objective is to get as close to the outcome of the previous step as possible.

2.2.1 STIFFNESS OPTIMISATION

A stiffness optimisation is not performed directly on the elements of the stiffness matrix, since the terms of the stiffness matrices are linked to each other. Rather, the lamination parameters are used, which describe the elements stiffness matrices linearly. A more detailed explanation of the lamination parameters (LP) is given in section 3.2. The advantage of the lamination parameters is that a general laminate can be described using 12 lamination parameters, and the total laminate thickness. Often, laminates have to be symmetric, in which case only 8 lamination parameters and the thickness are necessary. Hence, no matter how many plies the laminate has, only 9 design variables have to be optimised. Another reason for choosing the lamination parameters as design variables is that it has been shown that the optimisation problem in terms of the lamination parameters is convex[42]. This is not the case when the fibre angles are used as design variables; then a highly non-convex design space is found. Gradient-based methods can be used to find the global optimum since the design space is convex, .

Three options are possible using LP optimisation: a constant stiffness laminate is

found by defining only one set of lamination parameters and thickness. A variable stiffness laminate is found when the thickness is constant and the lamination parameters are varying over the structure. a variable stiffness variable thickness laminate is found when the thickness and the lamination parameters are varying. Theoretically, variable thickness laminates can also be obtained, however, when dropping a ply, the lamination parameters will change as well. Hence to obtain variable thickness laminates, both the thickness and lamination parameters have to change. A possible solution is limiting the change in lamination parameters from one point to another, which has been shown to lead to combinations of lamination parameters and thickness that can be matched more closely in terms of the fibre angles[97,98].

Due to the limited number of design variables and the convexity of the problem, optimising in terms of the lamination parameters has attracted quite some attention. Examples include standard structural responses such as compliance[53], buckling[61,127], strength[78], and fundamental frequency[7,17] while aero-elastic properties have also been optimised[98,143].

An example of a V_1 distribution, one of the optimised lamination parameters, is shown in Figure 2.12. One of the disadvantages of lamination parameters can be seen in this figure: no information about the physical lay-up of the laminate is available. By staying inside the feasible region, it is theoretically possible to find a laminate with exactly the same stiffness properties, but in reality this hardly ever happens. This has several reasons: the number of layers is limited, so the number of different stiffness properties within the laminate is limited. Furthermore, there is no one-on-one match between lamination parameters and stacking sequence. Finally, during the optimisation of the lamination parameters, no constraint on the change between points is posed, meaning the change may not be achievable when manufacturing the laminate, which is taken into account in subsequent steps. How these difficulties are handled is explained in the next part about fibre angle retrieval.

2.2.2 FIBRE ANGLE RETRIEVAL

Step two in the three-step optimisation approach is fibre angle retrieval, which can be done in many ways, depending on the desired outcome and the number of layers in the laminate. Enumeration can be used when constant stiffness laminates are to be designed, the number of layers is low, and the possible fibre angles are restricted to a small set (e.g., $0°$, $\pm 45°$, and $90°$)[56]. The total number of possibilities has to be small for enumeration to be feasible, but one is guaranteed to find the global optimum. To improve computational efficiency it is possible to first optimise the outer layers, since they have the most influence on the bending stiffness, and consequently move inward[108]. If the number of layers and/or the number of possible fibre angles increases, enumeration becomes too costly in which case a
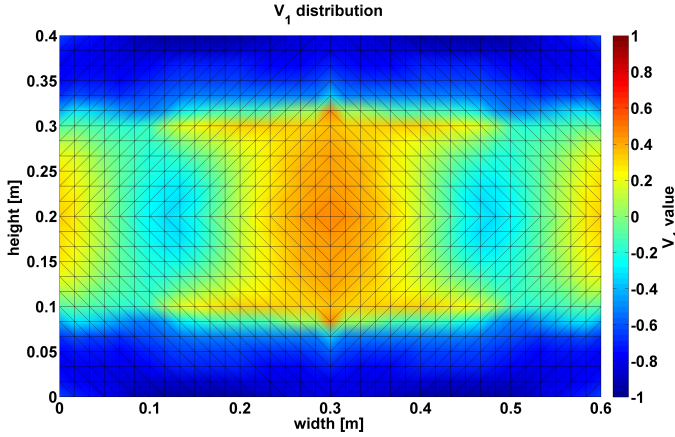
Figure 2.12: Example of the outcome of a lamination parameter optimisation, this is a V_1 distribution.

genetic algorithm (GA) might be used[90]. Using a GA has the advantage that not all possibilities are checked, and when the parameters related to the GA (for example cross-over or mutation) are chosen well, the global optimum is found. However, there is no guarantee one finds the global optimum using a GA[21,55]. It is possible to match the in- and out-of-plane matrices as closely as possible using a combination of a GA and a modified Shepard's interpolation to further improve the computational efficiency[64,104].

The previous possibilities work fine when the fibre angle is not changing within a layer, however, when the fibre angle does change, additional constraints need to be taken into account. Besides trying to retrieve the fibre angles at different points based on the outcome of the lamination parameter optimisation, the change in fibre angle needs to be considered as well: when this change is too large, the panel cannot be manufactured using AFP. A possible approach is describing a non-linear variation using Lagrangian polynomials, and using a GA to optimise the fibre angle distribution at a set of control points, as has been done by Raju et al.[121]. This leads to a general fibre angle distribution, which is matching the lamination parameters fairly well.

The constraint limiting the change in fibre angle is called the *steering constraint.* IJsselmuiden in his PhD thesis only takes an average steering constraint into account[59]. This has the advantage that only a single constraint per layer needs to be taken into account, but it also implies that locally the steering constraint

can be violated. Van Campen et al. use a different approach that does take local steering constraints into account, consisting of two steps[151]. In the first step, the LP distribution is matched as closely as possible using a GA, and the laminates are passed on to a gradient-based optimiser that is combined with cellular automaton. The second step takes the curvature per cell into account, making sure the outcome is manufacturable. Considering that the first step in the work by Van Campen et al. is using a GA, expanding it to large structures with a large number of layers and cells will be computationally expensive. On the other hand, using an average steering constraint like IJsselmuiden, leads to designs that are impossible to manufacture. The ideal would be a combination of both methods: posing a local steering constraint without having to use a GA.

Even when using a local steering constraint, it can be debated whether retrieval leads to the best possible lay-up: the fibre angles may need to be optimised after the retrieval step if the steering constraint prevents a good match to the lamination parameters. Due to the steering constraint, a perfect match is not possible, so it may pay off to perform an optimisation starting from the outcome of the fibre angle retrieval. As a final remark, it is noted that the retrieval steps that are available so far only consider variable stiffness or variable thickness laminates, not the combination.

An example of the outcome of a fibre angle retrieval step can be seen in Figure 2.13. Only a quarter of all fibre angles at the nodes are shown to keep the figure clear. This figure depicts a single layer of a laminate, for each layer such a distribution is found. From this figure one has a good idea of what each layer could look like, but it is not enough to manufacture the laminate. For manufacturing, a description of the exact fibre paths per layer is necessary, which is obtained in the next section about fibre path retrieval.
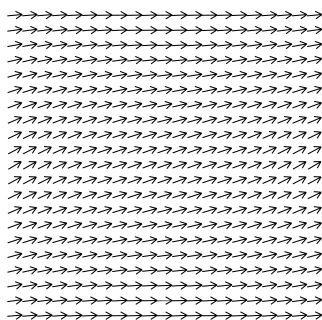
Figure 2.13: Example of the outcome of a fibre angle retrieval of a single layer.

2.2.3 FIBRE PATH RETRIEVAL

The fibre angle distribution found in the previous step needs to be 'translated' to fibre paths to manufacture the laminate. To do this, a streamline analogy can be used, where each streamline represents the centre line of a course[15]. A short summary of the work by Blom[15] is given in this section. A streamline is mathematically represented by a stream function:

$$\Psi\left(x, y\right) = c, \tag{2.2}$$

which connects all points with value c. The streamline function $\Psi\left(x, y\right)$ can be found from a given fibre angle distribution $\theta\left(x, y\right)$ by solving

$$\frac{d\Psi}{ds} = \frac{\partial\Psi}{\partial x}\frac{dx}{ds} + \frac{\partial\Psi}{\partial y}\frac{dy}{ds} = 0, \tag{2.3}$$

where s denotes the direction of the streamline. The solution of this partial differential equation depends on the boundary conditions, for which the physics of the problem play an important role. Blom found that the thickness at a certain point is directly proportional to the partial derivative of the stream function with respect to the normal of the streamline n:

$$t \propto \frac{\partial\Psi}{\partial n}. \tag{2.4}$$

Using this equation, a direct correlation between the thickness and fibre angle distribution can be found:

$$\mathbf{s}\boldsymbol{\nabla}\left(ln(t)\right) = \mathbf{n}\boldsymbol{\nabla}\theta, \tag{2.5}$$

where the following definitions are used:

$$\mathbf{n} = \begin{bmatrix} -sin(\theta) \\ cos(\theta) \end{bmatrix} \quad \boldsymbol{\nabla}\theta = \begin{bmatrix} \frac{\partial\theta}{\partial x} \\ \frac{\partial\theta}{\partial y} \end{bmatrix} \quad \mathbf{s} = \begin{bmatrix} cos(\theta) \\ sin(\theta) \end{bmatrix} \quad \boldsymbol{\nabla}\left(ln(t)\right) = \begin{bmatrix} \frac{\partial t}{\partial x} \cdot \frac{1}{t} \\ \frac{\partial t}{\partial y} \cdot \frac{1}{t} \end{bmatrix}. \tag{2.6}$$

Physically, eq. (2.5) states that the change in thickness along a certain streamline depends on the change in fibre angles perpendicular to the streamline: if the fibre angle changes towards the streamline, the thickness increases, if the angle is turned away, the thickness decreases. Eq. (2.5) is only dependent on the fibre angle distribution θ and thickness distribution t. Since θ is known, the thickness distribution can be found from this equation. The boundary condition that determines the overall thickness distribution is the thickness distribution at the inflow. By changing this inflow distribution, the overall thickness distribution is changed. Rewriting eq. (2.5) using $\tau = ln(t)$ leads to

$$\mathbf{s}\boldsymbol{\nabla}\tau = \mathbf{n}\boldsymbol{\nabla}\theta. \tag{2.7}$$

The outcome of step two is a fibre angle distribution at certain points, not a fibre angle distribution as a function of x and y. Hence, eq. (2.7) is discretised and rewritten as

$$\mathbf{M}\boldsymbol{\tau} = \mathbf{b}, \tag{2.8}$$

where **M** is the matrix that represents **s**, $\boldsymbol{\tau}$ is the discretisation of τ at every grid point, and **b** is the discretisation of $\mathbf{n}\nabla\theta$. A nominal solution $\boldsymbol{\tau}_0$ can be found by assuming an inflow $\boldsymbol{\tau}_{in}$ that is equal to one everywhere. The general solution of eq. (2.8) is found to be

$$\boldsymbol{\tau} = \boldsymbol{\tau}_0 + \mathbf{T}\boldsymbol{\tau}_{in}, \tag{2.9}$$

where each column j of matrix **T** represents the influence of inflow point j on the total thickness distribution. These columns are independent of each other. Since eq. (2.8) is a linear equation, every linear combination of columns represents a solution. Hence, the thickness distribution can be optimised by changing the thickness distribution at the inflow. The objective of the optimisation is not uniquely defined: either the maximum thickness is minimised, or the smoothness is maximised. A combination of both is possible as well. The details of this optimisation are omitted in this work, the interested reader is referred to the work of Blom [15].

From the thickness distribution, the streamline can be found by integrating over the normal of the streamline dn:

$$\Psi(x,y) = \int \frac{\partial \Psi}{\partial n} dn = \int \frac{d\Psi}{dx}\frac{dx}{dn} dn + \int \frac{d\Psi}{dy}\frac{dy}{dn} dn = \int \frac{\partial \Psi}{\partial x} dx + \int \frac{\partial \Psi}{\partial y} dy. \tag{2.10}$$

The derivatives of Ψ with respect to x and y can be written as

$$\frac{\partial \Psi}{\partial x} = \frac{\partial \Psi}{\partial s}\cos(\theta) - \frac{\partial \Psi}{\partial n}\sin(\theta)$$
$$\frac{\partial \Psi}{\partial y} = \frac{\partial \Psi}{\partial s}\sin(\theta) + \frac{\partial \Psi}{\partial n}\cos(\theta), \tag{2.11}$$

which can be simplified since $\frac{\partial \Psi}{\partial n} = t$ and $\frac{\partial \Psi}{\partial s} = 0$. Hence, the stream function can be written as

$$\Psi(x,y) = -\int_0^x t(x^*,y^*)\sin\theta(x^*,y^*)dx^* + \int_0^y t(x^*,y^*)\cos\theta(x^*,y^*)dy^*. \tag{2.12}$$

Since both the thickness and fibre angle distribution are known, the streamline function can be found. By plotting certain contours, single streamlines are found. These stream lines represent the centre lines of courses laid down by the fibre placement machine.

In a follow-up work, Kayin Wurpel did his Master thesis at Delft University of Technology on determining the tow-by-tow description of a flat panel [167]. To determine the places to cut the tows, the streamlines were not only used as centre lines for a pass of the fibre placement machine, but extra streamlines were requested halfway between the centre lines. These lines are used as cut lines: when a tow hits this line, it is cut. An example of the stream lines (in red) and the cut lines (in black) is shown in Figure 2.14.
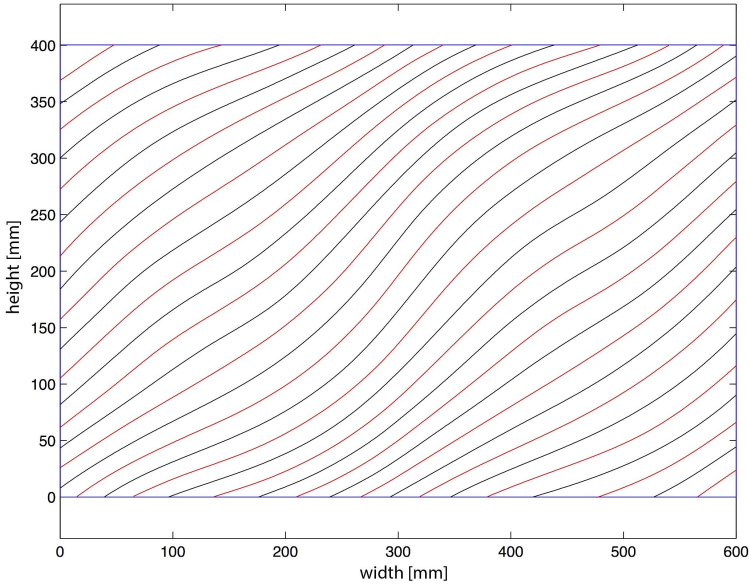
Figure 2.14: Example of the stream lines (in red) and the cut lines (in black) of a single layer.

Starting from the centre lines, the edge of each tow can be found by shifting the streamline perpendicular to the centre line [15]:

$$x_e = x_c \pm w \cdot \sin(\theta_c)$$
$$y_e = x_c \mp w \cdot \cos(\theta_c), \tag{2.13}$$

where the subscript c denotes the centre line, e denotes the edge and the width w is chosen to be the width over which the centre line needs to be offset. When this width is one time the tow width, the edge of the first tow next to the centre line is found. When it is two times the width of a tow, the edge of the second tow is found. For the example, it is assumed the fibre placement machine places eight tows during one pass, meaning four fibres on each side. Furthermore, the full gap strategy is used, meaning that when the outer edge of a tow touches the cut line, the tow is cut. If a full overlap strategy were to be used, the tow would be cut when the inner edge of the tow touches the cut line. An example is shown in Figure 2.15.

Figure 2.15 clearly shows the tow-by-tow description, without any overlap appearing. However, at the edges there are clearly large gaps appearing: the streamline needs to be extrapolated to fill up the complete layer. Furthermore, there are single tows that are too short to be laid down, so they need to be either extended such that they can be laid down, or removed completely. As a final remark, the strategy to cut at each cut line is a good first approximation, but a substantial
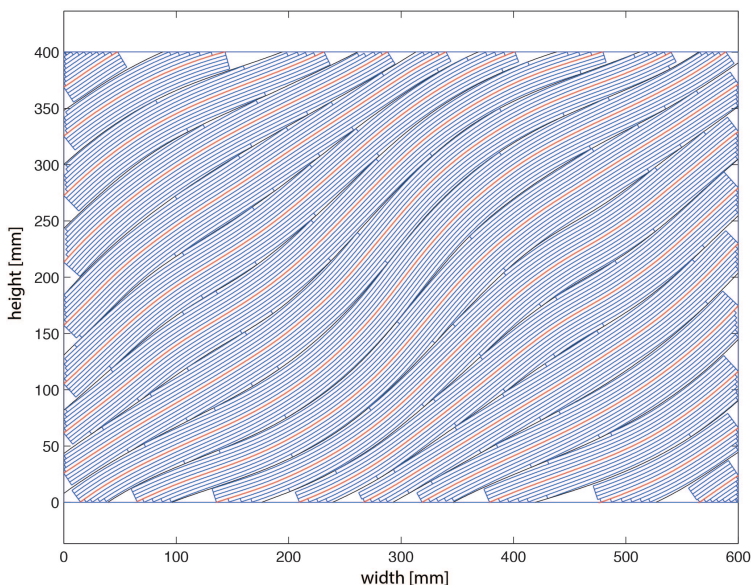
Figure 2.15: Example of the tows in a single layer.

number of tows can be extended without creating an overlap, hence the cutting strategy can be improved as well. While more research is necessary about this step, which is currently ongoing, the results presented already give a clear picture of the physical lay-out of the laminate.

2.2.4   CONCLUSION AND OUTLOOK

Considering the three-step optimisation approach, it is clearly a general approach: no limitations are posed on the fibre paths, hence the design space is as large as it can be. However, manufacturability is not guaranteed: the average steering constraint is not sufficient to guarantee that the steering radius is adhered to everywhere in the structure. Furthermore, step two where the fibre angle distribution is determined using retrieval can be improved: due to the manufacturing constraints the design space during this step differs from the design space during step one, which does not account for manufacturing constraints. Hence, it is likely that by performing fibre angle optimisation, a better performance can be obtained than by just performing retrieval.

In this work, step two will be turned into a retrieval-optimisation step, and instead of constraining the average steering radius, the steering will be constrained at each element, resulting in additional constraints on the fibre angle distribution within a

single layer. A predictor-corrector interior-point optimisation will be implemented since these additional constraints cannot be handled in an efficient way by the dual optimiser currently implemented.

In terms of industrial acceptance of the optimised laminates, not a lot of work has been performed so far. For conventional laminates, design guidelines, such as the 10% rule, are posed during optimisation, however, for non-conventional laminates no work has been found. Since a lot of experience is encapsulated in the design guidelines, it may be worth taking them into account during optimisation to make industry more likely to embrace non-conventional laminates. This will be done in this thesis by implementing extra constraints on the stacking sequence through the thickness.

Finally, in terms of varying the thickness of laminates, more development is necessary as well. During stiffness optimisation, the thickness can be changed, but during step two and three varying the number of plies is not possible. Based on the promising results when the thickness was changing during the stiffness optimisation, it is expected that extending step two to include ply drops will lead to even more efficient structures. This will be done in this work.

On this rock I will build my church.
Matthew 16:18

3

COMPOSITE LAMINATE PARAMETRISATION

A key decision in optimisation is: how to parametrise the design? Which design variables to use? In designing a structure maximising its performance is interesting: for example reducing its weight, while satisfying requirements on functionality, for example no buckling or, more evidently, no breaking of the structure. The prediction of the performance and functionality of the design is quantified in structural responses. These are dependent on the behaviour of the structure under loading, which is described, in the context of finite element analysis, by the structure's stiffness matrix. The stiffness matrix of the structure depends on its geometry and the stiffness properties of various components. Design parametrisation considers the question of associating design variables, which are to be chosen by the optimiser, to either stiffness properties or geometry.

For a composite structure, the property that controls the structural behaviour is the laminate stiffness. The laminate stiffness is derived in the classical laminate theory[75], reviewed in section 3.1. The classical laminate theory starts from the stress-strain relation of a single layer, which is rotated to the global coordinate system. The resulting forces and moments per unit length are found by integrating the stress through the thickness. Three parts of the stiffness matrix are identified: one part describes the in-plane behaviour, another describes the out-of-plane behaviour, and the third part describes the link between in- and out-of-plane behaviour. The integral form of the stiffness matrices can be rewritten as a sum-

mation over the different layers of the layer's stiffness matrices. Hence, the terms of the stiffness matrices are linked, making them hard to use as parametrisation.

Using trigonometric relations, the stiffness matrix of a single layer can be rewritten as summations of laminate invariants multiplied with sines and cosines of the angle with respect to the global coordinate system. By normalising the integral over the thickness, the lamination parameters are found as described in section 3.2. Lamination parameters can be used to parametrise the stiffness matrices. Another possible parametrisation is to describe the laminate by the layer thickness, represented by the ply density, and the rotation of the ply, described by the fibre angle. This is described in section 3.3.

3

3.1 CLASSICAL LAMINATE THEORY

An overview of the classical laminate theory[75,146,147] is given in this section. A single layer of a composite material can be seen as an orthotropic material. Assuming plane-stress, the stress-strain relationship of a single layer is given by

$$
\begin{bmatrix} \sigma_1 \\ \sigma_2 \\ \tau_{12} \end{bmatrix} = \begin{bmatrix} Q_{11} & Q_{12} & 0 \\ Q_{12} & Q_{22} & 0 \\ 0 & 0 & Q_{66} \end{bmatrix} \cdot \begin{bmatrix} \epsilon_1 \\ \epsilon_2 \\ \gamma_{12} \end{bmatrix}, \tag{3.1}
$$

where 1 denotes the fibre direction, and 2 the direction perpendicular to the fibre in the same plane. The terms of the stiffness matrix **Q** are given by

$$
\begin{aligned}
Q_{11} &= \frac{E_1}{1 - \nu_{12} \cdot \nu_{21}} \\
Q_{22} &= \frac{E_2}{1 - \nu_{21} \cdot \nu_{12}} \\
Q_{12} &= \frac{\nu_{12} \cdot E_2}{1 - \nu_{12} \cdot \nu_{21}} \\
Q_{66} &= G_{12},
\end{aligned} \tag{3.2}
$$

where E is the Young's modulus, ν is the Poisson ration, and G is the shear modulus.

Each ply can have a different orientation θ with respect to the global xy Cartesian coordinate system, as shown in Figure 3.1. When rotating the axes from the material to the global coordinate system by an angle θ, the terms in the stiffness

matrix are given in the global system by

$$
\begin{array}{rcl}
\bar{Q}_{11} & = & m^4 \cdot Q_{11} + n^4 Q_{22} + 2m^2 n^2 Q_{12} + 4m^2 n^2 Q_{66} \\
\bar{Q}_{22} & = & n^4 Q_{11} + m^4 Q_{22} + 2m^2 n^2 Q_{12} + 4m^2 n^2 Q_{66} \\
\bar{Q}_{12} & = & m^2 n^2 Q_{11} + m^2 n^2 Q_{22} + \left(m^4 + n^4 \right) Q_{12} - 4m^2 n^2 Q_{66} \\
\bar{Q}_{66} & = & m^2 n^2 Q_{11} + m^2 n^2 Q_{22} - 2m^2 n^2 Q_{12} + \left(m^2 - n^2 \right)^2 Q_{66} \\
\bar{Q}_{16} & = & m^3 n Q_{11} - mn^3 Q_{22} + \left(mn^3 - m^3 n \right) Q_{12} + 2 \left(mn^3 - m^3 n \right) Q_{66} \\
\bar{Q}_{26} & = & mn^3 Q_{11} - m^3 n Q_{22} + \left(m^3 n - mn^3 \right) Q_{12} + 2 \left(m^3 n - mn^3 \right) Q_{66},
\end{array}
\tag{3.3}
$$

where $m = cos(\theta)$ and $n = sin(\theta)$.
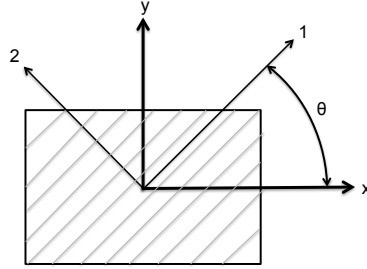
Figure 3.1: Rotation from 1-2 to x-y coordinate system.

The stress-strain relation in the global coordinate system for a single layer is given by

$$
\left[
\begin{array}{c}
\sigma_x \\
\sigma_y \\
\tau_{xy}
\end{array}
\right]
=
\left[
\begin{array}{ccc}
\bar{Q}_{11} & \bar{Q}_{12} & \bar{Q}_{16} \\
\bar{Q}_{12} & \bar{Q}_{22} & \bar{Q}_{26} \\
\bar{Q}_{16} & \bar{Q}_{26} & \bar{Q}_{66}
\end{array}
\right]
\cdot
\left[
\begin{array}{c}
\epsilon_x \\
\epsilon_y \\
\gamma_{xy}
\end{array}
\right],
\tag{3.4}
$$

in tensor form:

$$
\boldsymbol{\sigma} = \bar{\mathbf{Q}} \cdot \boldsymbol{\epsilon}.
\tag{3.5}
$$

Kirchhoff plate theory is assumed to hold, meaning plane sections remain plane and perpendicular to the neutral axis, and the strains are a superposition of membrane strains and curvatures [36,67]:

$$
\boldsymbol{\epsilon} = \boldsymbol{\epsilon_0} + z\boldsymbol{\kappa},
\tag{3.6}
$$

where the subscript 0 denotes the reference plane, $\boldsymbol{\kappa}$ the curvature, and z the through the thickness coordinate, with the mid-plane typically used as reference xy plane, as is shown in Figure 3.2. Resultant forces $\mathbf{N}$, and moments $\mathbf{M}$ per unit

length are obtained by integrating the stresses through the thickness:

$$\mathbf{N} = \int_{-\frac{h}{2}}^{\frac{h}{2}} \boldsymbol{\sigma} dz = \int_{-\frac{h}{2}}^{\frac{h}{2}} \bar{\mathbf{Q}} \cdot (\boldsymbol{\epsilon_0} + z\boldsymbol{\kappa}) \, dz$$

$$\mathbf{M} = \int_{-\frac{h}{2}}^{\frac{h}{2}} z\boldsymbol{\sigma} dz = \int_{-\frac{h}{2}}^{\frac{h}{2}} z\bar{\mathbf{Q}} \cdot (\boldsymbol{\epsilon_0} + z\boldsymbol{\kappa}) \, dz. \tag{3.7}$$

The complete constitutive equation takes the form

$$\begin{bmatrix} \mathbf{N} \\ \mathbf{M} \end{bmatrix} = \begin{bmatrix} \mathbf{A} & \mathbf{B} \\ \mathbf{B} & \mathbf{D} \end{bmatrix} \cdot \begin{bmatrix} \boldsymbol{\epsilon_0} \\ \boldsymbol{\kappa} \end{bmatrix}, \tag{3.8}$$

where

$$\mathbf{A} = \int_{-\frac{h}{2}}^{\frac{h}{2}} \bar{\mathbf{Q}} dz$$

$$\mathbf{B} = \int_{-\frac{h}{2}}^{\frac{h}{2}} z\bar{\mathbf{Q}} dz \tag{3.9}$$

$$\mathbf{D} = \int_{-\frac{h}{2}}^{\frac{h}{2}} z^2 \bar{\mathbf{Q}} dz.$$

The matrices **A**, **B**, and **D** encapsulate all the information about the laminate stiffness. The A-matrix describes the membrane deformations under in-plane loads, hence it is referred to as in-plane stiffness matrix. The D-matrix describes the bending deformations under pure bending so out-of-plane loading, hence it is called the out-of-plane stiffness matrix. The B-matrix describes the possible coupling between in- and out-of-plane loading and deformations, and is therefore called the coupling matrix.

The integrals defining the laminate stiffness matrices, eq. (3.9), can be rewritten as summations since the material stiffness is constant in a single layer:

$$\mathbf{A} = \sum_{k=1}^{n} \bar{\mathbf{Q}}_k \cdot (z_{k-1} - z_k)$$

$$\mathbf{B} = \frac{1}{2} \sum_{k=1}^{n} \bar{\mathbf{Q}}_k \cdot (z_{k-1}^2 - z_k^2) \tag{3.10}$$

$$\mathbf{D} = \frac{1}{3} \sum_{k=1}^{n} \bar{\mathbf{Q}}_k \cdot (z_{k-1}^3 - z_k^3),$$
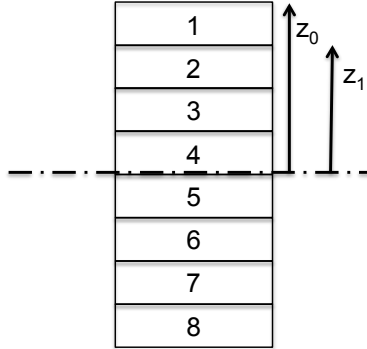
Figure 3.2: Z-coordinates of the different plies.

where n denotes the number of layers. The height z_k is defined in Figure 3.2: z_k is the distance to the bottom of the ply, while z_{k-1} is the distance to the top of the ply from the mid-plane. When the reference plane is chosen as the mid-plane z_k can be calculated using

$$z_k = \frac{1}{2} \sum_{i=1}^{n} t_i - \sum_{i=1}^{k} t_i, \tag{3.11}$$

where t_i denotes the thickness of the ith ply.

Considering eq. (3.10), it can be observed that the A-matrix is independent of the stacking sequence: the location of the layers has no influence. For the B- and D-matrix, the location of the layer is important: the further from the mid-plane, the larger the influence of the layer. Furthermore, it can be seen that if a laminate is symmetric about the mid-plane, the B-matrix is zero. Physically this means there is no membrane-bending coupling. In the remainder of this work the laminate is assumed to be symmetric, and hence $\mathbf{B} = \mathbf{0}$.

Assuming symmetry, the equations for the A- and D-matrices simplify. The integral-form is reduced to

$$\mathbf{A} = 2 \int_{0}^{\frac{h}{2}} \bar{\mathbf{Q}} dz$$

$$\mathbf{D} = 2 \int_{0}^{\frac{h}{2}} z^2 \bar{\mathbf{Q}} dz. \tag{3.12}$$

Thus, the A- and D-matrix can be written as

$$\mathbf{A} = 2\sum_{k=1}^{s} \bar{\mathbf{Q}}_{\mathbf{k}} \cdot (z_{k-1} - z_k)$$

$$\mathbf{D} = \frac{2}{3} \cdot \sum_{k=1}^{s} \bar{\mathbf{Q}}_{\mathbf{k}} \cdot (z_{k-1}^3 - z_k^3), \tag{3.13}$$

where s denotes the number of plies in the symmetric part.

3

3.2   LAMINATION PARAMETERS

Starting from eq. (3.3), using trigonometry, the elements of the stiffness matrix can be rewritten as[145]

$$\bar{Q}_{11} = \frac{1}{8}(3 \cdot Q_{11} + 3 \cdot Q_{22} + 2 \cdot Q_{12} + 4 \cdot Q_{66}) +$$
$$\frac{1}{2}(Q_{11} - Q_{12})\cos(2\theta) + \frac{1}{8}(Q_{11} + Q_{22} - 2 \cdot Q_{12} - 4 \cdot Q_{66})\cos(4\theta)$$

$$\bar{Q}_{22} = \frac{1}{8}(3 \cdot Q_{11} + 3 \cdot Q_{22} + 2 \cdot Q_{12} + 4 \cdot Q_{66}) -$$
$$\frac{1}{2}(Q_{11} - Q_{12})\cos(2\theta) + \frac{1}{8}(Q_{11} + Q_{22} - 2 \cdot Q_{12} - 4 \cdot Q_{66})\cos(4\theta)$$

$$\bar{Q}_{12} = \frac{1}{8}(Q_{11} + Q_{22} + 6 \cdot Q_{12} - 4 \cdot Q_{66}) -$$
$$\frac{1}{8}(Q_{11} + Q_{22} - 2 \cdot Q_{12} - 4 \cdot Q_{66})\cos(4\theta) \tag{3.14}$$

$$\bar{Q}_{66} = \frac{1}{8}(Q_{11} + Q_{22} - 2 \cdot Q_{12} + 4 \cdot Q_{66}) -$$
$$\frac{1}{8}(Q_{11} + Q_{22} - 2 \cdot Q_{12} - 4 \cdot Q_{66})\cos(4\theta)$$

$$\bar{Q}_{16} = \frac{1}{4}(Q_{11} - Q_{12}+)\sin(2\theta) + \frac{1}{8}(Q_{11} + Q_{22} - 2 \cdot Q_{12} - 4 \cdot Q_{66})\sin(4\theta)$$

$$\bar{Q}_{26} = \frac{1}{4}(Q_{11} - Q_{12}+)\sin(2\theta) - \frac{1}{8}(Q_{11} + Q_{22} - 2 \cdot Q_{12} - 4 \cdot Q_{66})\sin(4\theta).$$

Using these relations, the stiffness matrix of a single layer $\bar{\mathbf{Q}}$ can be written as

$$\bar{\mathbf{Q}} = \mathbf{\Gamma_0} + \mathbf{\Gamma_1} \cdot cos(2\theta) + \mathbf{\Gamma_2} \cdot sin(2\theta) + \mathbf{\Gamma_3} \cdot cos(4\theta) + \mathbf{\Gamma_4} \cdot sin(4\theta), \tag{3.15}$$

with the matrices $\mathbf{\Gamma}_i$ defined as

$$\mathbf{\Gamma_0} = \begin{bmatrix} U_1 & U_4 & 0 \\ U_4 & U_1 & 0 \\ 0 & 0 & U_5 \end{bmatrix} \qquad \mathbf{\Gamma_1} = \begin{bmatrix} U_2 & 0 & 0 \\ 0 & -U_2 & 0 \\ 0 & 0 & 0 \end{bmatrix}$$

$$\mathbf{\Gamma_2} = \begin{bmatrix} 0 & 0 & \frac{U_2}{2} \\ 0 & 0 & \frac{U_2}{2} \\ \frac{U_2}{2} & \frac{U_2}{2} & 0 \end{bmatrix} \qquad \mathbf{\Gamma_3} = \begin{bmatrix} U_3 & -U_3 & 0 \\ -U_3 & U_3 & 0 \\ 0 & 0 & -U_3 \end{bmatrix} \qquad (3.16)$$

$$\mathbf{\Gamma_4} = \begin{bmatrix} 0 & 0 & U_3 \\ 0 & 0 & -U_3 \\ U_3 & -U_3 & 0 \end{bmatrix},$$

where the material invariants U_i are given by

$$
\begin{aligned}
U_1 &= \frac{3 \cdot Q_{11} + 3 \cdot Q_{22} + 2 \cdot Q_{12} + 4 \cdot Q_{66}}{8} \\
U_2 &= \frac{Q_{11} - Q_{12}}{2} \\
U_3 &= \frac{Q_{11} + Q_{22} - 2 \cdot Q_{12} - 4 \cdot Q_{66}}{8} \\
U_4 &= \frac{Q_{11} + Q_{22} + 6 \cdot Q_{12} - 4 \cdot Q_{66}}{8} \\
U_5 &= \frac{Q_{11} + Q_{22} - 2 \cdot Q_{12} + 4 \cdot Q_{66}}{8}.
\end{aligned} \qquad (3.17)
$$

The A- and D-matrix are calculated using (3.9):

$$\mathbf{A} = \int_{-\frac{h}{2}}^{\frac{h}{2}} (\mathbf{\Gamma_0} + \mathbf{\Gamma_1} \cdot cos(2\theta) + \mathbf{\Gamma_2} \cdot sin(2\theta) + \mathbf{\Gamma_3} \cdot cos(4\theta) + \mathbf{\Gamma_4} \cdot sin(4\theta))\, dz$$

$$(3.18)$$

$$\mathbf{D} = \int_{-\frac{h}{2}}^{\frac{h}{2}} z^2 (\mathbf{\Gamma_0} + \mathbf{\Gamma_1} \cdot cos(2\theta) + \mathbf{\Gamma_2} \cdot sin(2\theta) + \mathbf{\Gamma_3} \cdot cos(4\theta) + \mathbf{\Gamma_4} \cdot sin(4\theta))\, dz.$$

Introducing the normalised thickness coordinate

$$\bar{z} = \frac{z}{h}, \qquad (3.19)$$

the expressions in eq. (3.18) become

$$\mathbf{A} \quad = \quad h \int_{-\frac{1}{2}}^{\frac{1}{2}} \left(\mathbf{\Gamma_0} + \mathbf{\Gamma_1} \cdot cos(2\theta) + \mathbf{\Gamma_2} \cdot sin(2\theta) + \mathbf{\Gamma_3} \cdot cos(4\theta) + \mathbf{\Gamma_4} \cdot sin(4\theta)\right) d\bar{z}$$

(3.20)

$$\mathbf{D} \quad = \quad \frac{h^3}{12} \int_{-\frac{1}{2}}^{\frac{1}{2}} \bar{z}^2 \left(\mathbf{\Gamma_0} + \mathbf{\Gamma_1} \cdot cos(2\theta) + \mathbf{\Gamma_2} \cdot sin(2\theta) + \mathbf{\Gamma_3} \cdot cos(4\theta) + \mathbf{\Gamma_4} \cdot sin(4\theta)\right) d\bar{z}.$$

3

Defining the in-plane lamination parameters as V and out-of-plane lamination parameters as W:

$$(V_1, V_2, V_3, V_4) =$$
$$\int_{-\frac{1}{2}}^{\frac{1}{2}} \left(\cos\left(2\theta(\bar{z})\right), \sin\left(2\theta(\bar{z})\right), \cos\left(4\theta(\bar{z})\right), \sin\left(4\theta(\bar{z})\right)\right) d\bar{z}$$
$$(W_1, W_2, W_3, W_4) =$$
$$\int_{-\frac{1}{2}}^{\frac{1}{2}} \bar{z}^2 \left(\cos\left(2\theta(\bar{z})\right), \sin\left(2\theta(\bar{z})\right), \cos\left(4\theta(\bar{z})\right), \sin\left(4\theta(\bar{z})\right)\right) d\bar{z},$$

(3.21)

the A- and D-matrix expressions simplify considerably to

$$\mathbf{A} = h\left(\mathbf{\Gamma_0} + \mathbf{\Gamma_1} \cdot V_1 + \mathbf{\Gamma_2} \cdot V_2 + \mathbf{\Gamma_3} \cdot V_3 + \mathbf{\Gamma_4} \cdot V_4\right)$$
$$\mathbf{D} = \frac{h^3}{12}\left(\mathbf{\Gamma_0} + \mathbf{\Gamma_1} \cdot W_1 + \mathbf{\Gamma_2} \cdot W_2 + \mathbf{\Gamma_3} \cdot W_3 + \mathbf{\Gamma_4} \cdot W_4\right),$$

(3.22)

where the laminate stiffness matrices are found as functions of the lamination parameters (LPs) and laminate thickness.

The feasible region of the lamination parameters is defined as the region where a stacking sequence can be found that gives the combination of lamination parameters. From their definition in eq. (3.21), the feasible region of the in- or out-of-plane lamination parameters separately can be found to be [53]

$$2 \cdot V_1^2 \cdot (1 - V_3) + 2 \cdot V_2^2 \cdot (1 + V_3) + V_3^2 + V_4^2 - 4 \cdot V_1 \cdot V_2 \cdot V_4 \quad \leq \quad 1$$
$$V_1^2 + V_2^2 \quad \leq \quad 1 \text{ (3.23)}$$
$$-1 \leq V_3 \quad \leq \quad 1.$$

Where V and W can be changed. For the combination of in- and out-of-plane lamination parameters, the feasible region does not have an easy definition. It can be found in for example Setoodeh et al. [126], or Bloomfield et al. [20].

Observing eq. (3.21), it can be seen that if the laminate is balanced, meaning for every θ there is a $-\theta$, V_2 and V_4 are equal to zero. The out-of-plane LPs are generally all non-zero, also for balanced laminates.

The advantage of using lamination parameters as parametrisation is that, independent of the number of layers, nine design variables are used: 4 in-plane, 4 out-of-plane LPs and the laminate thickness. For optimisation of a constant stiffness laminate, one set of in-plane and out-of-plane LPs and a thickness is sufficient to describe the complete laminate. If variable stiffness or variable thickness laminates are optimised, multiple points across the structure will have a set of LPs. The feasible region only considers the feasibility of a single laminate, not whether the change from one set of LPs at one point to the set at an adjacent point is manufacturable. Disadvantage of using LPs is that the lay-up of the laminate is unknown: a set of LPs does not describe a unique stacking sequence.

3.3 FIBRE ANGLES AND PLY DENSITY

A laminate is physically described by the number of plies, the fibre angle, and thickness of each ply. To allow the thickness to vary, each ply is assigned a density that scales its thickness. By setting this density to zero, layers may be removed from the laminate (i.e., zero thickness), as such the number of plies in the optimisation is an upper bound on the number of plies. If the user chooses this sufficiently large, it is no limitation on the scope of the parametrisation. The calculation of the A- and D-matrix with the fibre angles as design variables has already been discussed in section 3.1. For a constant stiffness laminate, only one set of fibre angles and densities is defined. For variable stiffness laminates the fibre angles change from point to point, for variable thickness laminates the density distribution changes from point to point.

The density is used to scale the thickness of each ply:

$$t_i = \rho_i t_i^0, \tag{3.24}$$

where t_i^0 is the physical thickness of a layer, which is the thickness of the prepreg. In Figure 3.3 each layer has the same physical thickness, as can be seen on the left. On the right the same plies are shown with a different density per layer. Ideally, each density is one, indicating the ply is present, or zero, meaning zero thickness, hence the ply is not present. Forcing the density to either zero or one is discussed in chapters 8 and 9. To keep the discussion general, the density can be any value between zero and one in this chapter even though physically this is not possible.

Figure 3.3: Plies with the same physical thickness and different density value.

To ease the density implementation, the A- and D-matrix are reformulated:

$$
\begin{aligned}
\mathbf{A}_k^0 &= \bar{\mathbf{Q}}_\mathbf{k} \cdot (z_{k-1} - z_k) \\
\mathbf{A} &= 2 \sum_{k=1}^{s} \mathbf{A}_\mathbf{k}^\mathbf{0} \\
\mathbf{D} &= \frac{2}{3} \cdot \sum_{k=1}^{s} \mathbf{A}_k^0 \cdot \left(z_{k-1}^2 + z_k \cdot z_{k-1} + z_k^2 \right).
\end{aligned}
\tag{3.25}
$$

To implement the density per layer only the in-plane stiffness of each layer $\mathbf{A}_k$ is multiplied with the density of this layer. The A-matrix changes to

$$
\mathbf{A} = 2 \cdot \sum_{k=1}^{s} \rho_k \cdot \mathbf{A}_k^0.
\tag{3.26}
$$

The calculation of the z-coordinate does not change, but to make the relation with density explicit it is rewritten to

$$
z_k(\boldsymbol{\rho}) = \sum_{i=1}^{s} \rho_i \cdot t_i^0 - \sum_{i=1}^{k} \rho_i \cdot t_i^0.
\tag{3.27}
$$

The expression for the D-matrix follows from these two equations:

$$
\mathbf{D} = \frac{2}{3} \sum_{k=1}^{s} \rho_k \cdot \mathbf{A}_k^0 \cdot \left(z_k(\boldsymbol{\rho})^2 + z_k(\boldsymbol{\rho}) \cdot z_{k-1}(\boldsymbol{\rho}) + z_{k-1}(\boldsymbol{\rho})^2 \right).
\tag{3.28}
$$

Since the fibre angle and density per ply will be used as design variables (chapters 6-9), the derivative of the A- and D-matrix with respect to these variables is needed for the gradient based optimisation. Based on eqs. (3.26) and (3.28), the derivatives of the A- and D-matrix with respect to the densities are

$$
\begin{aligned}
\frac{\partial \mathbf{A}}{\partial \rho_k} &= 2 \mathbf{A}_k^0 \\
\frac{\partial \mathbf{D}}{\partial \rho_k} &= \frac{2}{3} \mathbf{A}_k^0 \cdot \left(z_k^2 + z_k \cdot z_{k-1} + z_{k-1}^2 \right) + \\
&\quad \frac{2}{3} \sum_{i=1}^{k} \rho_i \cdot \mathbf{A}_i^0 \cdot t_i \cdot (2 \cdot z_i + z_{i-1}) + \frac{2}{3} \sum_{i=1}^{k-1} \rho_i \cdot \mathbf{A}_i^0 \cdot t_i \cdot (z_i + 2 \cdot z_{i-1}).
\end{aligned}
\tag{3.29}
$$

The derivative with respect to the fibre angle is found starting from the stiffness matrix $\bar{\mathbf{Q}}$. From eq. (3.15), the derivative with respect to θ is

$$\frac{d\bar{\mathbf{Q}}}{d\theta} = -2\boldsymbol{\Gamma_1} \cdot sin(2\theta) + 2\boldsymbol{\Gamma_2} \cdot cos(2\theta) - 4\boldsymbol{\Gamma_3} \cdot sin(4\theta) + 4\boldsymbol{\Gamma_4} \cdot cos(4\theta). \qquad (3.30)$$

Using eq. (3.13), the derivative of the A- and D-matrix with respect to θ_k, the fibre angle of layer k, is

$$\begin{aligned} \frac{\partial \mathbf{A}}{\partial \theta_k} &= 2\frac{d\bar{\mathbf{Q}}_k}{d\theta_k} \cdot (z_{k-1} - z_k) \\ \frac{\partial \mathbf{D}}{\partial \theta_k} &= \frac{2}{3}\frac{d\bar{\mathbf{Q}}_k}{d\theta_k} \cdot \left(z_{k-1}^3 - z_k^3\right). \end{aligned} \qquad (3.31)$$

Symmetry of the laminate has been considered from the beginning and is built right into eq. (3.13). Balanced laminates are often desired in practice. The introduction of balance halves the number of design variables: each *design layer* has a balanced counterpart which has the same density ρ but an opposite angle $-\theta$. Linking matrices $\mathbf{L}$ are used to generate the symmetric part of the fibre angles $\boldsymbol{\theta}_s$ from the design layers $\boldsymbol{\theta}_d$ using

$$\boldsymbol{\theta}_s = \mathbf{L}_\theta \cdot \boldsymbol{\theta}_d. \qquad (3.32)$$

The same formula holds for the densities:

$$\boldsymbol{\rho}_s = \mathbf{L}_\rho \cdot \boldsymbol{\rho}_d. \qquad (3.33)$$

In this work, the balanced layers are assumed to be adjacent. The linking matrix $\mathbf{L}$ for the angles is given by

$$\mathbf{L}_\theta = \begin{bmatrix} 1 & & & & 0 \\ -1 & & & & \\ & 1 & & & \\ & -1 & & & \\ & & & \ddots & \\ 0 & & & & \ddots \end{bmatrix}, \qquad (3.34)$$

and for the densities by

$$\mathbf{L}_\rho = \begin{bmatrix} 1 & & & & 0 \\ 1 & & & & \\ & 1 & & & \\ & 1 & & & \\ & & & \ddots & \\ 0 & & & & \ddots \end{bmatrix}. \qquad (3.35)$$

The location of the rows linking two layers are determined by the location of the balanced layer.

When a laminate is balanced and symmetric, every design layer represents four layers in the physical laminate. The gradient with respect to the design variables, given in eqs. (3.29) and (3.31), also needs to be changed to combine the influence of all layers:

$$\frac{\partial(.)}{\partial \mathbf{x}_d} = \mathbf{L}^T \cdot \frac{\partial(.)}{\partial \mathbf{x}_s},$$

(3.36)

where the correct $\mathbf{L}$ needs to be chosen based on whether $\mathbf{x}$ denotes the densities or the fibre angles. Symmetry was already taken into account in eqs. (3.29) and (3.31) and is always assumed in this work. Not all laminates in this work are balanced, this will be stated with each example.

Citius, Altius, Fortius.
Faster, Higher, Stronger.
Olympic motto, introduced by Pierre de Coubertin

4

MULTILEVEL OPTIMISATION USING CONVEX CONSERVATIVE SEPARABLE APPROXIMATIONS

Once the design variables of the optimisation are selected, the next important decision is: which algorithm to use to perform the optimisation? Since variable stiffness laminates are described by the stacking sequence at multiple places in the structure, a large number of design variables will exist. This excludes the use of evolutionary algorithms. Instead, a gradient-based algorithm is used, which can handle a large number of design variables in a computationally limited time. One of the most popular gradient-based methods is the method of successive approximations, hence this will be used in this thesis as well. This method was also used by IJsselmuiden[59] to optimise variable stiffness laminates in terms of the lamination parameters.

The formulation of a general optimisation problem and the method of successive approximations are discussed in section 4.1. As was shown in the previous

---

This chapter is based on the journal papers 'Stacking sequence optimisation of variable stiffness laminates with manufacturing constraints'[118], 'Optimisation of Ply Drop Order in Variable Stiffness Laminates'[66], and 'Optimisation of Ply Drop Locations in Variable Thickness Composites'[117] and the conference paper 'Effect of Steering Constraints on the Performance of Variable Stiffness Laminates'[114].

chapter, the structural behaviour depends on the laminate stiffness matrices, while the laminate stiffness matrices are dependent on the fibre density and fibre angle. Hence, the structural behaviour is approximated using a two level approximation scheme: level one is in terms of the laminate stiffness matrices, level two approximates level one in terms of the design variables. This is explained in section 4.2. The predictor-corrector interior-point method is used to perform the optimisation of the successive approximations. This method replaces the dual algorithm that was previously used. The reason for the change is the large number of constraints that will appear due to the manufacturing constraints, discussed in chapter 6. The newly implemented method is explained in section 4.3. The method of successive approximations is not guaranteed to be globally convergent. To guarantee global convergence, each step should be an improvement step. This global convergence strategy is explained in section 4.4.

To optimise variable stiffness, variable thickness laminates both the fibre angles and ply densities need to be updated. This can be done in two ways: one, an approximation in terms of both design variables is made, two, different approximations in terms of the fibre angles and ply densities are made and optimised and combined. In this work the second option was chosen since it allows for the two optimisations being done separately, tested, and combined afterwards. This implies the fibre angle optimisation work does not need to be done again when adding the possibility of variable thickness laminates. How both optimisations can be combined into a single optimisation is discussed in section 4.5. While in the original three-step optimisation approach from IJsselmuiden [59], the second step was only retrieval, in this work it is turned into an optimisation. This optimisation can be connected to the outcome of the first step, leading to a multi-step approach, explained in section 4.6. Finally, a summary of the complete algorithm is given in section 4.7.

4.1 METHOD OF SUCCESSIVE APPROXIMATIONS

The method of successive approximations replaces the optimisation of the problem by a sequence of approximate sub-problems. The first approximate sub-problem is built at a user-defined point. The requirements for the approximation are discussed in 4.1.1. This approximate sub-problem is optimised to find the next iterate. The process continues by building an approximate sub-problem at the new iterate and optimising until convergence is reached [26,123]. A flowchart of the method of successive approximations can be found in Figure 4.1.

A standard structural optimisation problem is solved. The worst case response of a subset of the structural responses is optimised, subject to constraints on other
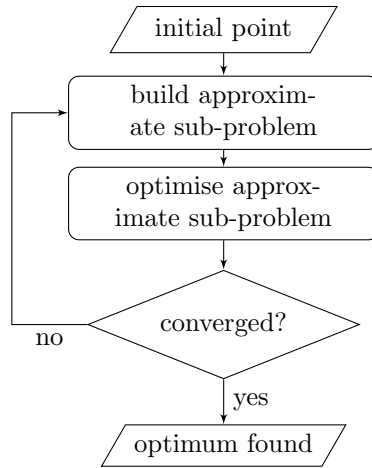
Figure 4.1: Flowchart of the method of successive approximations.

responses:

$$\min_{\mathbf{x}} \quad \max\{f_1, f_2, ..., f_n\}$$
$$s.t. \quad f_{n+1}, ..., f_m \leq 0, \tag{4.1}$$

where f_1 to f_n denote structural responses that are optimised and f_{n+1} up to f_m denote structural responses that are constrained. These responses are all functions of the design variables, denoted by $\mathbf{x}$ to indicate this holds for any design variable, not just lamination parameters, fibre angles or ply densities. If an equation only holds for a certain design variable, this will be indicated, if it holds in general $\mathbf{x}$ is used as design variable.

The problem is defined as a minimisation, hence if we want, for example, to maximise the buckling load, the inverse buckling load is minimised. Another example is maximising the stiffness, which is formulated as minimum compliance. As final example, the factor of safety is not maximised, instead the failure index is minimised. Defining the objective as worst case is useful when for example performing a buckling optimisation: by taking multiple modes into account, mode jumping is not a problem. Another example is stress optimisation: the maximum failure index appearing in the structure should be minimised.

The convergence criterion used is a soft convergence criterion. If the improvement of the objective function is less than a certain tolerance and the constraints are satisfied, the optimisation is assumed to have converged. The tolerance is usually a function of the initial value of the objective: an improvement smaller than 10^{-3} of the initial value is often used as tolerance in this work. The exact function is used to determine convergence, not the approximation.

4.1.1 REQUIREMENTS OF THE APPROXIMATION

An approximation has to have certain properties to be used during the method of successive approximations. Since the method is gradient-based, a first-order approximation is used, meaning [140]

$$f(\mathbf{x}_0) = \hat{f}(\mathbf{x}_0)$$

$$\frac{\partial f}{\partial x}(\mathbf{x}_0) = \frac{\partial \hat{f}}{\partial x}(\mathbf{x}_0), \tag{4.2}$$

where f denotes the exact function, $\hat{f}$ the approximation, and $\mathbf{x}_0$ the approximation point. For optimisation purposes, four more properties are favourable [22]:

- convex: if the approximation is convex, it is guaranteed to have a unique solution. Thus optimising the sub-problem will always give a solution when starting from a feasible point. Mathematically, a function f is convex if for any two points $\mathbf{x}_1$ and $\mathbf{x}_2$ in the feasible domain it holds that

$$f(t\mathbf{x}_1 + (1-t)\mathbf{x}_2) \leq tf(\mathbf{x}_1) + (1-t)f(\mathbf{x}_2), \tag{4.3}$$

  where t is any value between 0 and 1.

- separable: for problems with a large number of design variables, like in problems addressed in this work, a separable approximation is desirable. This means that the different design variables do not influence each other. This makes the optimisation computationally efficient. Mathematically, a function is separable if it can be written as a summation of functions of single variables:

$$f(\mathbf{x}) = \sum_i f_i(x_i). \tag{4.4}$$

  In this work, separable is interpreted slightly different: x_i does not need to be a scalar variable, it can be a (small) vector or a tensor.

- conservative: an approximation is conservative if the function that is approximated is, at each point, lower than or equal to the approximation. Mathematically, for a minimisation problem this means

$$f(\mathbf{x}) \leq \hat{f}(\mathbf{x}), \tag{4.5}$$

  where f and $\hat{f}$ denote the exact and approximate function respectively and $\mathbf{x}$ denotes any point in the design space. As we shall see in section 4.4, conservativeness plays an important role in guaranteeing global convergence of the total approximation problem.

- homogeneous: an approximation is homogeneous if the response scales with a certain factor when all design variables are scaled. Mathematically, a function is homogeneous of degree n if

$$f(\lambda\mathbf{x}) = \lambda^n f(\mathbf{x}). \tag{4.6}$$

This implies a solution can always be found, even if the starting point is infeasible, given that the upper and lower bounds on the design variables allow the required scaling.

These four properties are advantageous for the optimisation, but only convexity is required to use the method of successive approximations. The approximations used in this thesis are discussed in chapter 5. The approximations themselves are convex, separable, and, if possible, homogeneous. To render them conservative, an extra part, called damping function in this thesis, is added to the approximation. This is discussed in section 4.4.

4.2 MULTI-LEVEL OPTIMISATION ALGORITHM

As was explained in chapter 3, the structural behaviour of a composite structure depends on its geometry and the stiffness matrices of the laminate. The design variables chosen were either the lamination parameters, or the fibre angles and ply densities, both parametrising the laminate stiffness matrices. Hence, a logical choice is to have a two level approximation scheme. Level one approximates the structural responses in terms of the laminate stiffness matrices. Level two approximates the structural responses in terms of the design variables, derived from the level one approximations.

The general form of the level one approximation, which will be discussed in more detail in section 5.2, is

$$\overset{I}{f} = \sum_n \mathbf{A}_n : \boldsymbol{\phi}_n^m + \mathbf{D}_n : \boldsymbol{\phi}_n^b + \mathbf{A^{-1}}_n : \boldsymbol{\psi}_n^m + \mathbf{D^{-1}}_n : \boldsymbol{\psi}_n^b + c, \qquad (4.7)$$

where $\boldsymbol{\phi}$ and $\boldsymbol{\psi}$ denote the sensitivity in terms of the A- and D-matrix and their inverse, which are symmetric by construction. The superscript m denotes the membrane, b denotes bending, n ranges from 1 to the number of design points. Hence, for a constant stiffness laminate no summation is necessary. The : operator denotes the Frobenius inner product: $\mathbf{A} : \mathbf{B} = trace(\mathbf{A}^T \cdot \mathbf{B})$. The constant c is zero for responses that have homogeneous properties. The sensitivities are found from finite element analysis.

Since lamination parameters describe the stiffness matrices exactly, the level two approximation can be obtained by inserting the expression for the A- and D-matrix, eq. (3.22), into eq. (4.7). Details about the optimisation in terms of the lamination parameters, step one of the three-step optimisation approach, can be found in the work of IJsselmuiden[59]. This work focuses on the optimisation in terms of fibre angles and densities, which is step two in the three-step optimisation approach.

Two more level two approximations are developed in this work: one in terms of the fibre angles, and another in terms of the ply densities. In terms of the fibre angles, a second order Taylor series is used:

$$\overset{II}{f}(\boldsymbol{\theta}) \approx \overset{I}{f}_0 + \mathbf{g} \cdot \Delta\boldsymbol{\theta} + \frac{1}{2}\Delta\boldsymbol{\theta}^T \cdot \mathbf{H} \cdot \Delta\boldsymbol{\theta}, \tag{4.8}$$

where $\mathbf{g}$ is the gradient and $\mathbf{H}$ an approximation of the Hessian of the level one approximation as a function of the fibre angles. In terms of the ply densities, a linearisation is used:

$$\overset{II}{f}(\boldsymbol{\rho}) \approx \overset{I}{f}_0 + \mathbf{g} \cdot \Delta\boldsymbol{\rho}. \tag{4.9}$$

Details of the construction of the level two approximations can be found in section 5.3.

The level one and two approximation do not need to be built at the same point. When one builds a level one approximation at point $\mathbf{x}^*$, denoted by $\overset{I}{f}(\mathbf{x}, \mathbf{x}^*)$, one can build a level two approximation at this point based on $\overset{I}{f}(\mathbf{x}, \mathbf{x}^*)$, denoted by $\overset{II}{f}(\mathbf{x}, \mathbf{x}^*)$. When optimising the sub-problem based on $\overset{II}{f}(\mathbf{x}, \mathbf{x}^*)$, the new iterate $\mathbf{x}'$ is found. Next, another level two approximation at point $\mathbf{x}'$ based on $\overset{I}{f}(\mathbf{x}, \mathbf{x}^*)$, denoted by $\overset{II}{f}(\mathbf{x}, \mathbf{x}')$ can be built. Hence, the level two approximation can be updated multiple times without updating the level one approximation: optimising the approximate sub-problem of level one is done using the method of successive approximations. This is shown in Figure 4.2.

By performing several updates of the level one approximation without having to run an FEA to determine new sensitivities, considerable computational time may be saved since performing an FEA is much more expensive than calculating a level one approximation. In general, the larger the problem, the larger the time saving obtained by avoiding an FEA. However, a maximum number of updates is defined. This is done since the level one approximation has a limited range of validity.

4.3 PREDICTOR-CORRECTOR INTERIOR-POINT SOLVER

During optimisation, many side-constraints will be used in addition to the structural constraints. For example: the densities have to be between 0 and 1, and the fibre angles should not change too much from one point to the next. This implies a lot of constraints will be present, and a dual optimisation algorithm, which was implemented originally by IJsselmuiden, is no longer computationally efficient. To increase computational efficiency, a predictor-corrector interior-point optimiser is implemented based on the work of Zillober[172]. This has been shown
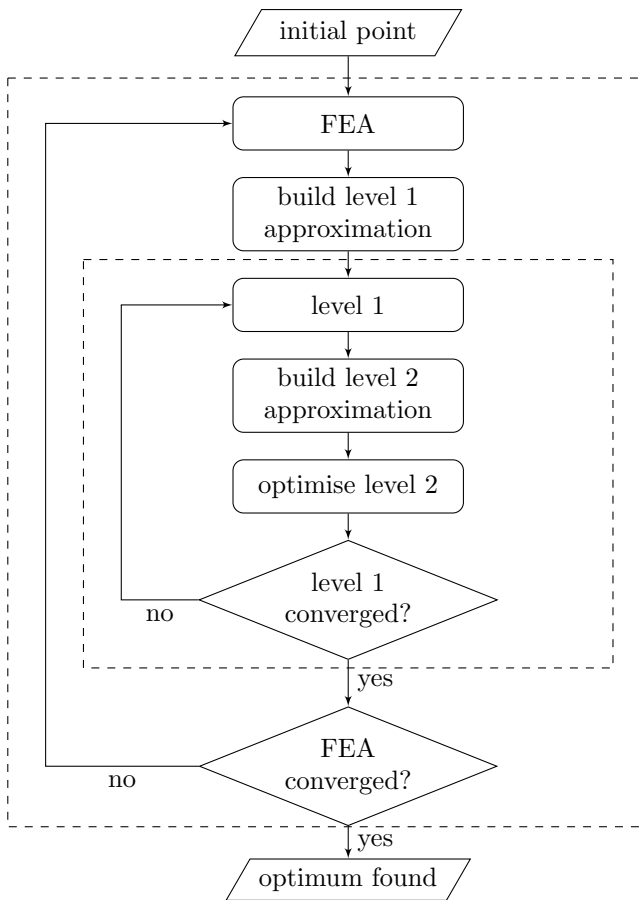
Figure 4.2: Flowchart of the method of successive approximations with two level approximations.

to be able to handle a large number of constraints. Furthermore, the computational efficiency is increased by implementing the optimisation algorithm, rather than calling a pre-defined function in Matlab: the sparsity of certain matrices can be exploited, and no computational time is lost on checking which sub-case of the function call is to be used.

The method presented in this chapter is generally applicable, hence the design vector is denoted by $\mathbf{x}$, and the upper and lower bound on design variables is denoted by $\bar{x}$ and $\underline{x}$ respectively. Instead of the min-max formulation from eq. (4.1), the problem is rewritten to

$$
\begin{aligned}
\min_{\mathbf{x}} \quad & z \\
s.t. \quad & \mathbf{f} - z \cdot \mathbf{e} \leq \mathbf{0} \\
& \underline{\mathbf{x}} \leq \mathbf{x} \leq \bar{\mathbf{x}},
\end{aligned}
\tag{4.10}
$$

where $\mathbf{e}$ contains only ones and zeroes: $e_i = 0$ if f_i is a constraint, and $e_i = 1$ if f_i is an objective. The inequality constraints are rewritten to equality constraints by adding slack variables, that have to be larger than zero:

$$
\begin{aligned}
\min_{\mathbf{x}} \quad & z \\
s.t. \quad & \mathbf{f} - z \cdot \mathbf{e} + \mathbf{s}_c = \mathbf{0} \\
& \mathbf{x} - \underline{\mathbf{x}} + \mathbf{s}_l = \mathbf{0} \\
& \bar{\mathbf{x}} - \mathbf{x} + \mathbf{s}_u = \mathbf{0}.
\end{aligned}
\tag{4.11}
$$

The Lagrangian is

$$
\mathcal{L} = z + \boldsymbol{\lambda}_c^T \cdot (\mathbf{f} - z \cdot \mathbf{e} + s_c) + \boldsymbol{\lambda}_l^T \cdot (\mathbf{x} - \underline{\mathbf{x}} + \mathbf{s}_l) + \boldsymbol{\lambda}_u^T \cdot (\bar{\mathbf{x}} - \mathbf{x} + \mathbf{s}_u) \\
- \mu \left(\mathbf{1}^T ln\,(\mathbf{s}_c) + \mathbf{1}^T ln\,(\mathbf{s}_l) + \mathbf{1}^T ln\,(\mathbf{s}_u) \right), \tag{4.12}
$$

where $\boldsymbol{\lambda}$ denotes the Lagrangian multipliers, which have to be larger or equal to zero, c denotes a constraint, u the upper limit, and l the lower limit. μ denotes the homotopy factor. The necessary optimality condition is $\nabla \mathcal{L} = 0$. Rewriting in terms of the variables leads to

$$
\begin{aligned}
\nabla x : -\mathbf{b}_x &= \boldsymbol{\lambda}_c^T \cdot \nabla \mathbf{f} + \boldsymbol{\lambda}_l - \boldsymbol{\lambda}_u \\
\nabla z : -b_z &= 1 + \boldsymbol{\lambda}_c^T \cdot \mathbf{e} \\
\nabla \lambda_c : -\mathbf{b}_{\lambda_c} &= \mathbf{f} - z \cdot \mathbf{e} + s_c \\
\nabla \lambda_u : -\mathbf{b}_{\lambda_u} &= \bar{\mathbf{x}} - \mathbf{x} + \mathbf{s}_u \\
\nabla \lambda_l : -\mathbf{b}_{\lambda_l} &= \mathbf{x} - \underline{\mathbf{x}} + \mathbf{s}_l \\
\nabla s_c : -\mathbf{b}_{s_c} &= \boldsymbol{\lambda}_c - \mu \mathbf{s}_c^{-1} \\
\nabla s_u : -\mathbf{b}_{s_u} &= \boldsymbol{\lambda}_u - \mu \mathbf{s}_u^{-1} \\
\nabla s_l : -\mathbf{b}_{s_l} &= \boldsymbol{\lambda}_l - \mu \mathbf{s}_l^{-1}.
\end{aligned}
\tag{4.13}
$$

To avoid numerical issues, the parts related to the slack variables are multiplied

with the slack. The linearised problem is

$$
\begin{bmatrix}
\boldsymbol{\lambda}_c \cdot \nabla^2 \mathbf{f} & \nabla \mathbf{f} & & & & & & \mathbf{I} & -\mathbf{I} \\
\nabla \mathbf{f} & & -\mathbf{e} & \mathbf{I} & & & & & \\
& -\mathbf{e}^T & & \mathbf{I} & & & & & \\
& \mathbf{s}_c & & & \boldsymbol{\lambda}_c & & & & \\
& & & & \boldsymbol{\lambda}_u & & \mathbf{s}_u & & \\
& & & & & \boldsymbol{\lambda}_l & & \mathbf{s}_l & \\
\mathbf{I} & & & & \mathbf{I} & & & & \\
-\mathbf{I} & & & & & \mathbf{I} & & &
\end{bmatrix}
\cdot
\begin{bmatrix}
\Delta \mathbf{x} \\
\Delta \boldsymbol{\lambda}_c \\
\Delta z \\
\Delta \mathbf{s}_c \\
\Delta \mathbf{s}_u \\
\Delta \mathbf{s}_l \\
\Delta \boldsymbol{\lambda}_u \\
\Delta \boldsymbol{\lambda}_l
\end{bmatrix}
=
\begin{bmatrix}
\mathbf{b}_x \\
\mathbf{b}_{\boldsymbol{\lambda}_c} \\
b_z \\
\mathbf{b}_{s_c} \\
\mathbf{b}_{s_u} \\
\mathbf{b}_{s_l} \\
\mathbf{b}_{\lambda_u} \\
\mathbf{b}_{\lambda_l}
\end{bmatrix},
$$
(4.14)

where the matrices of the slacks and Lagrangian multipliers are diagonal matrices, with the values of their respective vector on the diagonal.

The system in eq. (4.14) has to be solved. Instead of solving the large system, which requires a lot of computational time, the Schur complement [63] is used to reduce the size of the problem. The smaller problem is solved, and the change of all design variables is found by back-substituting.

Once the change in design variables is known, it has to be made sure that neither the slacks, nor the Lagrangian multipliers become negative. Hence, the maximum primal and dual step size are determined using

$$
\tilde{\delta}_p = \min \left\{ \frac{\hat{s}_c^k - \kappa}{-\Delta \hat{s}_c}, \frac{\hat{s}_u^k - \kappa}{-\Delta \hat{s}_u}, \frac{\hat{s}_l^k - \kappa}{-\Delta \hat{s}_l} \right\}
$$

$$
\tilde{\delta}_d = \min \left\{ \frac{\hat{\lambda}_c^k - \kappa}{-\Delta \hat{\lambda}_c}, \frac{\hat{\lambda}_u^k - \kappa}{-\Delta \hat{\lambda}_u}, \frac{\hat{\lambda}_l^k - \kappa}{-\Delta \hat{\lambda}_l} \right\},
$$
(4.15)

where κ is the machine accuracy, k denotes the current iterate, $\hat{s}$ and $\hat{\lambda}$ denote the terms of the respective vector that obey

$$
s_i^k + \Delta s_i < \kappa
$$
$$
\lambda_i^k + \Delta \lambda_i < \kappa,
$$
(4.16)

where i can be either c, u or l. The primal step size can be found from eq. (4.15):

$$
\delta_p = \begin{cases} 1 & \text{if } \tilde{\delta}_p \text{ not defined} \\ \min(1, 0.99995 \cdot \tilde{\delta}_p) & \text{otherwise.} \end{cases}
$$
(4.17)

The dual step size is

$$
\delta_d = \begin{cases} 1 & \text{if } \tilde{\delta}_d \text{ not defined} \\ \min(1, 0.99995 \cdot \tilde{\delta}_d) & \text{otherwise.} \end{cases}
$$
(4.18)

The change of the slacks, z and $\mathbf{x}$ are multiplied with the primal step size. The change of the Lagrangian multipliers are multiplied with the dual step size to determine the final change.

The system in eq. (4.14) is solved twice during the predictor-corrector step. The
left-hand side does not change, hence reducing the size of the large matrix only
needs to be done once. The right-hand side does change, compared to eq. (4.13).
During the predictor step the homotopy factor is zero.

After the predictor step, the homotopy factor is determined using the duality gap:

$$\mu = \epsilon \left((\mathbf{s}_c + \Delta \mathbf{s}_c \delta_p)^T \cdot (\boldsymbol{\lambda}_c + \Delta \boldsymbol{\lambda}_c \delta_d) + (\mathbf{s}_l + \Delta \mathbf{s}_l \delta_p)^T \cdot (\boldsymbol{\lambda}_l + \Delta \boldsymbol{\lambda}_l \delta_d) + \right.$$
$$\left. (\mathbf{s}_u + \Delta \mathbf{s}_u \delta_p)^T \cdot (\boldsymbol{\lambda}_u + \Delta \boldsymbol{\lambda}_u \delta_d) \right), \quad (4.19)$$

where ϵ is a factor to scale the duality gap, usually chosen to be

$$\epsilon = \frac{1}{c + l + u}, \quad (4.20)$$

where c is the number of constraints, l and u the number of lower and upper
bounds. Furthermore, the next terms are added to the right hand side:

$$
\begin{aligned}
\mathbf{b}_x &: & -\left(\sum_{j=1}^{m} \frac{\partial^2 h}{\partial x_k^2} \cdot \Delta \mathbf{x_k} \cdot \Delta \mathbf{y_j} \right)_{k=1,..,n} \\
\mathbf{b}_{s_c} &: & -\Delta \mathbf{s_c} \cdot \Delta \boldsymbol{\lambda_c} \\
\mathbf{b}_{s_u} &: & -\Delta \mathbf{s_u} \cdot \Delta \boldsymbol{\lambda_u} \\
\mathbf{b}_{s_l} &: & -\Delta \mathbf{s_l} \cdot \Delta \boldsymbol{\lambda_l},
\end{aligned}
\quad (4.21)
$$

where the terms with Δ are found during the predictor step, and the vector
products need to be done term-by-term.

The change in design variables found during the predictor step is only used to
determine the homotopy factor and the change in right-hand side for the corrector
step. After the corrector step, all design variables are updated, starting from the
value they had before the predictor step.

During the optimisation of the fibre densities, the predictor-corrector step is used
as explained in this chapter. When optimising the fibre angle distribution, an
extra constraint on the change in fibre angle from one point to the next has to
be taken into account. How this constraint is formulated and how this influences
the algorithm is explained in section 6.1.

4.4 GLOBAL CONVERGENCE

The method of successive approximations is not guaranteed to be globally conver-
gent[30]. To guarantee global convergence, each step should be an improvement
step. An improvement step means the objective has improv and all constraints
are satisfied. Hence, when updating the stiffness matrices after an optimisation

of $\overset{II}{f}$, $\overset{I}{f}$ has to improve to accept the new iterate. The same holds when an FEA is performed after $\overset{I}{f}$ has been optimised: the FEA has to improve to accept the new iterate.

The approximations in section 4.2 are not guaranteed to lead to an improvement step. If an approximation is conservative, as was mentioned in 4.1.1, an improvement step is guaranteed. Svanberg proposed to add an extra function[141], referred to as damping function in this work, to the approximation, to render the 'total' approximation conservative. The damping function d is scaled with a damping factor ζ:

$$\overset{I}{f} = \overset{I}{\tilde{f}} + \zeta \overset{II}{d}, \tag{4.22}$$

where $\overset{I}{\tilde{f}}$ is the approximation mentioned in section 4.2. The same expression holds for the level two approximations. The shape of the damping function depends on the shape of the approximation and does not change during the optimisation.

The damping factor is updated after each iteration: increased if the total approximation is not conservative, decreased if it is conservative.

The goal of adding a damping function is guaranteeing the approximation to be conservative[141]. However, the new iterate will be accepted if it is an improvement step, which implies the method is globally convergent. An example can be seen in Figure 4.3 where an example function $f(x)$, the black line, is approximated. The green line is a conservative approximation, and leads to an improvement step; the new iterate will be accepted and ζ decreased. The red line is an unconservative approximation and does not lead to an improvement step, hence the new iterate will be rejected and ζ increased. The blue line is an unconservative approximation, but does lead to an improvement step, hence the new iterate will be accepted, and ζ increased.

4.4.1 DAMPING FUNCTION

The damping function has to be designed such that the total approximation stays valid and convex. This means the damping function value and gradient at the approximation point should be zero, and the Hessian should be positive definite[141]:

$$
\begin{aligned}
d(\mathbf{x}_0) &= 0 \\
\nabla_x d(\mathbf{x}_0) &= 0 \\
\nabla_x \nabla_x d(\mathbf{x}_0) &\succ 0.
\end{aligned}
\tag{4.23}
$$

By changing the Hessian at the approximation point, and the values away from the approximation point, the new-found iterate is changed.

The damping function for each approximation has to be chosen carefully: it has to influence the step size taken, but should not influence the direction of the step

Figure 4.3: Example of a conservative (green) and two unconservative (red and blue) approximations.

4

too much. For $\overset{I}{f}$, the damping function is denoted by $\overset{I}{d}$ and chosen as[59]

$$\overset{I}{d} = \sum_n \left(\mathbf{A}_n : \mathbf{A}_{n0}^{-1} + \mathbf{D}_n : \mathbf{D}_{n0}^{-1} + \mathbf{A}_n^{-1} : \mathbf{A}_{n0} + \mathbf{D}_n^{-1} : \mathbf{D}_{n0} \right) - 12, \qquad (4.24)$$

where the subscript 0 denotes the value at the approximation point and the summation is over all nodes n. Comparing the damping function to the approximation, eq. (4.7), it is noticed they have the same form. Hence, no extra computational effort is required by adding the damping function: the sensitivities are updated, the optimisation does not change.

For $\overset{II}{f}(\boldsymbol{\theta})$, the damping function is

$$\overset{II}{d}(\theta) = \frac{1}{2} \Delta \boldsymbol{\theta}^T \cdot \mathbf{H}_d \cdot \Delta \boldsymbol{\theta}, \qquad (4.25)$$

where $\Delta \boldsymbol{\theta}$ is the change in angles from the approximation point of the level two approximation, and $\mathbf{H}_d$ is a regularisation matrix given by

$$\mathbf{H}_d = \frac{1}{s^2} \begin{bmatrix} 1 & -1 & & & \\ -1 & 2 & -1 & & \\ & \ddots & \ddots & & \\ & & -1 & 2 & -1 \\ & & & -1 & 1 \end{bmatrix} + \alpha \begin{pmatrix} 1 & \cdots & 1 \\ \vdots & \ddots & \vdots \\ 1 & \cdots & 1 \end{pmatrix}, \qquad (4.26)$$

where s stands for the number of layers in the symmetric part, with α given by

$$\alpha = \frac{\epsilon \cdot 2 \cdot (s-1)}{s^3}, \qquad (4.27)$$

where ϵ is a damping factor, usually chosen to be 1. This regularisation matrix, scaled with $\overset{II}{\zeta}_\theta$, is added to the Hessian, defined in eq. (4.8). Again the damping function has no influence on the form of the approximation and will not influence the optimisation.

For $\overset{II}{f}(\boldsymbol{\rho})$, the damping function is chosen to be

$$\overset{II}{d}(\rho) = \sum_i \left(\frac{\rho_i}{\rho_{0i}} + \frac{\rho_{0i}}{\rho_i} - 2 \right) \cdot w_i, \tag{4.28}$$

where w_i is defined as

$$w_i = \frac{A_i}{\sum_i A_i}, \tag{4.29}$$

where A_i denotes the area represented by node i. Considering the level two approximation, eq. (4.9), it is noticed that the damping does influence the form of the approximation. However, since linearisation is used, some non-linear terms are necessary to render the approximation convex.

Choosing a good initial value is important even though the damping factor is continuously updated. Choosing too small an initial damping factor will lead to a large number of rejected iterations before the new iterate is an improvement. Choosing it too large will lead to a small step size and thus a lot of iterations before the optimisation converges. The derivation of the initial damping factor for the different approximations can be found in Appendix A. For the stiffness optimisation the initial damping factor is found to be

$$\overset{I}{\zeta}^2 = \sum_n \frac{w_n}{2} \cdot \left(\left(||\boldsymbol{\phi}_{nm} : \mathbf{A}_n^{-1}|| + ||\boldsymbol{\psi}_{nm} : \mathbf{A}_n|| \right)^2 + \left(||\boldsymbol{\phi}_{nb} : \mathbf{D}_n^{-1}|| + ||\boldsymbol{\psi}_{nb} : \mathbf{D}_n|| \right)^2 \right). \tag{4.30}$$

For the fibre angle optimisation it is found to be

$$\overset{II}{\zeta}_\theta^2 = \frac{1}{2} \cdot \left(\mathbf{g}^T \cdot \mathbf{H}_d^{-1} \cdot \mathbf{g} \right). \tag{4.31}$$

For the density optimisation the initial damping factor is based solely on the magnitude of the sensitivities:

$$\overset{II}{\zeta}_\rho^2 = \sum_n \frac{w_n}{2} \cdot \left(\left(\boldsymbol{\phi}_{nm} : \boldsymbol{\phi}_{nm}^T + \boldsymbol{\psi}_{nm} : \boldsymbol{\psi}_{nm}^T \right)^2 + \left(\boldsymbol{\phi}_{nb} : \boldsymbol{\phi}_{nb}^T + \boldsymbol{\psi}_{nb} : \boldsymbol{\psi}_{nb}^T \right)^2 \right). \tag{4.32}$$

The damping function is updated after each iteration, regardless of whether the new iterate is an improvement or not. Contrary to the damping function and calculation of the initial damping factor, updating the damping factor is independent of the approximation. The update is solely based on the value of the exact function f, the total approximation $\hat{f}$, the damping function d, and the damping factor in the current iterate ζ. The derivation of the optimal damping

factor ζ_{opt} is given in teh work of IJssemuiden [59]. The ratio between the old and optimal damping factor is found to be

$$\zeta^* = e^{\frac{f(\mathbf{x}^*) - \hat{f}(\mathbf{x}^*)}{d}}. \tag{4.33}$$

Ideally, the new damping factor is equal to the optimal damping factor. However, some limits are posed to avoid the damping factor changing too much from one iteration to the next:

$$\bar{\zeta} = \begin{cases} 2 & \text{if } \zeta^* \geq 2 \\ \zeta^* & \text{if } 1.05 \leq \zeta^* \leq 2 \\ 1.05 & \text{if } 1.0 \leq \zeta^* \leq 1.05 \\ \zeta^* & \text{if } 0.5 \leq \zeta^* \leq 1 \\ 0.5 & \text{if } \zeta^* \leq 0.5. \end{cases} \tag{4.34}$$

The maximum of 2 and minimum of 0.5 are set to avoid large oscillations between consecutive updates. The minimum of 1.05 is set to avoid too many iterations that are just not conservative. The damping factor is updated using

$$\zeta_{new} = \bar{\zeta} \cdot \zeta. \tag{4.35}$$

4.5 COMBINING OPTIMIZATIONS WITH DIFFERENT DESIGN VARIABLES

Two different level two approximations are developed: one in terms of the fibre angles and one in terms of the ply densities. The method of successive approximations assumes a single set of design variables. However, both the fibre angles and ply densities are optimised when optimising a variable stiffness, variable thickness laminate. This could be done by building one approximation in terms of both fibre angles and ply densities, or by modifying the algorithm to combine the optimisations. In this work, the second option is chosen.

Combing both optimisations is done using the method of coordinate descent (CD) [5,169]: both optimisations are performed independently and the set of design variables that leads to the largest improvement is updated. Another option would have been to always update one, then the other, but it is expected that usually one of the two will have more influence, and this method allows for more updates of one over the other. The value of $\overset{I}{f}$ is used to determine the improvement:

$$i_\theta = \overset{I}{f}(\mathbf{A}(\boldsymbol{\theta}^*), \mathbf{D}(\boldsymbol{\theta}^*))$$
$$i_\rho = \overset{I}{f}(\mathbf{A}(\boldsymbol{\rho}^*), \mathbf{D}(\boldsymbol{\rho}^*)), \tag{4.36}$$

where the * denotes the optimal distribution found by optimising $\overset{II}{f}$. Before updating the set of design variables, it is checked whether this is an improvement

step. As was explained in section 4.2, $\overset{II}{f}$ is updated multiple times before an FEA is performed, this is still done: the set of design variables to be updated is determined right before an FEA is performed. To avoid one set of variables dominating the optimisation, a maximum of three consecutive updates of the same set of variables is allowed.

Once the set of design variables to be updated is selected, an FEA is performed to check whether an improvement is found. If this is the case, the set of design variables is updated, and $\overset{I}{f}$ is built again. If no improvement step is found, only $\overset{I}{\zeta}$ is updated, and the optimisation in terms of the chosen set of design variables is repeated. Based on this new improvement, the set of design variables to be updated is determined again. This loop is repeated until an improvement step is found. The convergence criterion for the overall algorithm does not change.

4.6 MULTI-STEP APPROACH

One of the advantages of the three-step optimisation approach is that in the first step the optimal lamination parameters are found and no more FEA is necessary afterwards: during the second step fibre angle retrieval is performed and the third step is building the fibre paths. The fibre angle retrieval of step two can be performed using the framework of this chapter. Instead of using the sensitivities at the user-defined initial guess, the sensitivities at the optimal stiffness distribution can be used. The level one approximation $\overset{I}{f}$ found is then solved until convergence of $\overset{I}{f}$ without doing an FEA to update the sensitivities.

Mathematically, the approximation $\overset{I}{f}$ is not even a zero-th order approximation: the function value and gradient at the initial guess are not the same as the ones found using an FEA. However, the closer the optimal stiffness distribution is approached, the better the approximation will be. Hence, at convergence, the function value found by the approximation will be close to the value found using FEA. Furthermore, during retrieval one wants to find a best fit to the lamination parameters, so an improvement step is almost guaranteed, whether or not the approximation is conservative.

Another possibility would be to match the A- and D-matrix as closely as possible. However, this does not take into account how sensitive the different responses are with respect to the A- and D-matrix at certain points. Furthermore, feasibility is not guaranteed: the constraints may slightly decrease meaning the required performance is not achieved.

When retrieving the fibre angle distribution from the optimal lamination para-

meters, the structural performance generally decreases. Due to manufacturing constraints the change in lamination parameter from one point to the next is limited, while this was not constrained during step one of the three-step optimisation approach. Hence, at certain points a bad fit will be obtained that can be improved. By updating the sensitivities and building a new $\overset{I}{f}$, an optimum in terms of fibre angles can be found rather than a bad fit to the lamination parameters. This leads to a retrieval-optimisation algorithm.

The retrieval-optimisation algorithm has advantages to both performing only retrieval or only optimisation. By first doing a retrieval step, a good 'initial guess' is found for the optimisation algorithm: the best fit to the optimal lamination parameters. This is found at a low computational cost: no FEA is done to obtain this best fit. Furthermore, by performing a fibre angle optimisation after the retrieval step, the places where the fit is not exact are optimised in terms of the fibre angles. This leads to an optimum in terms of the physical fibre angles rather than a bad fit in terms of the laminate stiffness matrices.

4.7 SUMMARY OF THE COMPLETE OPTIMISATION ALGORITHM

To wrap up the discussion about the methodology an overview of the complete algorithm is given for the general case where both design variables can be updated. The part related to updating the densities does not need to be performed if the thickness is kept constant. A graphical flowchart is shown in Figure 4.4. The algorithm is shown in algorithm 1.
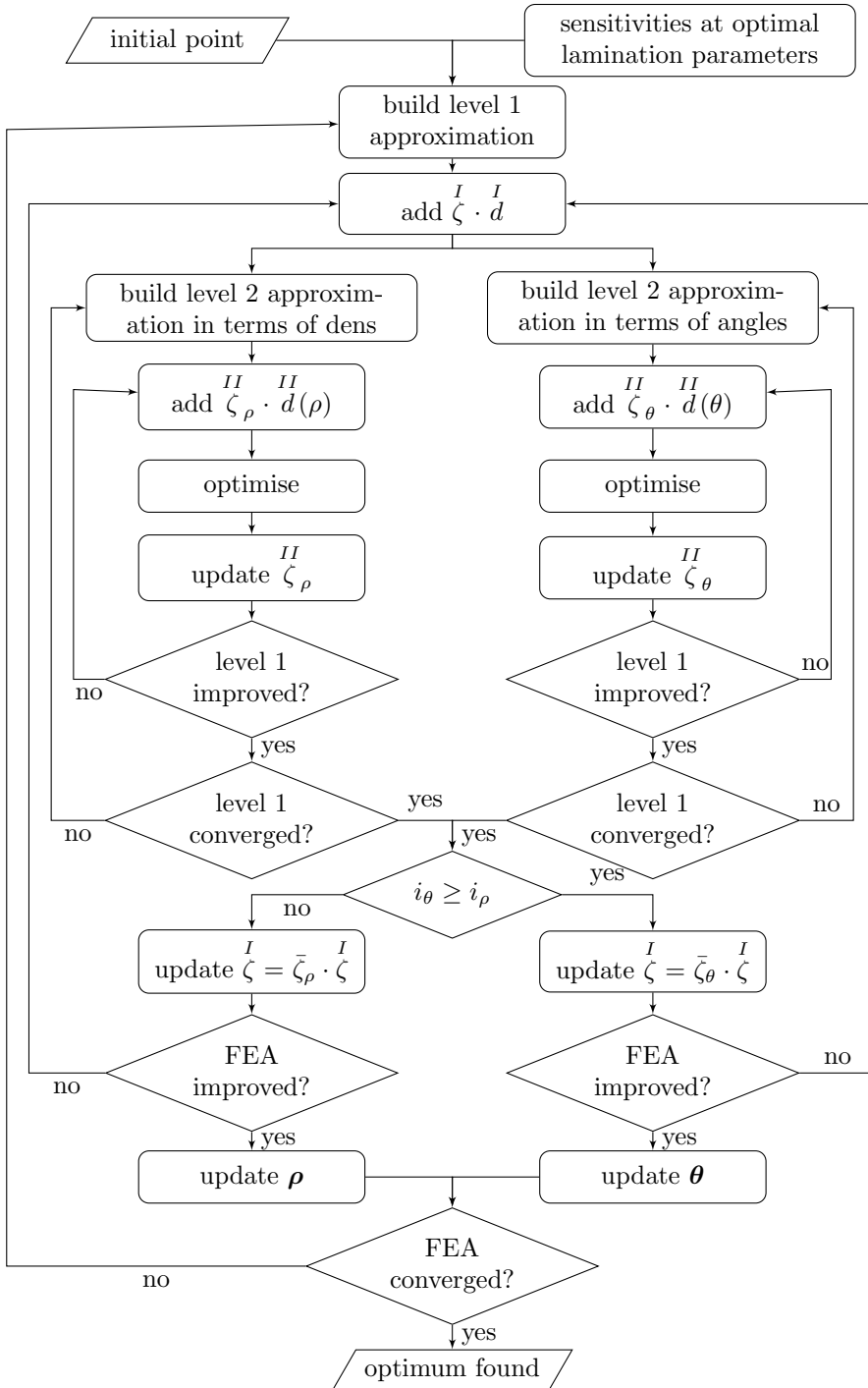
Figure 4.4: Flowchart of the complete algorithm.

Algorithm 1 Overview of the algorithm

1: start from an initial fibre angle distribution and sensitivities at the optimal lamination parameter distribution.
2: build the level one approximation $\overset{I}{f}$ using eq. (4.7).
3: add the damping function to the level one approximation using eqs. (4.24) and (4.30).
4: calculate the gradient and Hessian for the level two approximations, eqs. (4.8) and (4.9).
5: add the damping function to the level two approximations using eqs. (4.25), (4.28), (4.31), and (4.32).
6: optimise both level two approximations.
7: calculate level one approximation and update damping factors of level two using eq. (4.35).
8: check whether the level one approximation improved. If level one has improved, continue, else go back to step 5.
9: check whether the level one approximation has converged, or the maximum number of iterations is reached. If either of these conditions is met, continue, else return to step 4.
10: determine whether changing the fibre angles or densities leads to a higher improvement using eq. (4.36).
11: perform an FEA and update the damping factor of the level one approximation based on the chosen design variable using eq. (4.35).
12: check whether the FEA response has improved. If it has improved, the point is accepted, continue, else go back to step 3.
13: update the chosen design variable.
14: perform an FEA and calculate the sensitivities for the level one approximation.

15: check whether FEA has converged, if it has, the optimal fibre angle distribution is found, else return to step 2.

Truth is much too complicated to allow anything but approximations.

John Von Neumann

5

STRUCTURAL APPROXIMATIONS FOR COMPOSITE MATERIALS

One of the key ingredients in the method of successive approximations is how the approximations are built. The general forms used were already shown in the previous chapter. How they are constructed is explained in this chapter. The approximation strategy combines two methods. One, the convex linearisation method originally proposed by Fleury[40], which is extended to matrices in this work. Two, the force approximations originally proposed by Vanderplaats[155]. The basic idea behind the two methods is explained in section 5.1.

The approximation strategy is a two-level approach: the level one approximation is in terms of the laminate stiffness matrices, the level two approximation is in terms of the design variables of the optimisation. First, the level one approximation in terms of the laminate stiffness matrices is derived. To start, compliance is approximated, followed by strength and buckling approximations. Finally, the general form is found. This is explained in section 5.2. Second, a level two approximation is made based on the level one approximation. The level two approximation is independent of the response, it is a general form. During step one of the three-step optimisation strategy, the level two approximation is in terms of

---

This chapter is based on the conference paper 'Structural Approximations for Composite Optimisation'[115].

the lamination parameters, describing the stiffness matrices exact. During step two, the level two approximation is in terms of either the fibre angles or the ply densities. All these approximations are discussed in section 5.3.

5.1 APPROXIMATION STRATEGY

The approximation strategy is based on two methods: the convex linearisation, proposed by Fleury[40], and the method of force approximation, proposed by Vanderplaats and Thomas[155]. Convex linearisation leads to approximations that are computationally cheap to build and optimise because they are separable. Furthermore, the idea of linear or reciprocal approximations are combined in this method, taking the best of both. Force approximations lead to a two-level approximation strategy, also used in this work, as was described in section 4.2. This method has been shown to be computationally efficient. Both methods are combined in this work.

The convex linearisation (ConLin) approximation of Fleury[40] uses mixed variables: both linear and reciprocal terms are used. Based on the sign of the derivative, the most convex option is used: if the derivative with respect to a certain design variable is positive, the approximation in terms of that design variable is linear, if the derivative is negative, the approximation is reciprocal[40,41]:

$$\hat{f}(\mathbf{x}) \approx f(\mathbf{x}^0) + \sum_+ \left(\frac{\partial f}{\partial x_i} \right)\bigg|_{\mathbf{x}^0} \left(x_i - x_i^0 \right) - \sum_- \left(\frac{\partial f}{\partial x_i} \right)\bigg|_{\mathbf{x}^0} \frac{x_i^0}{x_i} \left(x_i - x_i^0 \right), \quad (5.1)$$

where $\sum_+$ denotes the summation over all terms with a positive derivative, and $\sum_-$ the summation over all terms with a negative derivative. It is assumed each design variable is non-negative. Hence, only first-order derivatives are necessary to build the approximation: building the approximation is computationally inexpensive.

The approximation obtained using the ConLin method is separable and convex. Hence, two out of four properties mentioned in section 4.1.1 are achieved. Conservativeness cannot be guaranteed since only first-order information is used. Conservativeness can be achieved using the damping function explained in section 4.4. Homogeneity is not achieved since some terms are linear, and others are reciprocal, hence when scaling all terms, it cannot be predicted how the approximation will scale.

The force approximations were proposed by Vanderplaats and Thomas to improve stress approximations[155]. Instead of directly approximating the stress using a first-order Taylor series, the element forces are approximated. The approximate stresses are found in terms of the element forces using an explicit, exact formula. Hence, the cost of building the approximation does not increase: the level two

approximation is only filling in the element forces in an equation no extra calculations, such as gradients, are necessary. The stress can be highly non-linear while, in general, the element forces are less non-linear: part of the non-linearity is captured using the explicit formula relating element forces to stresses [155].

The method of force approximations can also be used for responses other than stresses. In general, an approximation in terms of a section property, for example element force or stiffness, is made. The physical design variables are used to approximate the section properties. The section properties may be related exactly to the physical design variables, or another approximation, this time of the section properties in function of the physical design properties, may be necessary. Essentially, the method of force approximations is a two-level approximation: the level one approximation is in terms of the section properties, the level two approximation in terms of the physical design variables. Vanderplaats already noted the computational advantages of using a two-level approximation scheme. Since the level one and two approximations are related through an exact relation, the computational cost to build a two-level approximation is the same as for a single level approximation. However, it was noted in numerical experiments that due to the better approximation, less iterations were needed [85,154,155,156]. Hence, overall computational cost is reduced. If the level two approximation is not an exact function but needs to be constructed, (part of) the cost increase to build the second approximation is compensated by the decrease in number of iterations.

The approximation strategy in this thesis combines the ConLin method and force approximations in a two-level approximation scheme. First, the structural responses are approximated in terms of the laminate stiffness matrices and their inverse, hence using mixed variables similar to the ConLin method. Next, a level two approximation is made in terms of the physical design variables. This can be in terms of either the lamination parameters, the fibre angles, or the ply densities.

5.2   LEVEL ONE APPROXIMATION IN TERMS OF STIFFNESS

Most structural approximations were made in terms of beams or trusses, and later on expanded for general structures. Hence, first the derivation is done for a truss made of an elastic material. Next, the approximations for a general two-dimensional structure are derived. This is done since the physical reasoning behind the approximations is clear when a truss made of elastic material is used. For the general two-dimensional plates the complexity of the equations may hide their physical meaning. The approximations will be developed for three structural responses: compliance, strength and buckling. These are the most widely used responses for the design of structures under static loading. The derivation

for buckling is not done for a truss, but for a two-dimensional plate and a shell. Finally, a general approximation is formulated which can be used for any (structural) response.

5.2.1 DEFINITION OF DESIGN VARIABLES

Before an approximation can be made, the location of the design variables has to be defined. Since the structural responses are calculated using a finite element analysis (FEA), it seems a logical choice to link the design variables to the elements. However, rather than at the elements, the design variables are defined at the nodes of an FE model. This has three advantages. One, the continuity of the design variables is more likely to happen. It cannot be mathematically guaranteed, but in all numerical results presented continuity was preserved. Two, the number of design variables is often reduced: triangular elements are used in this thesis, which in general leads to more elements than nodes. Three, the manufacturing constraint on the minimum turning radius can easily be defined, as will be shown in section 6.1: the design variables are not next to each other, but have a certain distance between them.

By defining design variables at the nodes, an extra step is necessary to find the element properties, which are necessary for the FEA. The properties of nodes and elements are linked according to [51]

$$\mathbf{A}_k^{-1} = \sum_{i=1}^{n} N_{ik} \cdot \mathbf{A}_i^{-1}, \tag{5.2}$$

where N_{ik} denotes the value of shape function of corner node i at Gauss point k. The number of nodes n can be either three or four. The same relationship holds for the D-matrix. The element stiffness matrix is found using [39]

$$K_e = \sum_{k=1}^{n} v_k \cdot \mathbf{B}_k^T \cdot \mathbf{A}_k \cdot \mathbf{B}_k, \tag{5.3}$$

where k ranges over the Gauss integration points, $\mathbf{B}_k$ denotes the strain-displacement matrix, and the constant v_k is defined as

$$v_k = w_k \cdot h \cdot \det(\mathbf{J}), \tag{5.4}$$

where w_k denotes the weight of the Gauss point, h denotes the thickness of the laminate, and $\mathbf{J}$ denotes the Jacobian. [39] From this, the complete stiffness matrix can be constructed. Based on the element stiffness matrix, the complete stiffness matrix $\mathbf{K}$ is found. Next, the loads $\mathbf{f}$ and boundary conditions are defined. The displacements and rotations of each node, $\mathbf{u}$, are found using

$$\mathbf{f} = \mathbf{K} \cdot \mathbf{u}. \tag{5.5}$$

Once the displacements and rotations of each node are found, the strains and curvatures are recovered from them using [39]

$$\boldsymbol{\epsilon} = \mathbf{B} \cdot \mathbf{u}. \tag{5.6}$$

For a more detailed description of an FEM, the reader is referred to, for example, Felippa[39].

5.2.2 COMPLIANCE APPROXIMATION

TRUSS MADE OF ELASTIC MATERIAL
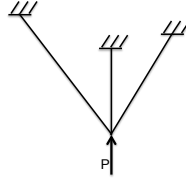
Figure 5.1: Example of a truss.

First, the compliance of a truss made of an elastic material will be derived. An example of a truss can be seen in Figure 5.1. The strain energy of a system is defined as

$$U = \sum_e \frac{1}{2} \cdot E \cdot \epsilon_e^2 \cdot A_e \cdot l_e, \tag{5.7}$$

where E denotes the Young's modulus, ϵ the strain, l the length, the subscript e denotes the element, and A_e denotes the area of element e. These are the design variables. The principle of minimum total potential energy is formulated as

$$\min_{\boldsymbol{\epsilon},\mathbf{u}} \quad \sum_e \frac{1}{2} \cdot E \cdot \epsilon_e^2 \cdot A_e \cdot l_e - \mathbf{f}^T \cdot \mathbf{u}$$
$$s.t. \qquad \epsilon_e - \mathbf{B_e}^T \cdot \mathbf{u} = 0. \tag{5.8}$$

The Lagrangian for this problem can be written as

$$\mathcal{L} = \min_{\boldsymbol{\epsilon},\mathbf{u}} \sum_e \frac{1}{2} \cdot E \cdot \epsilon_e^2 \cdot A_e \cdot l_e - \mathbf{f}^T \cdot \mathbf{u} + \max_{\boldsymbol{\sigma}} \sum_e \sigma_e \cdot A_e \cdot l_e \cdot \left(\epsilon_e - \mathbf{B_e}^T \cdot \mathbf{u} \right), \tag{5.9}$$

where σ_e are the Lagrangian multipliers of the constraints. The optimum can only be reached if the constraint is satisfied. If the constraint is not satisfied, the Lagrange multiplier will go to either $+\infty$ or $-\infty$, and thus the complete minimisation will go to $+\infty$. Rewriting to combine the terms involving the displacement vector:

$$\mathcal{L} = \min_{\boldsymbol{\epsilon},\mathbf{u}} \max_{\boldsymbol{\sigma}} \left(\sum_e A_e \cdot l_e \cdot \left(\frac{1}{2} \cdot E \cdot \epsilon_e^2 - \sigma_e \cdot \epsilon_e \right) + \left(\sum_e \sigma_e \cdot A_e \cdot l_e \cdot \mathbf{B}_e - f \right)^T \cdot \mathbf{u} \right). \tag{5.10}$$

f^* is defined as

$$f^* (\sigma_e) = \sigma_e \cdot \epsilon_e - \frac{1}{2} E \epsilon_e^2. \tag{5.11}$$

Interchanging the min and max, which is allowed in this case, eq. (5.10) is rewritten to

$$\max_{\boldsymbol{\sigma}} \left(- \left(\sum_e f^* \left(\sigma_e \right) A_e l_e \right) + \min_{\mathbf{u}} \left(\sum_e \sigma_e A_e l_e \mathbf{B_e} - \mathbf{f} \right)^T \cdot \mathbf{u} \right). \qquad (5.12)$$

Observing that $\mathbf{u}$ acts as a Lagrange multiplier of an equality constraint, this can be rewritten to the following minimisation problem:

$$\min_{\boldsymbol{\sigma}} \quad \sum_e f^* \left(\sigma_e \right) \cdot A_e \cdot l_e$$
$$s.t. \quad \sum_e F_e \cdot \mathbf{B_e} \cdot l_e = \mathbf{f}. \qquad (5.13)$$

Using

$$\sigma_e = \frac{F_e}{A_e}, \qquad (5.14)$$

and implementing the correct expression for f^*, eq. (5.11), the complementary strain energy is found to be

$$U^* = \frac{1}{2} \sum_e \frac{F_e^2 \cdot l_e}{E \cdot A_e}. \qquad (5.15)$$

The compliance can be formulated as

$$C = \min_{\mathbf{f}} U^*, \qquad (5.16)$$

and the minimum compliance can be formulated as

$$C^* = \min_{\mathbf{A}} \left(\min_{\mathbf{f}} U^* \right). \qquad (5.17)$$

Looking at equation (5.15), it can be seen the compliance is reciprocal in terms of the areas. Hence, the compliance can be approximated in terms of the areas as

$$C \approx \frac{1}{2} \sum_e \frac{F_e^{(k)2} \cdot \frac{l_e}{E}}{A_e}, \qquad (5.18)$$

where the superscript (k) denotes the force after the kth iteration, when the current iteration is $k + 1$.

The four desirable properties mentioned in section 4.1.1 are satisfied:

- convex: the approximation is reciprocal in terms of the area, the area is always strictly positive and the nominator is strictly non-negative.

- separable: the approximation is a summation of different functions of A_e

- conservative: only the element forces are approximated, by assuming they are the same as for the previous iteration. Each time the area is updated, the element forces $\mathbf{F}$ are still feasible. Hence when $\mathbf{F}$ is updated, the exact compliance will either improve or stay the same with respect to the approximation.

- homogeneous: the approximation is homogeneous of order -1.

GENERAL TWO-DIMENSIONAL PLATE
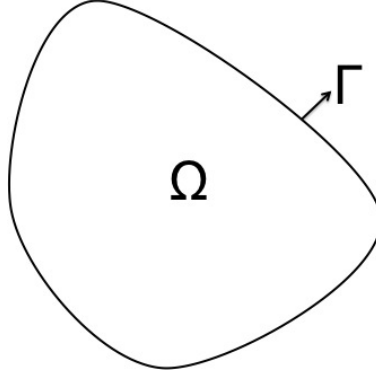
Figure 5.2: Example of a two-dimensional plate.

For a general two-dimensional plate with area Ω and boundary Γ, as shown in Figure 5.2, three equations need to be satisfied:

1. equilibrium: $\sum_{j=1}^{2} \frac{\partial N_{ij}}{\partial x_j} + b_i = 0$, for $i = 1, 2$

2. strain-displacement: $\epsilon_{ij}^0 = \frac{1}{2} \left(\frac{\partial u_i}{\partial x_j} + \frac{\partial u_j}{\partial x_i} \right)$, for $i, j = 1, 2$

3. material law: $N_{ij} = \mathbf{A}_{ijkl} \cdot \epsilon_{kl}$, for $i, j, k, l = 1, 2$,

where b_i is the external force in i-direction. Assuming the strain-displacement is satisfied in weak form and using a test function $\tilde{N}$ leads to

$$\sum_{i,j=1}^{2} \int_{\Omega} \tilde{N}_{ij} \cdot \epsilon_{ij}^0 - \frac{1}{2} \cdot \tilde{N}_{ij} \left(\frac{\partial u_i}{\partial x_j} + \frac{\partial u_j}{\partial x_i} \right) d\Omega = 0. \tag{5.19}$$

Using

$$\frac{\partial \tilde{N}_{ij} \cdot u_i}{\partial x_j} = \tilde{N}_{ij} \cdot \frac{\partial u_i}{\partial x_j} + \frac{\partial \tilde{N}_{ij}}{\partial x_j} \cdot u_i, \tag{5.20}$$

eq. (5.19) is rewritten to

$$\sum_{i,j=1}^{2} \int_{\Omega} \tilde{N}_{ij} \cdot \epsilon_{ij}^0 + \frac{1}{2} \left(\frac{\partial \tilde{N}_{ij}}{\partial x_j} \cdot u_i + \frac{\partial \tilde{N}_{ij}}{\partial x_i} \cdot u_j \right) - \frac{1}{2} \left(\frac{\partial \tilde{N}_{ij} \cdot u_i}{\partial x_j} + \frac{\partial \tilde{N}_{ij} \cdot u_j}{\partial x_i} \right) d\Omega = 0. \tag{5.21}$$

Applying the Gauss theorem on the last term:

$$\int_{\Omega} \tilde{N}_{ij} \cdot \epsilon_{ij}^0 + \frac{1}{2} \left(\frac{\partial \tilde{N}_{ij}}{\partial x_j} \cdot u_i + \frac{\partial \tilde{N}_{ij}}{\partial x_i} \cdot u_j \right) d\Omega - \oint_{\Gamma_t} \tilde{N}_{ij} \cdot u_i \cdot n_j + \tilde{N}_{ij} \cdot u_j \cdot n_i d\Gamma = 0. \tag{5.22}$$

Choosing the test function $\tilde{N}$ to be a change in stress distribution that satisfies equilibrium ∂N, the second term becomes zero since the external force $b_i = 0$ in each direction. Furthermore, the normal of ∂N is equal to zero since equilibrium is satisfied and the external force is zero, meaning the third term is zero as well. Hence, eq. (5.22) can be rewritten as

$$\int_\Omega \partial N_{ij} \cdot \epsilon_{ij}^0 d\Omega = 0, \tag{5.23}$$

which has to hold for $i, j = 1, 2$. Noting that the strain at mid-plane is defined as

$$\epsilon_{ij}^0 = \frac{\partial U^*(N_{ij})}{\partial N_{ij}}, \tag{5.24}$$

eq. (5.23) is rewritten as

$$\delta \int_\Omega U^*(\mathbf{N}) d\Omega = 0. \tag{5.25}$$

Using the material law the total strain energy is rewritten as

$$U^* = \frac{1}{2}\mathbf{N}^T \cdot \mathbf{A}^{-1} \cdot \mathbf{N}. \tag{5.26}$$

The minimum compliance is written as

$$C^* = \min_{\mathbf{A}} \min_{\mathbf{N}} \int_\Omega U^*(\mathbf{N}, \mathbf{A}) d\Omega. \tag{5.27}$$

Using the Frobenius product, the approximation of the compliance is rewritten to

$$C = \frac{1}{2} \int_\Omega \left(\mathbf{N} \cdot \mathbf{N}^T\right) : \mathbf{A}^{-1} d\Omega = \int_\Omega \phi : \mathbf{A}^{-1} d\Omega. \tag{5.28}$$

Observing the structure of this equation the following approximation can be used:

$$C \approx \sum_{n=1}^N \phi_\mathbf{n} : \mathbf{A_n}^{-1}, \tag{5.29}$$

where N denotes the number of nodes in the finite element model of the plate.

Analogous to the truss of elastic material, the four desirable properties mentioned in section 4.1.1 are satisfied:

- convex: the second variation of the approximation with respect to $\mathbf{A}^{-1}$ is non-negative.

- separable: the different contributions of the nodes do not influence each other.

- conservative: while for the truss of elastic material, the element forces were approximated, now the stresses $\mathbf{N}$ are assumed to be the same as for the previous iteration. Each time the area is updated, the stresses $\mathbf{N}$ are still feasible, such that the exact compliance can only improve or stay the same with respect to the approximation when $\mathbf{N}$ is updated.

- homogeneous: the approximation is homogeneous of order -1.

5.2.3 STRESS APPROXIMATION

Instead of stress, the failure index r is approximated. The failure index is based on the different strains, and avoids having to approximate the stresses in all directions. For the truss, only stress in the direction of the truss members exist, hence approximating the stress directly would be feasible. For the two-dimensional plate, the failure index is a combination of the strains (or stresses) in multiple directions. An example of the feasible space can be seen in Figure 5.3. For the truss made of an elastic material, the failure index is defined as the stress divided by the allowable stress σ_{all}. For the two-dimensional plate, a Tsai-Wu failure criterion based on the strains is implemented. The derivation of the failure index is outside the scope of this thesis, the interested reader is referred to the work by IJsselmuiden et al.[60] and Khani et al.[78].
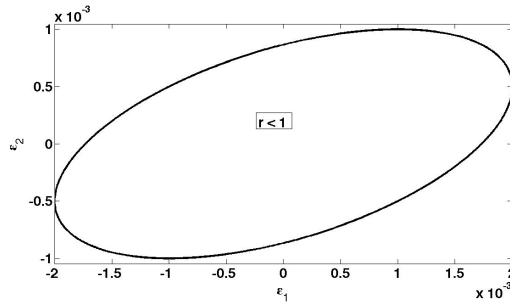
Figure 5.3: Example of a failure index as a function of strain in two directions.

TRUSS MADE OF ELASTIC MATERIAL

For a truss made of an elastic material, the failure index of an element is given by

$$r_e = \frac{F_e}{A_e \sigma_{all}}. \tag{5.30}$$

The failure index can be approximated analogous to the compliance approximation:

$$r_e \approx \frac{F_e^{(k)}}{A_e \sigma_{all}}. \tag{5.31}$$

However, changing the area of element e has an influence on the complete stress distribution, not just on the stress of element e. Therefore, a modification function $m(\mathbf{A})$ is added, that has to have two characteristics:

1. the value of the approximation at the current iterate should be zero, to have at least a zeroth order approximation: $m(\mathbf{A}^{(k)}) = 0$.

2. when scaling the current iterate, the approximation in eq. (5.31) is exact since the stress distribution does not change, hence the value of the added function should be zero: $m(c \cdot \mathbf{A}^{(k)}) = 0$,

where $\mathbf{A}$ is the design vector containing all element areas. A function that suits these requirements is

$$m = \frac{F_e(\mathbf{A}) - F_e(\mathbf{A}^{(k)})}{\sigma_{all} \cdot A_e^{(k)}} \approx \sum_e a_e \cdot A_e, \tag{5.32}$$

where a_e is found by matching the derivatives at the approximation point on both sides. The total approximation that takes the load redistribution into account is

$$r_e \approx \frac{F_e^{(k)}}{\sigma_{all} \cdot A_e} + \sum_e a_e \cdot A_e. \tag{5.33}$$

As for the compliance, it is checked again whether this approximation satisfies the requirements mentioned in section 4.1.1:

- convex: the reciprocal part is convex because the area is always strictly positive and the nominator is strictly non-negative; the linear part is always convex.

- separable: the function is not separable in terms of the element force, but separability is still achieved in terms of the element areas.

- conservative: the approximation is not conservative, hence, the damping function described in section 4.4 has to be added to this approximation to render it conservative.

- homogeneous: at the approximation point, the approximation is homogeneous of order -1: the linear part is homogeneous of order 0, the reciprocal part of order -1, hence the total approximation has homogeneity of order -1.

GENERAL TWO-DIMENSIONAL PLATE

For a general two-dimensional plate, the failure index is derived in the work by Khani et al.[78]. The failure index is linearised:

$$r \approx \boldsymbol{\epsilon}^T \cdot \mathbf{g}^{(k)}, \tag{5.34}$$

where

$$\mathbf{g}^{(k)} = \left. \frac{\partial r}{\partial \epsilon} \right|_{\boldsymbol{\epsilon} = \boldsymbol{\epsilon}^{(k)}}. \tag{5.35}$$

Using the material law, the strain is defined as

$$\boldsymbol{\epsilon} = \mathbf{A}^{-1} \cdot \mathbf{N}. \tag{5.36}$$

The failure index can be approximated as

$$r = \mathbf{N}^T \mathbf{A}^{-1} \mathbf{g} = \phi : \mathbf{A}^{-1}, \tag{5.37}$$

where ϕ is defined as

$$\phi = \frac{1}{2} \left(\mathbf{N} \mathbf{g}^T + \mathbf{g} \mathbf{N}^T \right). \tag{5.38}$$

The approximation in eq. (5.37) is only convex if ϕ is positive semi-definite. Since this is not guaranteed by construction, ϕ is split up in two parts: a part that is positive semi-definite ϕ^+ and the non-definite part ϕ^-. The non-definite part is approximated using a first-order Taylor expansion, leading to

$$r \approx \phi^+ : \mathbf{A}^{-1} + \psi : \mathbf{A} - \phi^- : \mathbf{A}^{(k)^{-1}}. \tag{5.39}$$

To ensure convexity, $\phi^- : \mathbf{A}^{(k)^{-1}}$ needs to be zero. This is ensured by taking the Cholesky factorisation of $\mathbf{A} = \mathbf{L} \cdot \mathbf{L}^T$ and imposing

$$trace \left(\mathbf{L}^{-1} \cdot \phi^- \cdot \mathbf{L}^{-T} \right) = 0. \tag{5.40}$$

Furthermore, ϕ^+ needs to be as large as possible, implying ϕ^- needs to be as small as possible. The following optimisation problem is solved to find ϕ^-:

$$\begin{aligned} min \qquad & ||\phi^-|| \\ s.t. \qquad & trace \left(\mathbf{L}^{-1} \cdot \phi^- \cdot \mathbf{L}^{-T} \right) = 0 \\ & \mathbf{L}^{-1} \cdot \phi \cdot \mathbf{L}^{-T} - \mathbf{L}^{-1} \cdot \phi^- \cdot \mathbf{L}^{-T} \le 0. \end{aligned} \tag{5.41}$$

ϕ^- is determined solving this optimisation problem, after which ϕ^+ and ψ can also be determined. The final approximation of the failure index is

$$r \approx \sum_{n=1}^{N} \psi_n : \mathbf{A}_n + \phi_n : \mathbf{A}_n^{-1}, \tag{5.42}$$

where the superscript $+$ has been removed from ϕ since only the positive part is taken into account in the approximation and thus no ambiguity exists by removing it. The summation over the nodes is required to capture the load redistribution effect. The details of the sensitivity analysis are outside the scope of this thesis, the interested reader is referred to the work by IJsselmuiden et al. [59,61].

Again the four desirable properties mentioned in section 4.1.1 are checked:

- convex: by construction, the approximation is convex: ϕ is guaranteed to be positive semi-definite.

- separable: the different contributions of the nodes do not influence each other.

- conservative: the approximation is not conservative, hence, the damping function described in 4.4 has to be added to this approximation to render it conservative.

- homogeneous: at the approximation point, the approximation is homogeneous of order -1: the linear part is homogeneous of order 0, the reciprocal part of order -1, hence the total approximation has homogeneity of order -1.

5.2.4   Buckling approximation

General two-dimensional plate

The buckling factor λ is calculated using[61]

$$(\mathbf{K}_b - \lambda \mathbf{K}_g) \cdot \mathbf{a} = 0, \tag{5.43}$$

where $\mathbf{K}_b$ is the global bending stiffness matrix and $\mathbf{K}_g$ is the global geometric stiffness matrix. $\mathbf{a}$ is the mode shape normalised to obey

$$\mathbf{a}^T \cdot \mathbf{K}_b \cdot \mathbf{a} = 1. \tag{5.44}$$

Differentiating equation (5.43) with respect to a design variable x and rearranging terms leads to

$$\frac{d\lambda}{dx} = \lambda \mathbf{a}^T \cdot \left(\frac{\partial \mathbf{K}_b}{\partial x} - \lambda \frac{\partial \mathbf{K}_g}{\partial x} \right) \cdot \mathbf{a}. \tag{5.45}$$

It is assumed that x only influences the properties of a single element. The first term is a local term: the bending stiffness is only dependent on the properties of a single element. The second term, the geometric stiffness matrix, depends on all elements: changing a single element will have an influence all over the panel due to the load redistribution.

The buckling load is homogeneous of order zero with respect to the in-plane stiffness matrix, much like the load redistribution part in the stress approximations. Furthermore, the buckling load is homogeneous of order one with respect to the bending stiffness matrix. As was mentioned in chapter 4, the optimisation is formulated as a minimisation problem, hence the inverse buckling load is approximated:

$$r = \frac{1}{\lambda}. \tag{5.46}$$

Consequently, the bending stiffness matrix becomes analogous to the compliance approximation, but since it is only dependent on the out-of-plane stiffness matrix for plates, the approximation is also only in terms of the inverse out-of-plane stiffness matrix $\mathbf{D}^{-1}$. Since the in-plane stiffness matrix is homogeneous of order zero, its shape does not change: it is a linear function of the inverse of the buckling load. The total approximation becomes

$$r \approx \sum_{n=1}^{N} \boldsymbol{\psi}_{mn} : \mathbf{A}_n + \boldsymbol{\phi}_{bn} : \mathbf{D}_n^{-1}. \tag{5.47}$$

The derivation of the sensitivities is outside the scope of this thesis: the interested reader is referred to the work by IJsselmuiden et al.[59,61]

General two-dimensional shells

The previous discussion holds for plates, for shells some extra terms appear. The bending stiffness matrix is no longer only a function of the D-matrix, but also

depends on the A-matrix, such that a term with $\mathbf{A}^{-1}$ will also appear. The load redistribution is no longer only dependent on the A-matrix: also the D-matrix has an influence due to the curved geometry. The resulting total approximation of the inverse buckling load for shells is

$$r \approx \sum_{n=1}^{N} \boldsymbol{\psi}_{mn} : \mathbf{A}_n + \boldsymbol{\psi}_{bn} : \mathbf{D}_n + \boldsymbol{\phi}_{mn} : \mathbf{A}_n^{-1} + \boldsymbol{\phi}_{bn} : \mathbf{D}_n^{-1}, \qquad (5.48)$$

where the subscripts m and b denote the membrane and bending part respectively.

Again the four desirable properties mentioned in section 4.1.1 are checked:

- convex: the approximation is convex by construction: $\boldsymbol{\psi}_m$ and $\boldsymbol{\psi}_b$ are guaranteed to be positive semi-definite.

- separable: the different contributions of the nodes do not influence each other.

- conservative: the approximation is not conservative, hence, the damping function described in 4.4 has to be added to this approximation to render it conservative.

- homogeneous: at the approximation point, the approximation is homogeneous of order -1: the linear part is homogeneous of order 0, the reciprocal part of order -1, hence the total approximation has homogeneity of order -1.

5.2.5 GENERAL FORM OF APPROXIMATION

The approximation in terms of the stiffness is the level one approximation as was explained in chapter 4. In general, it can be a function of the in- and out-of-plane stiffness matrices and their inverse, like eq. (5.48):

$$\overset{I}{f} \approx \sum_{n} \boldsymbol{\psi}_{mn} : \mathbf{A}_n + \boldsymbol{\psi}_{bn} : \mathbf{D}_n + \boldsymbol{\phi}_{mn} : \mathbf{A}_n^{-1} + \boldsymbol{\phi}_{bn} : \mathbf{D}_n^{-1} + c, \qquad (5.49)$$

where the constant c has been added for generality: all responses discussed so far enjoy homogeneous properties, and $c = 0$, but this is not always the case.

Compliance, strength and buckling approximations have been discussed in this chapter, but any structural response can be approximated using eq. (5.49). Examples include, but are not limited to, fundamental frequency[7], post-buckling behaviour[121,165], and aeroelastic tailoring[98,143].

5.3 LEVEL TWO APPROXIMATIONS

While only one level one approximation exists, multiple options exist for level two. In the level two approximation, the stiffness matrices are approximated in terms of physical design variables. During step one of the three-step optimisation approach, the level two approximation is in terms of the lamination parameters. This is not strictly speaking an approximation since the lamination parameters describe the stiffness matrices exact. During step two, two physical design variables exist: fibre angles, and ply densities. Both are approximated in a differently: a second-order Taylor series is used for the fibre angles, a linearisation is used for the ply densities.

5.3.1 LAMINATION PARAMETER APPROXIMATION

During step one of the three-step optimisation approach, the stiffness is optimised. As was explained in section 3.2, the terms of the stiffness matrices are linked, hence directly optimising them is not easy. One would need a lot of constraints to assure feasibility. By using the lamination parameters, the feasible region can easily be described. Since the lamination parameters describe the feasible region exact, the level two approximation is an explicit function, much like Vanderplaats proposed for the strength approximation.

Furthermore, the number of design variables is not dependent of the number of layers, and the feasible region is convex when using lamination parameters. A convex feasible region implies the optimum found during step one of the three-step optimisation approach is the global optimum. The details of the lamination parameter optimisation are not discussed here, the interested reader is referred to the PhD thesis of IJsselmuiden[59].

5.3.2 FIBRE ANGLE APPROXIMATION

During step two of the three-step optimisation approach, the fibre angles are optimised. This is done by building a level two approximation, denoted by $\overset{II}{f}(\boldsymbol{\theta})$. Contrary to the lamination parameters, the fibre angles only represent the stiffness matrices exact at the approximation point. As approximation a second-order Taylor series is chosen since it is guaranteed to be convex when the second derivative is positive. Based on equation 5.49, the approximation is found to be

$$\overset{II}{f}(\boldsymbol{\theta}) \approx \overset{I}{f}_0 + \mathbf{g} \cdot \Delta\boldsymbol{\theta} + \Delta\boldsymbol{\theta}^T \cdot \mathbf{H} \cdot \Delta\boldsymbol{\theta}, \tag{5.50}$$

where $\overset{I}{f}_0$ denotes the value, $\mathbf{g}$ the gradient and $\mathbf{H}$ is an approximation of the Hessian of the level one approximation at the approximation point. The gradient

and Hessian approximation can be calculated starting from

$$\overset{II}{f}(\theta) = \overset{I}{f}(\mathbf{s}(\theta)) \tag{5.51}$$

where $\mathbf{s}$ contains the components of the stiffness matrices $\mathbf{A}$ and $\mathbf{D}$. Differentiating this with respect to the fibre angle θ_i, the ith term of the gradient is found to be

$$g_i = \frac{\partial \overset{I}{f}}{\partial \theta_i} = \frac{\partial \overset{II}{f}}{\partial \theta_i} = \frac{\partial \overset{I}{f}}{\partial \mathbf{s}_\alpha} \cdot \frac{\partial \mathbf{s}_\alpha}{\partial \theta_i}, \tag{5.52}$$

where s_α denotes either the in- or out-of-plane stiffness matrix. The derivatives of the stiffness matrices with respect to an angle θ_i is given in eq. (3.31). Differentiating again with respect to fibre angle θ_j, the ij^{th} term of the Hessian is found to be

$$H_{ij} = \frac{\partial^2 \overset{I}{f}}{\partial \theta_i \partial \theta_j} = \frac{\partial^2 \overset{I}{f}}{\partial \mathbf{s}_\alpha \partial \mathbf{s}_\beta} \cdot \frac{\partial \mathbf{s}_\alpha}{\partial \theta_i} \cdot \frac{\partial \mathbf{s}_\beta}{\partial \theta_j} + \underline{\frac{\partial \overset{I}{f}}{\partial \mathbf{s}_\alpha} \cdot \frac{\partial^2 \mathbf{s}_\alpha}{\partial \theta_i \partial \theta_j}}. \tag{5.53}$$

Convexity is not guaranteed when using the exact Hessian. Convexity is guaranteed by omitting the underlined part of equation 5.53, which is not guaranteed to be positive definite, and leaving the positive semi-definite leading term, called the Gauss-Newton part. Only part of the Hessian does not influence the validity of the approximation since a first-order approximation only has to have equal function and gradient values at the approximation point as the approximated function.

5.3.3 DENSITY APPROXIMATION

Next to the fibre angles, the density distribution can be optimised during step two of the three-step optimisation approach. This way variable thickness laminates are obtained. Analogous to the fibre angle optimisation, one starts from equation 5.49, and linearises the A and D matrix in terms of the densities. The derivatives of the laminate stiffness matrices with respect to the ply density are given in eq. (3.29). The approximation can be used as is since a linear function is always convex.

Today's scientists have substituted mathematics for experiments, and they wander off through equation after equation, and eventually build a structure which has no relation to reality.

Nikola Tesla

6

MANUFACTURING CONSTRAINTS FOR VARIABLE STIFFNESS LAMINATES

The previous chapters focused on the structural optimisation and optimisation algorithm. This chapter focuses on formulating constraints to guarantee the optimised laminate is manufacturable. Whether or not a laminate is manufacturable depends on the turning radius: if the turning radius is too small, the fibres will wrinkle and lose (part of) their load-carrying capability. The turning radius is calculated from the change in fibre angles at the nodes of a finite element model. This is discussed in section 6.1. The implementation in the optimisation algorithm is discussed in section 6.2.

The lower bound on the turning radius depends on a lot of factors, for example material, tow width, number of tows in a course, and placement speed. Hence, the manufacturing time and cost are also dependent on the minimum turning radius that has to be laid down. Since all these variables are material- and case-specific, no exact number can be used, hence, the effect of the lower bound on the turning radius on the structural performance is investigated in section 6.3. The effect of the retrieval-optimisation algorithm introduced in section 4.6 is also

---

This chapter is based on the journal paper 'Stacking sequence optimisation of variable stiffness laminates with manufacturing constraints'[118], and the conference paper 'Effect of Steering Constraints on the Performance of Variable Stiffness Laminates'[114].

investigated. In section 6.4 it is verified that the algorithm leads to a reduction in computational effort compared to only using optimisation.

6.1 STEERING CONSTRAINTS

When laying down fibres in a curved path using automated fibre placement machines, three sorts of defects can appear[37,50,79,95]: fibre wrinkling, gaps and overlaps. Fibre wrinkling needs to be avoided because a fibre loses (part of) its load-carrying capability when it wrinkles. Gaps and overlaps on the other hand lead to local variations in the thickness which can have a large effect on the overall weight and structural performance[33,38,99,100]. The effect of these defects on the structural performance is a field of research on its own. In this work, a perfect structure is assumed: no gaps or overlaps are modelled. However, constraints are posed to avoid fibre wrinkling and to minimise the number of gaps and overlaps.

Fibre wrinkling is caused by the turning radius being too small. It is a local effect: if at one point the turning radius is too small, the fibre will wrinkle at that point. This is shown in Figure 6.1. Hence, to avoid fibre wrinkling, a local constraint needs to be formulated. Since the fibre angles are defined at the nodes, the turning radius is found per element, hence one constraint per layer per element is formulated to avoid fibre wrinkling. This is referred to in this work as the *local* steering constraint.
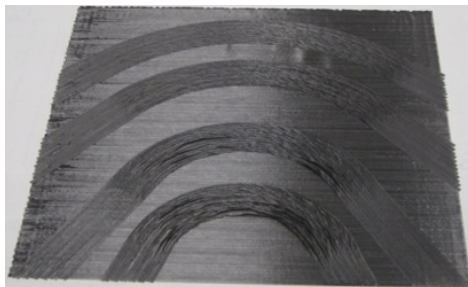
Figure 6.1: Wrinkling of the tows occurs when the turning radius is too small (courtesy of NLR).

Gaps and overlaps appear due to the fibres converging and diverging. The exact location of the gaps and overlaps is hard to predict based on the fibre angle distribution at the nodes: other decisions such as the start of the first tow, the tow width, and the cutting strategy have a large effect on their exact location. Hence, instead of defining an upper bound on the (local or total) size of gaps and overlaps, another measure is used: the average gradient of the fibre angle distribution. This average is a measure for the amount of convergence and divergence of the fibres,

and therefore provides a good indication of the total size of gaps and overlaps in the structure. Only one constraint per layer is formulated since it is an average. This is referred to in this work as the *global* constraint.

Steering is defined as

$$\varsigma^2 = \nabla\theta \cdot \nabla\theta. \tag{6.1}$$

The average steering over an area Ω can be found using

$$\bar{\varsigma^2} = \frac{1}{\Omega} \int_\Omega \varsigma^2 d\Omega. \tag{6.2}$$

Discretising this leads to

$$\varsigma^2 = \frac{2}{\Omega} \cdot \boldsymbol{\theta}^T \cdot \mathbf{L} \cdot \boldsymbol{\theta}, \tag{6.3}$$

where L is the standard FEM Laplacian: if it is chosen to be the Laplacian of an element, the local steering is found, if it is chosen to be the Laplacian of the complete structure, the global steering is found. During the optimisation, an upper bound on the local and/or global steering ς_U is defined. An equivalent lower bound on the turning radius r_l can be found from the upper bound on the steering ς_U using

$$\varsigma_U = \frac{1}{r_l}. \tag{6.4}$$

6.2 IMPLEMENTATION OF STEERING CONSTRAINTS

6

The global and local steering constraint can be posed at the same time, or only one of them can appear in the optimisation. For simplicity, the upper and lower bounds are removed from the optimisation problem. The optimisation problem with steering constraints is formulated as

$$
\begin{aligned}
\min \quad & z \\
s.t. \quad & f_i - z \cdot \mathbf{e} \le 0 \\
& \varsigma^2 - \varsigma_U^2 \le 0,
\end{aligned} \tag{6.5}
$$

where ς_U denotes the upper bound on steering. The predictor-corrector method, explained in section 4.3, is used to perform this optimisation. For this problem, the Lagrangian is formulated as

$$
\mathcal{L} = z + \boldsymbol{\lambda}_c^T \cdot (\mathbf{f} - z \cdot \mathbf{e} + s_c) + \boldsymbol{\lambda}_s^T \cdot \left(\boldsymbol{\varsigma}^2 - \varsigma_U^2 + s_s\right) \\
- \mu \left(\mathbf{1}^T ln\left(\mathbf{s}_c\right) + \mathbf{1}^T ln\left(\mathbf{s}_s\right)\right), \tag{6.6}
$$

where $\boldsymbol{\varsigma}$ is a vector containing each steering value that is constrained and s_s and $\boldsymbol{\lambda}_s$ denote the slack and Lagrange multipliers of the steering constraints. The

optimality criteria are formulated as

$$
\begin{aligned}
\nabla z : -b_z &= 1 - \lambda_c \cdot e^T \\
\nabla x : -\mathbf{b}_\theta &= \boldsymbol{\lambda}_c \cdot \mathbf{g} + 2 \cdot \sum_s \lambda_s \cdot \mathbf{L_s} \cdot \boldsymbol{\theta} \\
\nabla \lambda_c : \mathbf{b}_{\lambda_c} &= f - z \cdot \mathbf{e}^T + s_c \\
\nabla s_c : \mathbf{b}_{s_c} &= \lambda_c - \frac{\mu}{s_c} \\
\nabla \lambda_s : \mathbf{b}_{\lambda_s} &= \boldsymbol{\theta}^T \cdot \mathbf{L_s} \cdot \boldsymbol{\theta} - |\Omega_s| \cdot \varsigma_U^2 + s_s \cdot |\Omega_s| \\
\nabla s_s : \mathbf{b}_{s_s} &= \lambda_s \cdot |\Omega_s| - \frac{\mu \cdot |\Omega_s|}{s_s}.
\end{aligned}
\tag{6.7}
$$

To avoid numerical problems, the terms related to the slack are multiplied with the slacks:

$$
\lambda_c \cdot s_c - \mu = 0
\tag{6.8}
$$
$$
\lambda_s \cdot \Omega_s \cdot s_s - \mu \cdot \Omega_s = 0.
$$

Linearising and using

$$
\Delta s_c = \frac{s_c}{\lambda_c} \Delta \lambda_c
\tag{6.9}
$$
$$
\Delta s_s = \frac{s_s}{\lambda_s} \Delta \lambda_s,
$$

leads to the following problem:

$$
\begin{bmatrix}
\boldsymbol{\lambda_c} \cdot \mathbf{H} + 2 \cdot \lambda_s \cdot \mathbf{L_s} & \mathbf{g} & 2 \cdot \mathbf{L_s} \cdot \boldsymbol{\theta} & 0 \\
\mathbf{g}^T & -\frac{s_c}{\lambda_c} & 0 & -e^T \\
(2 \cdot \mathbf{L_s} \cdot \boldsymbol{\theta})^T & 0 & -\frac{s_s \cdot |\Omega_s|}{\lambda_s} & 0 \\
0 & -e & 0 & 0
\end{bmatrix}
\cdot
\begin{bmatrix}
\Delta\theta \\
\Delta\lambda_c \\
\Delta\lambda_s \\
\Delta z
\end{bmatrix}
=
\begin{bmatrix}
\mathbf{b}_\theta \\
\mathbf{b}_{\lambda_c} - \frac{\mathbf{b}_{s_c}}{\lambda_c} - \frac{\mu \mathbf{1}}{\lambda_c} \\
\mathbf{b}_{\lambda_s} - |\Omega_s| \frac{\mathbf{b}_{s_s} + \mu \mathbf{1}}{\lambda_s} \\
b_z
\end{bmatrix},
\tag{6.10}
$$

where the vector products in the right-hand side are done term-by-term. The size of this problem can be further reduced using the Schur complement [63] to remove the Lagrange multipliers of the steering constraints from this problem. This leads to the following problem:

$$
\begin{bmatrix}
\mathbf{H}^* & \mathbf{g} & 2 \cdot \mathbf{L_s} \cdot \boldsymbol{\theta} & 0 \\
\mathbf{g}^T & -\frac{s_c}{\lambda_c} & 0 & -e^T \\
0 & -e & 0 & 0
\end{bmatrix}
\cdot
\begin{bmatrix}
\Delta\theta \\
\Delta\lambda_c \\
\Delta z
\end{bmatrix}
=
\begin{bmatrix}
\mathbf{b}_\theta^* \\
\mathbf{b}_{\lambda_c} - \frac{\mathbf{b}_{s_c}}{\lambda_c} - \frac{\mu \mathbf{1}}{\lambda_c} \\
b_z
\end{bmatrix},
\tag{6.11}
$$

where $\mathbf{b}_\theta^*$ and $\mathbf{H}^*$ are given by

$$
\mathbf{H}^* = \boldsymbol{\lambda_c} \cdot \mathbf{H} + 2 \cdot \lambda_s \cdot \mathbf{L_s} + 2 \cdot \mathbf{L_s} \cdot \boldsymbol{\theta} \cdot \left(\frac{\lambda_s}{|\Omega_s|\mathbf{s_s}} \right) \cdot 2 \cdot \mathbf{L_s} \cdot \boldsymbol{\theta}
\tag{6.12}
$$

$$
\mathbf{b}_\theta^* = \mathbf{b}_\theta + \left(\mathbf{b}_{\lambda_s} - |\Omega_s| \frac{\mathbf{b}_{s_s} + \mu \mathbf{1}}{\lambda_s} \right) \cdot \left(2 \cdot \mathbf{L_s} \cdot \boldsymbol{\theta} \cdot \frac{\lambda_s}{|\Omega_s|\mathbf{s_s}} \right).
$$

From this small problem, all variables can be found, and the standard predictor-corrector method, explained in section 4.3, can be used.

6.3 INFLUENCE OF STEERING CONSTRAINTS

The lower bound on the turning radius depends on a many factors, such as material, tow width, tows laid down per course, placement speed, and of course manufacturing method. The manufacturing method considered during this work is automated fibre placement (AFP). This implies the lower bound on turning radius can be as low as about $300-400$ mm, but may also be up to 800 mm for other materials. Much smaller radii could be reached when tailored fibre placement is used[137].

The same structure is optimised multiple times with different upper bounds on steering to quantify the influence of the steering constraints. A buckling optimisation example is used for illustration. The problem is defined as a singly-curved plate under uni-axial compression optimised for maximum buckling load with stiffness constraint. The critical buckling load is maximised during the optimisation. The first two buckling loads are taken into account to account for possible mode jumping. A stiffness constraint is posed requiring the compliance to be no greater than the compliance of a quasi-isotropic (QI) laminate of the same thickness. A QI laminate is defined as all lamination parameters being zero. No lay-up is specified for the QI laminate, but it is a good way to normalise the results. The stiffness constraint has two reasons: one, making sure that a minimum stiffness is reached, two, making sure the post-buckling behaviour is stable. The stability in the post-buckling regime and the stiffness have earlier been shown to be linked[120]. The plate is 600 by 400 mm, with a sine-shaped height difference, with a maximum height of 75 mm attained in the middle. The left and right edge are constrained to remain straight and loaded in uni-axial compression with a unit force. All edges are constrained to not move out-of-plane. A graphical representation can be seen in figure 6.2.

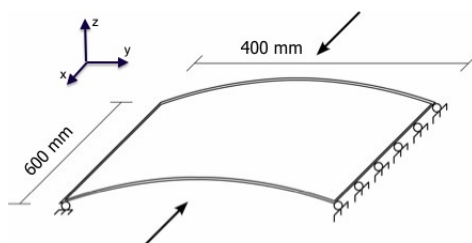**Figure 6.2:** Problem statement for the optimisation.

The material properties are: $E_1 = 154 GPa$, $E_2 = 10.8 GPa$, $G_{12} = 4.02 GPa$, $\nu_{12} = 0.317$, and $t_{ply} = 0.6$mm. The laminate is prescribed to be balanced, meaning for every θ-layer, a $-\theta$-layers is present. These balanced layers are assumed to be next to each other in this example. The physical laminate has 36 layers in total,

but only 9 *design layers* are part of the optimisation problem since symmetry is also imposed. The design layers are linked to the physical laminate as follows: if the design layers are $[\theta_1/\theta_2]$, the physical laminate is $[\theta_1/-\theta_1/\theta_2/-\theta_2]_s$.

A mesh convergence study indicated that a sufficiently fine mesh has 24 elements in y-direction, and 36 in x-direction, leading to 1728 triangular elements and 925 nodes in the model used during optimisation. Only a quarter of the plate is used during the optimisation ue to the symmetry of the problem, reducing the number of nodes in the optimisation to 247, and the number of elements to 432. The weights of the quarter of the plate are changed to reflect the complete plate. The complete model is used for the FE analysis and sensitivity calculation.

In step one of the three-step optimisation approach, the optimal stiffness distribution in terms of the lamination parameters is found. The buckling loads found are 2.2432 and 2.4656 times the lowest buckling load of a QI laminate while the stiffness is 1.0001 times the stiffness of the QI laminate. Since the laminate is balanced and symmetric, the lamination parameters V_2 and V_4 are both zero.

6.3.1 INFLUENCE OF LOCAL STEERING CONSTRAINTS

The influence of the local steering constraints is investigated first. The local steering constraint makes sure that the fibre does not wrinkle, which is to a certain degree material dependent, but also the width of the tow, the number of tows laid down in a single course and machine speed have an influence. Hence, a smaller turning radius may be obtained for the same material if a smaller tow is used, but the manufacturing time, and cost, will increase. Whether or not the increase in time and cost is worth the increase in performance is a question for the designer. By performing the optimisation for different steering constraints, all information needed to make this trade-off would be available.

The upper bound on local steering ς_U is changed from 1 m^{-1} to 5 m^{-1}, meaning a lower bound on turning radius of 1000 to 200 mm. The results are shown in Table 6.1, where the upper bound on local steering is shown in column one, the optimal buckling load in column two and three, the stiffness in column four. The difference with respect to the optimum in terms of the lamination parameters is shown in the last column. The steering constraint was always active: the maximum steering was always equal to the upper bound set.

The results are not surprising: the higher the steering (i.e., the smaller the minimal turning radius), the higher the buckling load. The stiffness is always close to 1: the constraint is adhered to, and active. Furthermore, it is noticed that the two buckling loads get close to each other, and sometimes even become exactly the same. This demonstrates the need to consider the first two buckling loads since the optimal design is bimodal. Had only one buckling load been considered, the buckling mode would have oscillated preventing convergence[128].

Table 6.1: Overview of the results using different local steering constraints.

upper bound on local steering $[\text{m}^{-1}]$	optimal normalised buckling load 1 [-]	optimal normalised buckling load 2 [-]	optimal normalised stiffness [-]	difference w.r.t. optimal stiffness distribution
1	1.3731	1.3735	1.0012	- 38.8%
2	1.5749	1.5752	1.0005	- 29.8%
3	1.7474	1.7474	1.0008	- 22.1%
4	1.8846	1.8852	1.0010	- 16.0%
5	1.9830	1.9835	1.0007	- 11.6%

When even tighter turning radii are permitted, one can plot the Pareto front that shows manufacturability versus performance. The performance is represented by the buckling load in this example. Manufacturability is represented by the turning radius: the smaller the turning radius, the higher the expected manufacturing time and cost are. Fewer tows can be laid down in one go when a smaller turning radius is required, or smaller tows have to be used, meaning the number of passes from the machine, resulting in increased manufacturing time. The steering constraint was always active, even for these lower bounds on the turning radius, . The Pareto front can be seen in Figure 6.3.

When observing the Pareto front, it stands out that it is not convex which is typical of the highly non-convex buckling optimisation problem. In the first region, roughly between a minimum turning radius of 1000 and 400 mm, a relatively large improvement in the buckling load as a consequence of the decrease in minimal turning radius can be seen. For even tighter turning radii, the structural improvement is less significant when the minimal turning radius is decreased.

The optimum in terms of the fibre angles does seem to converge towards the optimum found in terms of the lamination parameters for the smallest steering radii computed. This implies that the fibre angle optimisation is working well: it always obeys the constraints and, although it will always find a local optimum, it does approach to the global optimum found in terms of the lamination parameters as the manufacturing constraints are relaxed.

6.3.2 INFLUENCE OF GLOBAL STEERING CONSTRAINTS

While the local steering constraint makes sure the optimised laminate can be manufactured, it does not take into account the number of gaps and overlaps. As explained in section 6.1 the location and size of the gaps and overlaps cannot be taken into account exactly, but by formulating the global steering constraint the total area of gaps and overlaps is constrained.
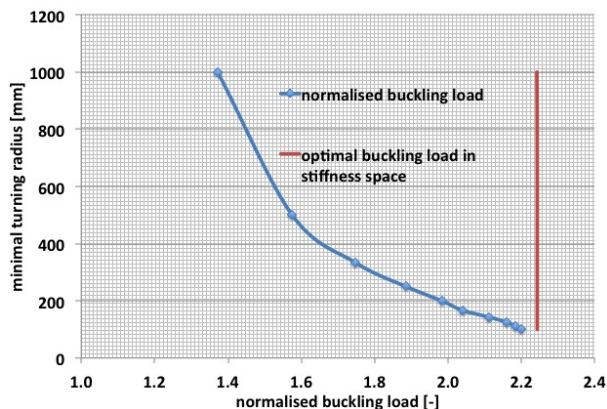
Figure 6.3: Normalised buckling load versus the minimum steering radius.

To assess the influence of the global steering constraint, the upper bound on local steering is fixed to 4m^{-1}, corresponding to an equivalent lower bound on the turning radius of 250 mm, which is an optimistic limit when using AFP, but reasonable for purposes of demonstration. The upper bound on global steering is changed from 0.01m^{-1}, which means that almost no steering is allowed leading to a more traditional CSL, to 4m^{-1}, meaning the lower bound on turning radius is allowed everywhere. The results can be seen in Table 6.2, where the upper bound on local steering is shown in column one, the optimal buckling load in columns two and three, the stiffness in column four, and the difference with respect to the optimum in terms of the lamination parameters is shown in the last column. Analogous to the local steering constraints, the global steering constraint was always active, except when the upper bound on local and global steering were the same.

Observing the results, it is noted that, analogous to the local steering constraint, the larger the upper bound on global steering, the higher the buckling load. Again the first two buckling loads are very close to each other. The stiffness constraint is always satisfied, and almost always active. For the upper bound on global steering of 0.01 m^{-1}, the stiffness constraint is not active, which is probably due to the relatively limited options the optimiser has: effectively, only one fibre angle per layer can be chosen, meaning the stiffness cannot be relaxed further without decreasing the buckling load.

It is interesting to note that the results with an upper bound on local steering of 4m^{-1} and an upper bound on global steering of $1, 2$ and 3m^{-1} are slightly better $(2-3.6\%)$ than the results when using only an upper bound on local steering of $1, 2$ and 3m^{-1}. This is due to the better local load redistribution: close to the supported edges steering is not as effective. This implies more gain can be

Table 6.2: Overview of the results using different global steering constraints.

upper bound on global steering $[\mathrm{m}^{-1}]$	optimal normalised buckling load 1 [-]	optimal normalised buckling load 2 [-]	optimal normalised stiffness [-]	difference w.r.t. optimal stiffness distribution
0.01	1.2132	1.2132	1.1067	- 45.9%
0.5	1.2888	1.2888	1.0011	- 42.6%
1	1.3992	1.3999	1.0011	- 37.6%
1.5	1.5192	1.5196	1.0007	- 32.3%
2	1.6330	1.6333	1.0007	- 27.2%
2.5	1.7436	1.7441	1.0006	- 22.3%
3	1.8034	1.8046	1.0005	- 19.6%
3.5	1.8467	1.8481	1.0013	- 17.7%
4	1.8846	1.8852	1.0010	- 16.0%

obtained by highly steering at places away from the edges and low steering close to the edges than by steering everywhere moderately.

6.4 INFLUENCE OF THE RETRIEVAL-OPTIMISATION ALGORITHM

The results shown in the previous section were obtained using the fibre angle optimisation algorithm. As was discussed in section 4.6, performing a retrieval step to try to match the optimal lamination parameters and starting the optimisation from that fibre angle distribution could lead to a higher computational efficiency. One possible advantage is that the final performance is less dependent on the initial guess, since the approximation used is not dependent on the initial guess. Another possible advantage is that the number of FEAs would be reduced compared to only using fibre angle optimisation: the outcome of the retrieval should be close to the optimum, requiring few FEAs to converge to an optimised solution. Another question that is still open is whether performing full optimisation after the retrieval step leads to considerable improvement. In this section two examples are presented: first the buckling optimisation of the previous section is revisited, then a strength optimisation is performed to answer these questions.

6.4.1 BUCKLING OPTIMISATION

A gradient-based optimiser may always get stuck in a local optimum. The only practical way to improve the likelihood of reaching the global optimum is starting from multiple initial guesses. In the retrieval step, section 4.6, the initial approximation is created around the continuous optimum and is not dependent on the initial guess. Thus it is expected that the optimised design should be (almost) the same regardless of the initial fibre angle distribution. For the same optimisation problem as in the previous section, three choices of the initial fibre angles are defined: all angles equal to 1°, all equal to 10°, and all equal to 20°. No larger angles were checked since the compliance constraint would not be satisfied, and the initial guess has to satisfy all constraints. To check the convergence history, the result after each fibre angle update is saved and an FEA is performed. The level one approximation is not updated. The lowest buckling load after each iteration can be seen in Figure 6.4.

Observing the results, it is noted that the final designs are close to each other, although the convergence history is different. The different convergence history is expected since the starting point is different. The same performance at the end indicates that the influence of the initial guess, at least for this case, is negligible. When observing the results in more detail, it is observed that the performance is not monotonously improving. This is because the criterion to accept a new fibre angle distribution is that the level one approximation has to improve, the FE response is not checked. A final note to be made is that the number of level two iterations for the different starting points differs significantly, from 8 to 17. However, the computational cost of building a level two approximation is negligible compared to performing an FEA, so in all cases the retrieval step is ran until convergence.
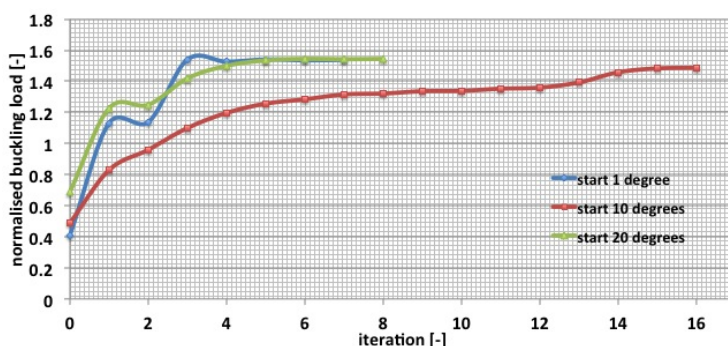

Figure 6.4: FE response after each level 2 optimisation (during fibre angle retrieval).

Since the performance after retrieval is independent of the initial guess, one may think that this is the optimal fibre angle distribution, and that the optimisation

step can be skipped. The same problem is solved with multiple values for the upper bound on local steering to verify whether the optimisation step leads to an improvement. The lowest buckling load after retrieval and after optimisation are shown in Table 6.3. The first column shows the maximum local steering, the lowest buckling load after retrieval and optimisation is shown in columns two and three respectively, the number of FEAs needed is shown in column four, and the difference obtained due to optimisation is shown in the last column. As previously seen, the steering constraint is always active.

Table 6.3: Overview of the results using different local steering constraints.

maximum local steering $[\mathrm{m}^{-1}]$	optimal normalised buckling load after fibre angle retrieval [-]	optimal normalised buckling load after optimisation [-]	number of FEAs	difference w.r.t. optimum after fibre angle retrieval
1	1.1210	1.3731	4	+ 22.5 %
2	1.2894	1.5749	5	+ 22.1 %
3	1.4867	1.7474	5	+ 17.5 %
4	1.6024	1.8846	4	+ 17.6 %
5	1.7550	1.9830	5	+ 13.0 %

Observing the results in Table 6.3, it is noted that performing optimisation leads to significant improvements while using a limited number of FEAs. The improvement is most likely due to the locations where the optimal lamination parameters have a steep gradient. Since the change in fibre angles is limited by the steering constraint, the match between the fibre angle distribution and the optimal lamination parameters distribution is bad in these regions. During the full optimisation, the fibre angle distribution is tailored to maximise performance directly rather than marginally improving a bad match with the optimal lamination parameters. The improvement due to the optimisation generally gets less and less for higher steering values. This is because the retrieval step performs better for higher steering values: the change in fibre angles can be larger and thus the optimal lamination parameters are more closely matched. Hence, the difference between the 'bad' match and the optimal distribution is reduced.

Computational efficiency is expected to increase when using the retrieval-optimisation algorithm rather than only optimisation. the number of FEAs, , which the largest computational cost, is expected to decrease. This is verified by performing the same optimisation as in the previous section for different starting angles with an upper bound on the local steering of $3\mathrm{m}^{-1}$. Table 6.4 shows the initial fibre angles in the first column, the optimal buckling load, and number of FEAs without and with the retrieval step in the second to fifth column.

Observing the results in Table 6.4, it is noted that the number of finite element analyses does decrease significantly by performing the retrieval step before the fibre angle optimisation. In most cases the number is almost halved. This is what was expected: before the first FEA is done, the fibre angle distribution is already optimised in the retrieval step, hence, only some fine-tuning needs to be done rather than completely starting from all straight fibres. The limited number of FEAs is due to the algorithm, it is not linked to the steering bound. This is clear from the number of FEAs needed for different upper bounds on steering in Table 6.3. The optimised buckling load is never exactly the same, but the difference is smaller than 1%, which can be attributed to the gradient-based optimisation finding a somewhat different local optimum.

Table 6.4: Overview of the results using different initial sensitivities.

initial fibre angles [deg]	optimal normalised buckling load without fibre angle retrieval [-]	number of FEAs without fibre angle retrieval	optimal normalised buckling load with fibre angle retrieval [-]	number of FEAs with fibre angle retrieval
0.1	1.7574	14	1.7696	8
1	1.7620	21	1.7671	5
10	1.7608	13	1.7486	8
20	1.7628	11	1.7645	5

6

6.4.2 STRENGTH OPTIMISATION

The second example problem is a problem previously solved by Khani et al.[78]. A plate with a circular cut-out loaded in uni-axial tension is optimised for strength. The plate is 400 by 400 mm, with a large circular cut-out with a diameter of 200 mm at the centre. The plate is simply supported all around, with all edges constrained to remain straight. A graphical representation can be seen in Figure 6.5. After taking symmetry into account, the plate was discretised into 217 triangular elements with 132 nodes. The material stiffness properties are: $E_1 = 142.9GPa$, $E_2 = 10.3GPa$, $G_{12} = 7.2GPa$, and $\nu_{12} = 0.27$. The failure is defined using the conservative omni-strain envelope[60,78,148]. The load is chosen such that the QI design has a minimum factor of safety of 1. The total laminate has 24 layers resulting in a thickness of 4.6 mm. As in the previous example, the laminate is designed to be balanced and symmetric, leading to 6 design layers.

When performing the optimisation in terms of the lamination parameters, the optimal design has a minimum factor of safety of 1.944. The optimisation is
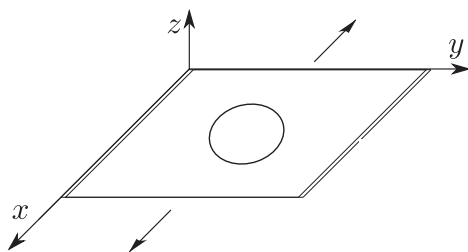
Figure 6.5: Load case and boundary conditions for the strength optimisation.

performed for different upper bounds on the local steering, global steering is not constrained. The values range from 0.01m^{-1}, representing a CSL, to 3m^{-1}, which is close to the highest steering possible using AFP. The results are shown in Table 6.5, where the local steering constraint is shown in the first column. The maximum failure index after angle retrieval and after optimisation are shown in the second and third column, the fourth column gives the number of FEAs needed to get to the optimum, the difference from angle retrieval due to full optimisation is shown in column five, the last column indicates the difference with respect to the optimal stiffness distribution.

Observing the results in Table 6.5, it is noted that the retrieval step is not as effective for strength as it is for buckling. The improvement due to the optimisation is significantly larger than in the previous example. This is probably due to the extreme gradients in the optimal lamination parameters close to the cut-out as can be seen in Figure 6.6. At this location lamination parameters matching does not perform well, and thus a lot of improvement can be made during fibre angle optimisation. Another difference is that the computational efficiency is not as high: this time $10 - 15$ FEAs are necessary while for the previous problem around 5 FEAs were needed. This is again due to the bad match during the retrieval step. Only for a local steering of 0.01m^{-1}, the number of FEAs is lower, probably because effectively one fibre angle per layer needs to be chosen, hence the number of design variables is lower and the optimisation converges faster.

What stands out in the results in Table 6.5 is that the difference between the optimal performance found with the different upper bounds on steering and the performance using the optimal lamination parameters is small. Even with a steering of 1m^{-1}, meaning a minimum turning radius of 1000 mm, the strength is only 7% worse than for the optimal lamination parameters. The performance increase due to higher steering values is limited, certainly when comparing to the previous example. This is probably due to the few places where steering is used: the load has to be redirected from the hole, which apparently is already possible using a steering of 1m^{-1}. Increasing the steering further improves the strength a bit, but it probably will not be worth the additional manufacturing cost.

Table 6.5: Overview of the results using different local steering constraints.

maximum local steering [m^{-1}]	minimum factor of safety after fibre angle retrieval [-]	optimal factor of safety [-]	number of FEAs	difference w.r.t. optimum after fibre angle retrieval	difference w.r.t. optimal stiffness distribution
0.01	1.288	1.578	4	+ 22.5 %	- 18.8 %
1	1.345	1.811	10	+ 34.6 %	- 6.8 %
2	1.357	1.830	12	+ 34.9 %	- 5.9 %
3	1.395	1.869	15	+ 34.0 %	- 3.9 %

For this example, the lamination parameter distribution is interesting to examine. Since the strength is only dependent on the in-plane stiffness matrix, only the in-plane lamination parameters V are of interest. Furthermore, the laminate is balanced, thus V_2 and V_4 are zero, leaving only V_1 and V_3. In Figure 6.6 V_1 and V_3 are shown after stiffness optimisation, fibre angle retrieval and fibre angle optimisation for an upper bound on steering of 3m^{-1}. Observing the lamination parameters, the previous conclusions are supported: after fibre angle retrieval, the lamination parameter distribution is not even close to the optimal lamination parameter distribution. The reason can be seen in the plot of the optimal lamination parameter distribution: it shows a strong variation, steep gradients that cannot be matched, making it difficult to achieve the optimum stiffness variation during the angle retrieval step.

The optimum in terms of lamination parameters and fibre angles is considerably different at places. This illustrates a drawback of the lamination parameter optimisation: it only looks for the optimum without paying any attention to the gradient of the design. It is also very interesting to see that two structures with such different lamination parameters distributions have a performance that is within 4% of each other. This shows that in this case the local changes that are found during lamination parameter optimisation only have a small effect on the overall performance.

(a) V_1 distribution for optimal stiffness.

(b) V_3 distribution for optimal stiffness.

(c) V_1 distribution after fibre angle retrieval step for maximum local steering of $3\mathrm{m}^{-1}$.

(d) V_3 distribution after fibre angle retrieval step for maximum local steering of $3\mathrm{m}^{-1}$.

(e) V_1 distribution after fibre angle optimisation for maximum local steering of $3\mathrm{m}^{-1}$.

(f) V_3 distribution after fibre angle optimisation for maximum local steering of $3\mathrm{m}^{-1}$.
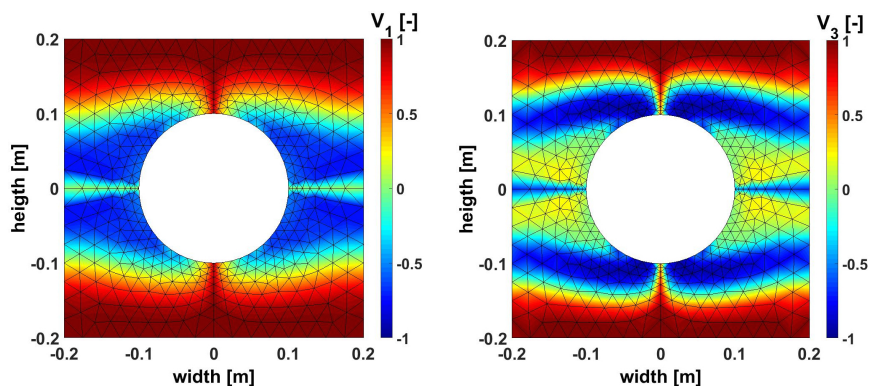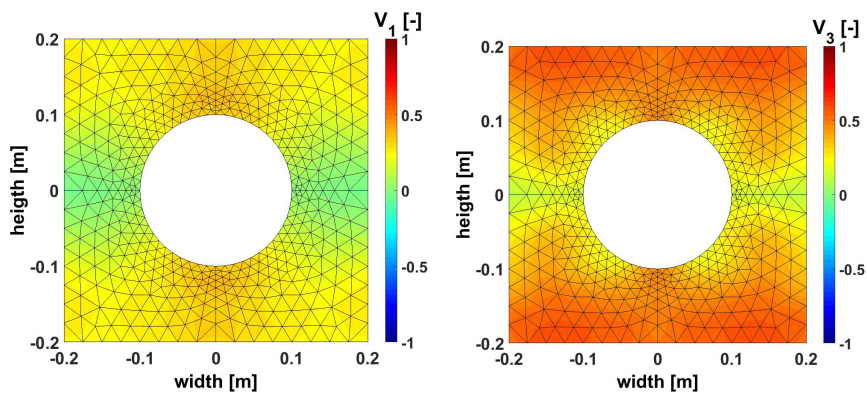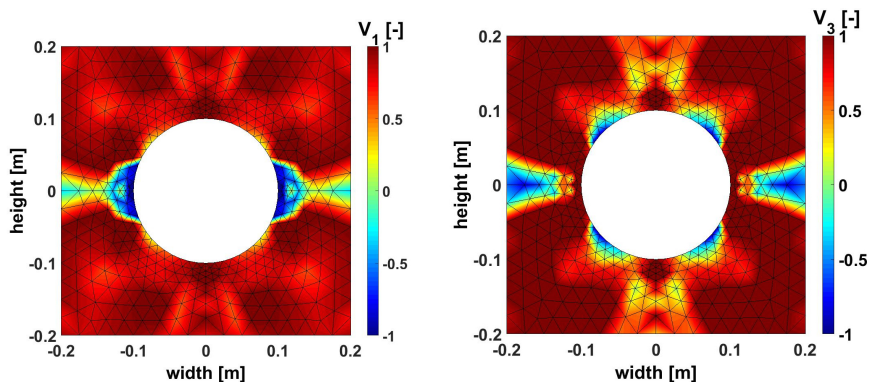
Figure 6.6: In-plane lamination parameters for different cases.

The only source of knowledge is experience.
Albert Einstein

7

DESIGN GUIDELINES FOR NON-CONVENTIONAL LAMINATES

While the previous chapter focused on the manufacturability of the optimised design, this chapter focuses on its (industrial) feasibility. The aerospace industry has a lot of experience with conventional laminates, with plies from a limited set, usually consisting of $0°$, $\pm 45°$, and $90°$. Design guidelines have been formulated for these laminates, based on different reasons. For example, the laminate should be symmetric based on experience with manufacturing, the outer layers should be $\pm 45°$ fabric plies based on experience with impact (and for stability)[9,10], and the 10% rule was proposed based on experience with secondary failure modes. A more complete overview of the design guidelines that exist for conventional laminates related to the stacking sequence is given in section 7.1. Since a lot of experience, that cannot be quantified, is encapsulated in the design guidelines, it is worthwhile to try and interpret them in such a way that they can be posed as constraints in the proposed gradient-based optimisation algorithm. By taking the design guidelines into account during the optimisation, the experience that has been accumulated over decades is taken into account and the optimised designs will be more easily accepted by industry; it could be a step towards certification of non-conventional laminates.

This chapter is based on the journal paper 'Design Guidelines in Nonconventional Composite Laminate Optimization'[116].

The design guidelines are split up into three categories for implementation in the optimisation. The first category are the guidelines that can be interpreted as bounds on fibre angles, the second category is the 10% rule, the third category can be implemented without explicitly posing them as constraints in the optimisation but instead by properly choosing the design variables. For example, having $\pm 45°$ layers on the outside is done by defining the outer layers as being $\pm 45°$ and excluding them from the optimisation. Two different bounds on fibre angles exist: the fibre angle itself can be constrained to not be too close to $0°$ or $90°$, or the difference between the fibre angles of adjacent layers can be constrained. The bounds on the difference between adjacent layers has multiple reasons: it should not be too low to stop crack growth, and it should not be too high to avoid large interlaminar stresses. The bounds on fibre angles are discussed in section 7.2. The 10% rule cannot be posed as a ply-count rule in the optimisation: it would prescribe at least 40% of the layers and be too restrictive. Instead, it is interpreted as a lower bound on degree of isotropy [6] and posed as a positive semi-definite constraint during the optimisation. This is discussed in detail in section 7.3. The last category of design guidelines, the ones that are not posed as constraint, are discussed in section 7.4. The optimisation with the different design guidelines as constraints is discussed in section 7.5. Finally, the influence of the design guidelines is assessed for CSL performing a strength optimisation of a bi-axially loaded square plate, and for VSL performing a buckling optimisation of a uni-axially loaded rectangular plate. These results are discussed in section 7.6.

7.1 DESIGN GUIDELINES FOR CONVENTIONAL LAMINATES

7

As mentioned in section 1.3, dispersed and APPLY laminates improve post-impact behaviour compared to conventional laminates. Hence, it is worth taking requirements for these two configurations into account as design guidelines. These design guidelines can be formulated as

1. For APPLY laminates each pair of interwoven layers is balanced (i.e., in the form $\pm\theta$). An upper and lower bound on the fibre angle is imposed to ensure the unit cell is not too large.

2. For dispersed laminates a lower bound on the difference between adjacent fibre angles is imposed.

Besides these constraints for specific NCL, industry uses constraints on the stacking sequence. The following list is based on the work by Beckwith [10] and a NASA report [9]:

3. The ply contiguity rule, which enjoins the designer to avoid stacking too many plies, usually the limit is set to 4, with the same fibre angle next to each other.

4. Minimise the difference between adjacent fibre angles. If this is not done, the chance of delaminations increases and residual stresses are more likely.

5. The 10% rule, which states that 10% of the plies has to be in 0°, 45°, 90° and −45° direction. This makes sure the laminate is not too anisotropic and has at least some resistance against longitudinal (0°), transverse (90°) and shear loading (±45°). This will also reduce the free-edge stresses and avoid micro-cracking.

6. A laminate should be symmetric about its middle surface. This avoids extension-bending coupling, in other words: the B-matrix is zero.

7. The balance constraint which states that 45° layers should be added in pairs (i.e., with a −45° layer).

8. Put the 45° and −45° layer in contact with each other to minimise inter-laminar shear.

9. Add a fabric layer to the inner or outer layer to improve impact damage resistance.

10. Add ±45° layers on the outside. This improves the buckling resistance and has a better damage tolerance.

11. Maintain a homogeneous stacking sequence by banding several plies of the same orientation together.

12. Keep a reasonable number or primary load-carrying plies away from the outer surfaces. This rule avoids impact damage on the outside to be critical for the primary load-carrying capability.

More guidelines, related to thermal effects, bonding and bolted joints exist, but these guidelines are not mentioned here because these are not used in the current work.

7.2   BOUNDS ON FIBRE ANGLE AND ANGLE DIFFERENCE

Multiple guidelines can be implemented as bounds on fibre angle and angle difference. First, the bounds on the fibre angle exist due to APPLY, rule 1: since the balanced layers are next to each other, the fibre angle should not be too close to 0° or 90° to avoid the unit cell becoming too large. Dispersed laminates, rule 2,

are based on a lower bound on the difference between adjacent fibre angles. The ply contiguity rule, rule 3, is taken into account using the lower bound on the difference between adjacent fibre angles as well. Effectively, the limit of plies with the same orientation next to each other is set to one. This is possible because the set of fibre angles is no longer limited and having the same fibre angle next to each other can be avoided completely. Finally, the rule to minimise the fibre angle difference, rule 4, is interpreted as an upper bound on the difference between adjacent fibre angles. All bounds (upper and lower bound on fibre angle and angle difference) have a similar formulation. Only the formulation of the upper bound on angle difference is derived in this section, the other constraints have a similar form and are shown without derivation.

The difference between fibre angles of adjacent layers cause interlaminar stresses. These occue due to the mismatch in stiffness properties between the layers. According to Herakovich[54], the two most important properties are the Poisson's ratio ν and the coefficient of mutual influence η, defined as

$$\nu_{xy} \quad = \quad \frac{-\epsilon_y}{\epsilon_x} = \frac{a_{12}}{a_{11}} \tag{7.1}$$

$$\eta_{xy,x} \quad = \quad \frac{\gamma_{xy}}{\epsilon_y} = \frac{a_{16}}{a_{11}}, \tag{7.2}$$

where **a** is the inverse of the in-plane stiffness matrix **A**. Using $E_1 = 181\text{GPa}$, $E_2 = 11.3\text{GPa}$, $G_{12} = 7.17\text{GPa}$ and $\nu_{12} = 0.28$ as material data, the plots of the Poisson's ratio and the coefficient of mutual influence as a function of the fibre angle were made. These are shown in Figure 7.1.

(a) η.   (b) ν.
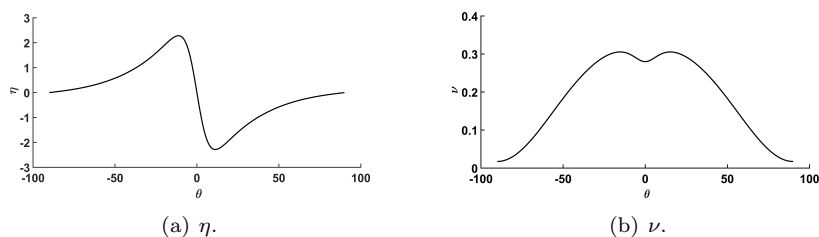
Figure 7.1: η and ν as a function of the fibre angle.

To estimate the interlaminar stresses occurring, the difference of η and ν between different layers is important. Observing Figure 7.1, it can be seen that the difference will be dependent on both angles, not just on the difference. Hence, to plot the difference, multiple lines are plotted in the same figure varying the average angle from 0° to 90° in steps of one degree, and for each average angle, a plot is made of the change in η and ν as a function of the angle difference. The plots with the difference are shown in Figure 7.2. Observing this figure, the difference in η is very large for a relatively small difference in fibre angle, with a maximum for a

difference of around $20°$, hence if the change in η was to be limited, the constraint would be very restrictive. Hence, the upper bound on difference in fibre angle is determined by the difference in Poisson's ratio ν. Observing this difference in Figure 7.2(b), it is noticed that the upper bound can be fairly well captured using a sine squared function. Thus, a constraint is proposed in the form of

$$(\sin(\theta_k - \theta_{k+1}))^2 \le (\sin(\Delta\theta_u))^2 , \tag{7.3}$$

where k and $k+1$ denote the layer of the laminate, and θ_u is user-defined, based on the material used. An extra advantage of the sine squared-formulation is that the constraint value for an angle of $89°$ and $-88°$ comes out small (and hence the constraint is satisfied) without the need to have an extra check (Note that $90°$ and $-90°$ are essentially the same fibre orientation).

(a) $\Delta\eta$.　　　(b) $\Delta\nu$.
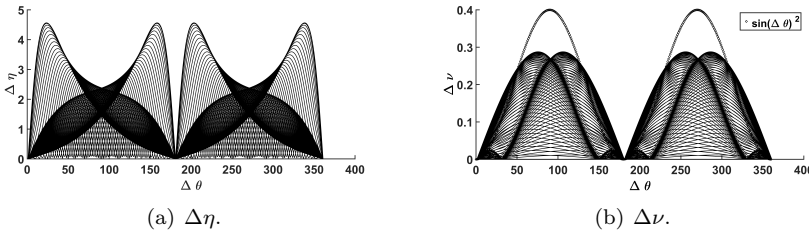
Figure 7.2: Difference in η and ν as a function of the change in fibre angle.

Analogous to the upper bound on the difference between angles, the other three bounds are formulated as

$$
\begin{aligned}
\text{lower bound on angle difference:} \quad & (\sin(\theta_k - \theta_{k+1}))^2 \ge (\sin(\Delta\theta_l))^2 \\
\text{upper bound on angle:} \quad & (\sin(\theta_k))^2 \le (\sin(\theta_u))^2 \\
\text{lower bound on angle:} \quad & (\sin(\theta_k))^2 \ge (\sin(\theta_l))^2 .
\end{aligned} \tag{7.4}
$$

7.3   10% RULE

Implementing the 10% rule as stated in section 7.1 is not easy in the context of NCL design. When using a limited set of fibre angles, having a minimum number of layers in $0°$, $45°$, $90°$, and $-45°$ can be relatively easily enforced. However, in the current optimisation, the fibre angle is a continuous variable, making it hard to enforce angles of exactly $0°$, $90°$, and $\pm45°$ in the optimisation. Furthermore, the 10% rule prescribes at least 40% of the layers, considerably limiting the design space. Hence, it will be interpreted in a wider sense to allow it to be used in a gradient-based optimisation as constraint. Generally, the rule is referred to as 10% rule, but other values are also possible for the minimum number of layers for

each orientation, depending on the position in the structure. Hence, from now on the rule will be referred to as ply-count percentage rule.

The ply-count percentage rule can be seen as a ratio of the laminate having to be quasi-isotropic. Using this idea, the rule can be reformulated as a bound on an eigenvalue problem, as has been done by Abdalla et al.[6]. This interpretation has been used to replace the ply count-based rule even in the context of CL[65]. The advantage of this interpretation is that it is continuous, thus it can be used in a gradient-based optimiser. Disadvantage is that the dispersion of the plies is no longer guaranteed, which can be (partly) counter-acted by the lower bound on the fibre angle difference.

According to Abdalla et al.[6], the 10% rule can be written as a constraint on the minimum eigenvalue of the problem[6]:

$$\mathbf{A} : \epsilon = \gamma \bar{\mathbf{A}} : \epsilon, \tag{7.5}$$

where ϵ is the in-plane eigen-strain vector, and $\bar{\mathbf{A}}$ is the quasi-isotropic A-matrix of an arbitrary in-plane stiffness matrix $\mathbf{A}$, defined as

$$\bar{\mathbf{A}} = \begin{bmatrix} \bar{A}_{11} & \bar{A}_{12} & 0 \\ \bar{A}_{12} & \bar{A}_{11} & 0 \\ 0 & 0 & \bar{A}_{66} \end{bmatrix}, \tag{7.6}$$

with

$$\bar{A}_{11} = \frac{3A_{11} + 3A_{22} + 2A_{12} + 4A_{66}}{8} \tag{7.7}$$

$$\bar{A}_{12} = \frac{A_{11} + A_{22} + 6A_{12} - 4A_{66}}{8} \tag{7.8}$$

$$\bar{A}_{66} = \frac{A_{11} + A_{22} - 2A_{12} + 4A_{66}}{8}. \tag{7.9}$$

The degree of isotropy of the laminate is given by the minimum eigenvalue γ_{min}: the laminate is considered robust if

$$\gamma_{min} \geq \alpha. \tag{7.10}$$

The lower bound on α depends on the minimum percentage in ply count p, and on the material used. For carbon fibre materials the conversion is given by[6]

$$1 - \alpha = \frac{5}{6}(1 - 4p), \tag{7.11}$$

where the fraction $\frac{5}{6}$ is only valid for a whole range of carbon composites, but not for glass fibre composites for example. For the traditional 10% rule $p = 0.1$ which corresponds to $\alpha = 0.5$. The eigenvalue constraint can be rewritten as a semi-definite matrix constraint:

$$(\mathbf{A} - \alpha \bar{\mathbf{A}}) \succeq 0. \tag{7.12}$$

Using the Cholesky product: $\bar{\mathbf{A}} = \mathbf{L} \cdot \mathbf{L}^T$, $\mathbf{X}$ can be defined as

$$\mathbf{X} = \mathbf{L}^{-1} \cdot \mathbf{A} \cdot \mathbf{L}^{-T}, \tag{7.13}$$

and the constraint on positive semi-definiteness can be written as

$$\mathbf{X} - \alpha \cdot \mathbf{I} \geq 0. \tag{7.14}$$

7.4   OTHER DESIGN GUIDELINES

The guidelines that have not yet been discussed do not require constraints on the stacking sequence. Some are hard-coded in the optimisation, others are options. How each guideline can be adhered to is discussed in this section.

The following options define how the *design layers* are related to the actual lay-up:

- the symmetric constraint, rule 6, is hard-coded: every laminate is symmetric. Only half the stack, the design layers are optimised and mirrored to obtain the complete laminate.

- the balance constraint, rule 7, and setting the $\pm 45°$ pair next to each other, rule 8, can be implemented by changing the way design layers describe the laminate. If a laminate is to be balanced the design layers $[\theta_1/\theta_2]$ describe the laminate $[\theta_1/-\theta_1/\theta_2/-\theta_2]_S$, meaning a negative fibre angle is added, and if an angle is $45°$, the adjacent angle is $-45°$.

- adding a fabric layer on the outside, rule 9, can be done by defining a fabric layer in the initial guess and removing this layer from the optimisation. Hence, the design layers $[\theta_1/\theta_2]$ describe the laminate $[\text{fabric}/\theta_1/-\theta_1/\theta_2/-\theta_2]_S$, assuming the laminate is also balanced.

- adding the $\pm 45°$ layers on the outside, rule 10, can be done in the same way as the fabric layer: by defining the outer layer(s) and removing them from the optimisation. This means that the design layers $[\theta_1/\theta_2]$ describe the laminate $[45°/-45°/\theta_1/-\theta_1/\theta_2/-\theta_2]_S$, assuming the laminate is to be balanced as well.

The homogeneity rule, rule 11, which states several plies of the same orientation should be bunched together is not implemented. When only four different orientations are possible, from a certain number of plies it is unavoidable to have plies with the same direction. When this happens, the question whether or not to group them arises. Sometimes grouping is unavoidable: if 70% of the layers is in $0°$ direction, and 10% in the other three directions, some $0°$ plies have to be stacked together. However, in this work the orientation is continuous, so having plies of the same orientation next to each other can be avoided all together, hence the need for this rule does not arise. Furthermore, this rule directly contradicts the idea of dispersed laminates, rule 2.

Finally, rule 12, which states that a reasonable number of primary load-carrying plies should be kept away from the outer surfaces is not implemented. This has two reasons. One, the outer surface can already be defined if wanted: depending on the load case, a $\pm 45°$ ply is usually not considered to be a primary load-carrying ply, hence defining it on the outside can be done. Two, this rule relies

on engineering judgement: it cannot be formulated as a constraint which plies are load-carrying without knowledge of the structural optimization problem. The idea behind the rule, which is improving the impact-resistance, is implemented using the dispersed and/or APPLY laminates.

7.5 OPTIMISATION PROCEDURE WITH DESIGN GUIDELINES

Two different types of constraints appear when implementing the design guidelines: one, functional constraints, based on the bounds on angle and angle difference, eqs. (7.3)-(7.4), two, the positive semi-definite matrix constraint, based on the ply-count percentage rule, eq. (7.14). To keep the derivation as simple as possible and focus on the design guideline constraints, a single-response optimisation without constraints on structural performance is considered:

$$
\begin{aligned}
\min_{\mathbf{x}} \quad & f \\
s.t. \quad & \mathbf{X} - \alpha \cdot \mathbf{I} \geq 0 \\
& g\left(\theta_k, \theta_{k+1}\right) \quad k = 1, ..., n-1 \\
& h\left(\theta_k\right) \quad k = 1, ..., n.
\end{aligned}
\tag{7.15}
$$

The functions g and h are linearised. The linearised versions are referred to as $\hat{g}$ and $\hat{h}$. $\mathbf{X}$ can be approximated as

$$
\mathbf{X} = \mathbf{X}_0 + \sum_{i=1}^{L} \mathbf{X}_i x_i,
\tag{7.16}
$$

where $\mathbf{X}_i$ is defined as

$$
\mathbf{X}_i = \mathbf{L}^{-1} \cdot \frac{\partial \mathbf{A}}{\partial x_i} \cdot \mathbf{L}^{-T}.
\tag{7.17}
$$

A slack variable and a damping function, to guarantee global convergence, are added to both constraints:

$$
\begin{aligned}
\min_{\mathbf{x}} \quad & f + \zeta_1 d_1(x) \\
s.t. \quad & \mathbf{X}_0 + \sum_{i=1}^{L} \mathbf{X}_i x_i - \alpha \cdot \mathbf{I} - \zeta_2 \cdot d_2(x) \cdot \mathbf{I} - \mathbf{Z} = \mathbf{0} \\
& \hat{g}\left(\theta_k, \theta_{k+1}\right) + \zeta_3 \cdot d_{(3k)}(x) + s_g = 0 \quad k = 1, ..., l-1 \\
& \hat{h}\left(\theta_k, \theta_{k+1}\right) + \zeta_4 \cdot d_{(4k)}(x) + s_h = 0 \quad k = 1, ..., l-1 \\
& \mathbf{Z} \geq 0 \\
& s_g \geq 0 \\
& s_h \geq 0.
\end{aligned}
\tag{7.18}
$$

The damping functions are defined as

$$
d_2 = \Delta\theta \left(\frac{1}{n_l^2} \begin{bmatrix} 1 & -1 & & & \\ -1 & 2 & -1 & & \\ & \ddots & \ddots & & \\ & & -1 & 2 & -1 \\ & & & -1 & 1 \end{bmatrix} + \alpha \begin{pmatrix} 1 & \cdots & 1 \\ \vdots & \ddots & \vdots \\ 1 & \cdots & 1 \end{pmatrix} \right) \cdot \Delta\theta^T
$$

$$
d_{(3k)}(x) = \frac{(\Delta\theta_k - \Delta\theta_{k+1})^2}{2} \tag{7.19}
$$

$$
d_{(4k)}(x) = \frac{(\Delta\theta_k)^2}{2}.
$$

The Lagrangian is found to be

$$
\begin{aligned}
\mathcal{L} \;=\; & f(x) + \zeta_1 d_1(x) - \mathbf{Y} : \left(\mathbf{X}_0 + \sum_{i=1}^{L} \mathbf{X}_i x_i - \alpha \cdot \mathbf{I} - \zeta_2 d_2(x) \cdot \mathbf{I} - \mathbf{Z} \right) - \\
& \mu ln\left(det(\mathbf{Z}) \right) + \sum_k \lambda_k \cdot \left(\hat{g} + \zeta_3 d_{(3k)}(x) + s_{g_k} \right) + \mu \cdot ln(s_{g_k}) + \\
& \sum_k \gamma_k \cdot \left(\hat{h} + \zeta_4 d_{(4k)}(x) + s_{h_k} \right) + \mu \cdot ln(s_{h_k}),
\end{aligned} \tag{7.20}
$$

where $\mathbf{Y}$, λ_k, and γ_k denote Lagrangian multipliers. The solution procedure is explained in Appendix B.

7.6 RESULTS

To assess the influence of the different constraints, two examples will be used: a strength optimisation for a CSL and a buckling optimisation for a VSL. In both examples, the starting point has to be feasible, since the proposed interior point method is designed to conserve feasibility. The influence of the ply-count percentage rule, and of the bounds on the fibre angles and angle difference is investigated for the CSL. Only the influence of the ply-count percentage rule is investigated for the VSL. The results are obtained using only fibre angle optimisation, no retrieval or LP optimisation is performed.

7.6.1 CONSTANT STIFFNESS LAMINATES

A strength optimisation is performed for CSLs. The model is a square panel with sides of 500 mm, simply supported all around, and with the edges constrained to remain straight. The plate is loaded under bi-axial tension N_x and N_y. A graphical representation can be seen in Figure 7.3. The material used has the

following properties: $E_1 = 154$GPa, $E_2 = 10.8$GPa, $G_{12} = 4.02$GPa, $\nu_{12} = 0.317$, $t_{ply} = 0.6$mm. The laminate consists of 36 layers, and is balanced and symmetric, such that 9 design layers are optimised. Failure is defined using the conservative omni-strain envelope[60,78,148]. The factor of safety, which is the inverse of the failure index, is normalised with respect to a quasi-isotropic laminate, defined as all lamination parameters equal to zero.
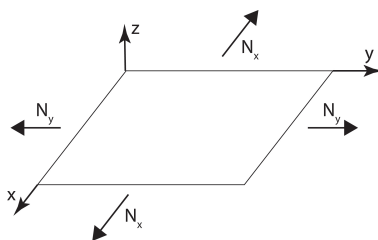
Figure 7.3: Sketch of the plate loaded in tension.

INFLUENCE OF THE PLY-COUNT PERCENTAGE RULE

The influence of the ply-count percentage constraint, or 10% rule, is investigated: different values for the ply-count percentage are checked, without any bound on the fibre angles or angle difference. Only one ratio of the loads is optimised: $N_y/N_x = 1/6$. First, the optimisation is performed without the ply-count percentage constraint. The optimal laminate then has a ply-count percentage of 3.67% and a factor of safety of 2.72. This was back-calculated from the value found for γ. Next, the optimisation is repeated for values of the ply-count percentage from 4 to 16%. The normalised factor of safety for both conventional and non-conventional laminates is shown in Figure 7.4. The conventional design is found by enumeration: the performance of all conventional designs and selecting the best one. Since the factor of safety is optimised, only the in-plane stiffness matrix has an influence on the performance of the structure, meaning only the number of layers with a certain orientation is important, not their location in the stack. This means enumeration can be done by checking a limited number of options, such that the global optimum is found for the conventional design.

Observing the results it is noted that the general trend is as expected: the higher the bound on ply-count percentage, the lower the factor of safety is. The graph in Figure 7.4 is monotonically decreasing, as it should be. During the numerical experiments it was observed that sometimes a better performance was found with a higher bound on ply-count percentage, depending on the initial guess. This may be explained by the fact that the optimiser is prone to getting stuck in a local optimum. Another interesting point is the drops at 8 and 15%. These are most likely caused by the optimiser getting pushed to a different local optimum since
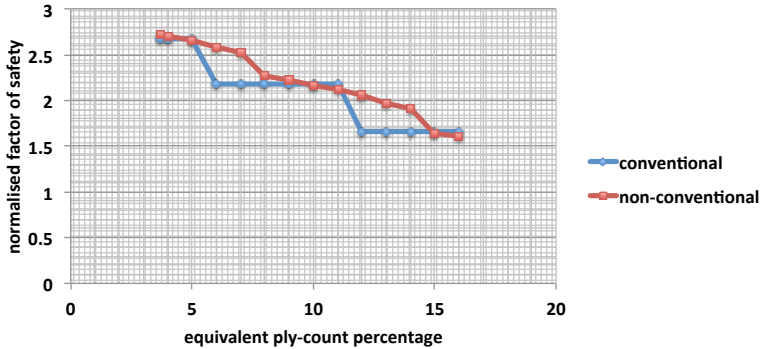
Figure 7.4: Factor of safety for different values of the ply-count percentage, both for conventional (blue) and non-conventional (red) laminates.

the direction for the optima found for lower values of the ply-count percentage constraint is no longer feasible. This shows that local optima can work both ways: one might be lucky and find a better local optimum with a higher ply-count percentage constraint, or the performance could significantly decreases.

The conventional design stays constant for a certain range of ply-count percentages: since the laminate has to be balanced and symmetric and consists of 36 layers in total, most of the time the ply-count percentage is higher than strictly necessary. At places where the conventional design is very conservative with respect to the ply-count percentage, the non-conventional one is clearly outperforming the conventional design. This demonstrates a secondary advantage using non-conventional laminates: the design is not more conservative than it needs to be, leading to a better performance. For the cases where the constraint on the non-conventional design and the actual percentage of the conventional design are close to each other, the performance is very close as well. At some places the conventional design is even performing slightly better than the non-conventional one. This is due to the optimiser getting stuck in a local optimum, while for the conventional design the global optimum is found.

INFLUENCE OF OTHER DESIGN GUIDELINES

All constraints implemented are imposed during the optimisation: the 'traditional' 10% rule is used as ply-count percentage, a lower bound on the fibre angle of 5° is used, an upper bound on the fibre angle of 85°, a lower bound on the fibre angle difference of 10° and an upper bound on the fibre angle difference of 45°. The same optimisation problem is considered, for a range of N_y/N_x ratios. By increasing the ratio from 0 to 1, the optimal design will get closer and closer

to the quasi-isotropic design. With a ratio of 1 the optimal design should be a quasi-isotropic laminate.

As was shown in the previous design study, the optimisation is prone to getting stuck in a local optimum. This is an inherent disadvantage of using a gradient-based optimisation. The advantage is that the optimisation is quite quick, thus multiple starting points can be checked. The results for different ratios and different starting points are shown in Table 7.1. In this table, the ratio of N_y/N_x is shown in column one, column two to four show the results using three different starting points. Start 1 is $[\pm 10/\pm 40/\pm 70/\pm 45/\pm 30/\pm 50/\pm 75/\pm 40/\pm 15]_S$, start 2 is $[\pm 6/\pm 17/\pm 28/\pm 39/\pm 50/\pm 61/\pm 72/\pm 63/\pm 50]_S$, and start 3 is $[\pm 30/\pm 60/\pm 30/\pm 60/\pm 30/\pm 60/\pm 30/\pm 60/\pm 30]_S$.

The results show the normalised factor of safety. Normalisation is always done with respect to the factor of safety of the QI laminate for the specific loading condition. All constraints are satisfied for all optimised results: each optimised design is feasible.

Table 7.1: Factor of safety normalised with respect to the quasi-isotropic factor of safety for different ratios of N_y/N_x.

ratio	start 1	start 2	start 3
0	1.522	1.156	1.266
0.25	1.870	1.815	1.431
0.5	1.543	1.638	1.635
0.75	1.222	0.999	1.220
1	0.995	0.995	0.999

Observing the results in Table 7.1 it is noticed that the factor of safety for the different starting points can differ significantly, showing again that the optimisation is prone to getting stuck in a local optimum. However, except for a ratio of 0, meaning uni-axial loading in x-direction, the highest two values are close together. From a ratio of 0.25 onward, the normalised factor of safety is always decreasing, indicating that the laminate is getting closer to the behaviour of a quasi-isotropic laminate. This is expected since the closer the ratio of N_y/N_x gets to one, the closer the ideal stiffness E_y/E_x gets to one, and thus the closer the laminate gets to quasi-isotropic behaviour.

For a ratio of 1, the theoretical optimum is a quasi-isotropic laminate, and this is almost what was found. At least, the performance of the laminate is almost identical to a quasi-isotropic one: the lay-up, however, for the three optima is very different. From start 1, the optimum found is $[\pm 13/\pm 34/\pm 69/\pm 48/\pm 31/\pm 58/\pm 79/\pm 51/\pm 21]_S$, from start 2 $[\pm 8/\pm 20/\pm 30/\pm 40/\pm 50/\pm 66/\pm 83/\pm 65/\pm 42]_S$, and from start 3 $[\pm 28/\pm 59/\pm 32/\pm 60/\pm 31/\pm 63/\pm 34/\pm 67/\pm 33]_S$. This proves that different lay-ups may lead to (almost) the same stiffness properties and hence the same factor of safety.

7.6.2 INFLUENCE OF THE PLY-COUNT PERCENTAGE RULE ON VARIABLE STIFFNESS LAMINATES

A different optimisation problem is chosen to assess the influence that the ply-count percentage has on the performance of a VSL, since a CSL is optimal for the bi-axial loading case of the previous section. The problem for VSL is defined as a buckling optimisation of a flat plate of 400 by 600 mm, under uni-axial compression on the short edge, with the stiffness constrained to be at least the stiffness of a quasi-isotropic laminate. A graphical representation can be seen in Figure 7.5. The plate is meshed using 1200 triangular elements and 651 nodes. By taking symmetry into account, the stacking sequence has to be optimised at 176 nodes. The ply-count percentage has to be satisfied at each node. A minimum steering radius of 333 mm is imposed to ensure the laminate is manufacturable. This is imposed at each design layer and each of the 300 elements in the symmetric model. The same material is used as in the previous example and the laminate consists of 36 layers, which due to balance and symmetry is equivalent to 9 design layers.
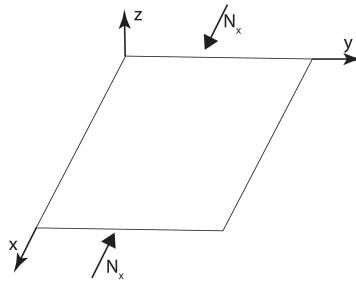
Figure 7.5: Sketch of the plate loaded in compression.

An exhaustive search for the best conventional lay-up is not possible: the position of the layers is important for a buckling optimisation, hence the number of possible stacking sequences is too large to be enumerated. Rather, a suitably efficient reference design is constructed: the number of $\pm 45°$ plies is maximised, and the minimum number of $0°$ layers is determined based on the stiffness constraint, for which the place in the stack is not important. Next, the layers found are shuffled to find the reference design. This lay-up is found to be $[\pm 45/0/\pm 45/90/\pm 45/0/\pm 45/0/\pm 45/90/0_2/\pm 45/0_2]_S$.

As in the CSL case, the optimisation is first performed without a constraint on the ply-count percentage. The ply-count percentage of the optimal design was found to be 0.57%. This low equivalent ply-count percentage is mainly caused by the stacking sequence near the centre of the plate which consists almost exclusively of $\pm 45°$ layers. On the panel sides the ply count percentage is higher due to the

stiffness constraint. Next, the optimisation is performed varying the ply-count percentage constraint from 1 to 12%. The results, normalised with respect to the conventional reference lay-up, are shown in Figure 7.6.
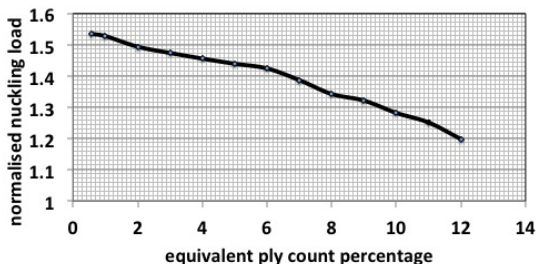
Figure 7.6: Optimal factor of safety for different ply-count percentages, normalised with respect to the reference conventional laminate.

Observing the results, it is noticed that a 53.5% improvement in buckling load can be obtained without constraint on the ply-count percentage, while only a 28.2% improvement can be obtained when applying the 'traditional' 10% rule. Almost half of the improvement over conventional laminates is lost due to the ply-count percentage rule. This is due to the restricted possibility for stiffness changes over the panel, which causes a reduction in the load redistribution, and hence a reduction in the buckling load with respect to the unconstrained laminate. However, an improvement of more than 28% is still significant. Furthermore, by adhering to the 10% rule, these laminates are more likely to be used in practical structures. Hence, by sacrificing some performance (16.5% compared to the optimal steered panel), the feasibility of the design is increased. The exact ply-count percentage that has to be used is case-dependent: if the minimum ply-count percentage is 5%, the performance is 43.9% higher than the conventional reference laminate.

However beautiful the strategy, you should occasionally look at the results.
Winston Churchill

8

TWO DIMENSIONAL TOPOLOGY OPTIMISATION OF COMPOSITE LAMINATES

The previous chapters focused on optimising the material characteristics by tailoring the stacking sequence of composite laminates. Other ways to optimise structural performance involve the design of the structural layout. These types of problems are usually divided into two broad disciplines: shape and topology optimisation. In this chapter, topology optimisation of composite laminates is considered.

Often, the material used during topology optimisation is isotropic, and the objective is to minimise compliance[11,12,13,28,86,87,130]. A method to optimise the topology of composite laminates for minimum compliance is presented in this chapter. The first step of the three-step optimisation approach is extended to include topology optimisation, in addition to lamination parameter optimisation. This means both the location where material is placed and the material properties are optimised. How topology optimisation and lamination parameter optimisation are combined is explained in section 8.1.

This chapter is based on the journal paper 'Combining topology and lamination parameter optimisation'[119].

A known problem in topology optimisation is finding a clear description of the topology: the fictitious density that describes whether or not a given location has material or void should be close to zero or one. When using an isotropic material, a popular method to generate clear topology descriptions is the solid isotropic material penalisation (SIMP) approach. This is an implicit penalisation technique. The SIMP approach is extended to anisotropic materials in section 8.2. Furthermore, an explicit penalisation approach is implemented in the same section. The outcome of the optimisation consists of both lamination parameter and density distributions. The material boundaries need to be found to obtain a clear picture of the optimised structure. The recovery of laminate boundaries and the smoothing of the recovered boundaries are explained in section 8.3. In section 8.4 the new approach is applied to two different compliance optimisation problems to compare the implicit and explicit penalisation, and show the advantages of combining lamination parameter and topology optimisation.

8.1 COMBINATION OF TOPOLOGY AND LAMINATION PARAMETER OPTIMISATION

Minimising compliance is the most commonly used objective in topology optimisation. In this work, compliance minimisation of two dimensional laminates is considered. Thus, instead of using the general approximation, eq. (5.49), where both the in- and out-of-plane stiffness matrices are used, it is sufficient to consider only the in-plane stiffness. The feasible region for in-plane lamination parameters is well known (see equation (3.23)). Although the methodology proposed in this chapter is only applied to the in-plane stiffness matrix, the implementation may be easily extended to pure plate bending problems involving the out-of-plane stiffness.

8.1.1 PROBLEM FORMULATION

The problem solved is a standard compliance minimisation, subject to a volume constraint:

$$
\begin{aligned}
\min_{\mathbf{x}} \quad & \max(f_1, f_2, ..., f_n) \\
s.t. \quad & V \leq \eta \cdot V_0 \\
& \mathbf{x}_i \in \mathcal{D}_i,
\end{aligned}
\tag{8.1}
$$

where V denotes the volume, η is the maximum volume fraction to be used, and V_0 the total volume of the domain. The vector of design variables $\mathbf{x}$ is split up per node. The vector per node $\mathbf{x}_i$ consists of a set of in-plane LPs and fictitious density ρ. The feasible region of the LPs is defined in eq. (3.23), for the densities

it is defined by

$$\rho_\ell \leq \rho \leq 1, \tag{8.2}$$

where ρ_ℓ is the lower bound on the density, which is ideally zero, but to avoid a singular stiffness matrix it is set to a small value, typically 10^{-3} is used.

Similarly to the previous chapters, the design variables are defined at the nodes. Quadrilateral rather than triangular elements are used in this chapter. Similar formulae can be easily derived for triangular elements. The volume used is calculated using

$$V = \sum_{i=1}^{N} A_i \cdot \rho_i, \tag{8.3}$$

where A_i is the volume associated with the ith node. This is calculated using

$$A_i = \sum_{e_i} \frac{1}{4} A_e, \tag{8.4}$$

where A_e denotes the area of element e, and the summation ranges over all elements e_i that have node i as one of the corner nodes.

8.1.2 OPTIMISATION STRATEGY

As was explained in section 5.2, the general form of the approximation of compliance is

$$C \approx \sum_{i=1}^{N} \phi_{\mathbf{i}} : \mathbf{A_i}^{-1}. \tag{8.5}$$

The fictitious density is incorporated in the A-matrix as

$$\mathbf{A} = \rho \cdot \mathbf{A}^0, \tag{8.6}$$

where $\mathbf{A}^0$ is the physical A-matrix, depending only on the LPs. The total approximation is

$$f_j = \sum_{i=1}^{N} \frac{\phi_{ij} : \left(\mathbf{A}_i^0\right)^{-1}}{\rho_i}. \tag{8.7}$$

The method of successive approximations is used to perform the optimisation. A dual technique is used to optimize the approximate sub-problem [52]. The Lagrangian is constructed:

$$\mathcal{L} = \sum_{j=1}^{n} \lambda_j \cdot f_j + \mu \cdot (V - \eta \cdot V_0). \tag{8.8}$$

Using Falk's dual method, the dual function can be written as

$$\mathcal{L}_c(\boldsymbol{\lambda}, \mu) = \min_{\mathbf{x} \in \mathcal{D}} \left(\sum_{j=1}^{n} \lambda_j \cdot f_j + \mu \cdot (V - \eta \cdot V_0) \right). \tag{8.9}$$

The minimisation of this problem is done in two steps. First, node-by-node optimisation with respect to lamination parameters is performed:

$$\beta_{ij} = \min_{\mathbf{V}} \boldsymbol{\phi}_{ij} : \left(\mathbf{A}_i^0\right)^{-1}. \tag{8.10}$$

This step is performed numerically using the `fmincon` function in Matlab. Next, without updating the approximation, the densities are optimised node-by-node solving

$$\mathcal{L}_c(\boldsymbol{\lambda}, \mu) = \sum_{i=1}^{N} \min_{\rho_i} \frac{\sum\limits_{j=1}^{n} \lambda_j \beta_{ij}}{\rho_i} + \mu\alpha_i\rho_i - \mu\eta V_0. \tag{8.11}$$

The Lagrange multipliers λ_j and μ can be obtained solving the maximization problem

$$\begin{aligned} \max_{\boldsymbol{\lambda}, \mu} \quad & \mathcal{L} = \mathcal{L}_c(\boldsymbol{\lambda}, \mu) \\ s.t. \quad & \sum_{j=1}^{n} \lambda_j = 1 \\ & \mu \geq 0. \end{aligned} \tag{8.12}$$

This is done using a dual optimisation algorithm. The approximation is updated after both the lamination parameters and density are optimised. The optimisation is considered converged when the change in compliance between two consecutive iterations is less than a user-specified tolerance.

8.2 ELIMINATING GREY AREA

A known problem in topology optimisation is obtaining a clear topology description, meaning all values of the fictitious density are close to either zero or one, called a black-and-white design. Some form of penalisation has to be used to achieve a this. Two different penalisation approaches exist: implicit and explicit. Both are implemented in this work and compared in section 8.4 to determine which is best suited when combining topology and lamination parameter optimisation.

8.2.1 IMPLICIT PENALISATION

One of the most used implicit penalisation strategies for isotropic materials is the SIMP approach, which penalises the Young's modulus E according to

$$E(\rho) = \rho^p \cdot E^0, \tag{8.13}$$

where p is the penalisation power, and E^0 denotes the physical Young's modulus. The penalisation power p is used to penalise densities away from zero or one, usually $p = 3$ is a good choice. Analogous to the SIMP approach, the A-matrix, which

is the equivalent of the Young's modulus for anisotropic materials, is penalised according to

$$\mathbf{A}(\rho) = \rho^p \cdot \mathbf{A}^0. \tag{8.14}$$

The calculation of the volume does not change. The stiffness decreases faster than the density, meaning the specific stiffness is unfavourable for a density away from zero or one.

The implementation of this penalisation is straightforward from the method described in the previous section: only the expression for the A-matrix as a function of ρ needs to be changed. The disadvantage of this method is that at convergence, there is no guarantee the design is black-and-white. The penalisation power has a significant influence on the outcome: if it is chosen too low, the final design will contain a lot of grey, if it is chosen too high, the structural performance is not optimal.

8.2.2 EXPLICIT PENALISATION

Explicit penalisation[13] uses a two-step approach: step one is the same as implicit penalisation, with a penalisation power $p = 1$, meaning no penalisation. It must be made clear this is still only step one of the three-step optimisation approach: the two steps that are discussed here can be seen as step 1.1 and 1.2 in the general three-step optimisation approach. The outcome will be a design with a lot of grey area.

In step two, a measure of the grey area is defined as

$$g = \frac{\sum_{i=1}^{N} A_i \cdot (\rho_i - \rho_\ell) \cdot (1 - \rho_i)}{V_0}, \tag{8.15}$$

which measures how far the design is from a completely black-and-white design. Since the grey area indicator is not convex, it needs to be approximated. This is done using

$$g = a_0 + \sum_{i=1}^{N} a_i \cdot \rho_i, \tag{8.16}$$

with

$$a_i = \frac{A_i \cdot (1 + \rho_\ell - 2 \cdot \rho_i)}{V_0}. \tag{8.17}$$

The term a_0 in eq. (8.16) is chosen such that the exact and approximation function have the same value at the approximation point.

During step two, the amount of grey is minimised, while the compliance is allowed to slightly increase:

$$\begin{aligned} \min \quad & g \\ s.t. \quad & V \leq \eta \cdot V_0 \\ & f_j \leq \bar{f} \\ & \mathbf{x}_i \in \mathcal{D}_i. \end{aligned} \tag{8.18}$$

8

The bound on compliance is given by

$$\bar{f} = \max_j f_j + \kappa \frac{g}{\sum_j \lambda_j}, \qquad (8.19)$$

where κ denotes the relaxation factor of the compliance allowed. In the first iteration, $\kappa = 0$ is used, next the relaxation factor is changed to a positive non-zero value. Hence, the performance is allowed to decrease in return for a decrease in grey area. Eventually, a black-and-white design is found. The convergence criterion during step two is a limit on the amount of grey, usually $1 \cdot 10^{-3}$ is chosen. For this amount of grey, the topology is considered to be sufficiently resolved, and more iterations will not have a large effect on the final outcome. Another stopping criterion is the volume constraint no longer being active: at that moment nodes that have a density close to zero will be forced to the lower bound on density, and not to one, since this would increase the amount of grey according to the approximation. Hence, the optimisation is stopped if the volume drops below a certain threshold, for example 95% of the volume constraint.

The advantage of this method is that the final design is guaranteed to be black-and-white. The disadvantage is that an extra step is needed, thus increasing computational cost. While in the implicit penalisation the penalisation power p had to be chosen carefully, using explicit penalisation, the relaxation factor κ has to be selected carefully: choosing it too low will lead to extra iterations, while choosing it too high will lead to a suboptimal structural performance.

8.3 POST-PROCESSING

The outcome of the optimisation is an LP and density distribution. Clear material boundaries and fibre paths are actually required to manufacture the structure. The fibre paths can be found using the 'standard' three-step optimisation approach: the fibre angles are retrieved using the method described in section 4.6, without any FE updates. Then the fibre paths are found based on the fibre angle distribution, as explained in section 2.2.

A continuous interpolation of the density is performed to find the material boundary and the boundary is identified as the contour line $\rho = \rho^*$, where ρ^* is a threshold value, usually chosen to be 0.7. The resulting boundaries are not very clear, as can be seen in Figure 8.1(a). The density distribution is first interpolated to a finer mesh, which improves the quality of the boundaries as can be seen in Figure 8.1(b). The contour lines are extracted from this finer mesh. The result can be seen in Figure 8.1(c). The edges are not usually smooth, hence, the smooth command in Matlab is used to obtain a smooth boundary, shown in Figure 8.1(d).

(a) Initial topology.

(b) Topology after mesh refinement.

(c) Contour lines.

(d) Smooth contour lines.
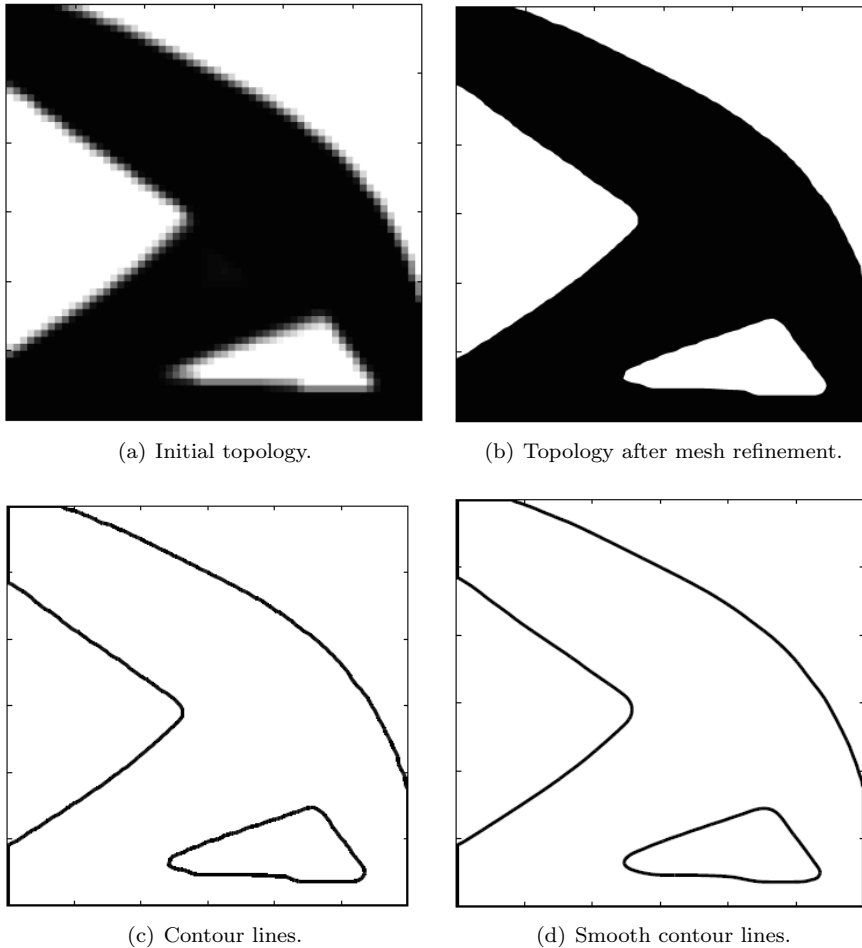
Figure 8.1: Mesh refinement steps.

8

8.4 COMPARISON BETWEEN IMPLICIT AND EXPLICIT PENALISATION

Two example problems are worked out in detail. The first example is used to compare the performance of implicit and explicit penalisation. The second example is used to show the advantage of combining LP and topology optimisation.

The first example is a well-known topology optimisation problem: a flat plate that is clamped in on the left and loaded with a downward force on the right

bottom corner is optimised. The plate is 300 by 300 mm and is divided into 60 equally-spaced elements in x- and y-direction. This number was found after a mesh convergence study. The load has a magnitude of 10 N. The material properties are: $E_1 = 177$ GPa, $E_2 = 10.8$ GPa, $G_{12} = 7.6$ GPa, $\nu_{12} = 0.27$, and $t_{ply} = 0.225$ mm. The maximum volume fraction η is set to 0.6. It is assumed the laminate is symmetric and balanced and has a total of 16 layers. Implicit penalisation, based on the SIMP approach, is used as a benchmark since it is quite well known. The penalisation power p is chosen to be 3, which is considered a reasonable value. The optimisation is run until convergence. For the benchmark an optimal compliance of 0.1757 is found after 67 iterations with the amount of grey area g equal to 0.0157.
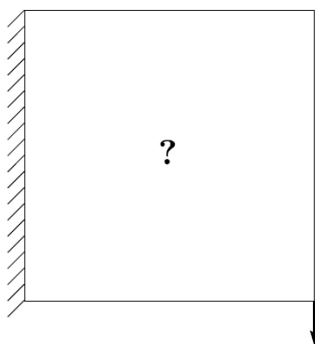
Figure 8.2: Cantilever with boundary condition and load indicated.

Using explicit penalisation, the relaxation factor κ is to be chosen by the user. The results for different values of κ are compared at the same compliance, same grey area, and at convergence. The compliance and grey area can never be matched exactly, hence the iteration where the compliance or grey area is closest to the benchmark is used.

The results at the same grey area as the benchmark are compared first. The results can be seen in Table 8.1 where the relaxation term κ is shown in the first column, the grey area in the second column, the compliance in the third column, and in the final column the number of iterations is shown. Observing the results, it can be noticed that, if the same grey area is reached, the compliance is always lower than for the benchmark. This suggests that using explicit penalisation is the better option when looking at it from a structural performance point-of-view.

The relaxation factor has a large influence on the results: the higher κ is, the higher the compliance is. Furthermore, as was expected, when κ is too large, the optimiser does not perform well. For this case, $\kappa = 0.05$ is too large: the grey area is not even reduced to the level of the benchmark. The influence of the relaxation factor is also seen when the number of iterations is inspected: the

number of iterations when using $\kappa = 0.3$ is clearly higher than for $\kappa = 0.045$ while the difference in compliance is small. However, only when using $\kappa = 0.03$ the number of iterations is slightly increased compared to the benchmark. Thus, also from a computational point-of-view, using explicit penalisation seems to be better than using implicit penalisation.

Table 8.1: Overview of the results of the explicit penalisation scheme to reach the grey area found to be optimal using the implicit penalisation scheme.

κ	grey area	compliance	iterations
0.03	0.01531	0.1691	70
0.04	0.01559	0.1698	53
0.0425	0.01551	0.1699	49
0.045	0.01509	0.1705	47
0.0475	0.01603	0.1719	43
0.05	not	reached	-
benchmark	0.0157	0.1757	67

Next, the results at the same compliance as the benchmark are compared in Table 8.2 where the relaxation term κ is shown in the first column, the compliance in the second column, the grey area in the third column, and in the final column the number of iterations is shown. When inspecting the results, it can be seen that a larger number of iterations is needed compared to the results at the same grey area, while the compliance is worse. This may seem counter-intuitive, however, one has to keep in mind that during step two of the optimisation, the compliance always increases and the objective is to minimise the grey area. Another difference compared to the same grey area is that the compliance is much closer to the benchmark. This is because the compliance is gradually increasing, while the grey area sometimes takes a big leap in one iteration.

Analogue to the previous results, the grey area is decreasing for smaller values of κ, as is expected. The number of iterations also follows the same trend: it increases for decreasing κ. However, the number of iterations is increasing this time: for $\kappa = 0.03$, the number of iterations increases significantly, and even for $\kappa = 0.04$, the number of iterations is slightly increasing. Again, the value $\kappa = 0.05$ is too high and the same compliance as the benchmark is not reached.

The most important result from Table 8.2 is that the grey area significantly decreases when using explicit penalisation. For most cases the grey area is more than halved, meaning that the material boundaries are much clearer. It can be concluded that explicit penalisation is comparable in numerical efficiency to implicit penalisation since only for $\kappa = 0.03$ the number of iterations significantly increases.

Finally, the results at convergence are compared in Table 8.3. The compliance

Table 8.2: Overview of the results of the explicit penalisation scheme to reach the compliance found to be optimal using the implicit penalisation scheme.

κ	compliance	grey area	iterations
0.03	0.1759	0.00629	95
0.04	0.1759	0.00705	71
0.0425	0.1759	0.00755	61
0.045	0.1757	0.00757	60
0.0475	0.1758	0.00933	49
0.05	not	reached	-
benchmark	0.1757	0.0157	67

and grey area do not show a clear trend, but the number of iterations does. As expected, the lower κ is, the more iterations are needed. However, the number of iterations is usually close the the benchmark. Only for $\kappa = 0.03$ the number of iterations is significantly higher, and for $\kappa = 0.05$ the number of iterations is significantly lower. These extreme values of the relaxation factor are not the most useful: the grey area for $\kappa = 0.05$ is so high that the topology is not clear, and the extra computational cost for $\kappa = 0.03$ is not worth the decrease in either compliance or grey area.

When comparing the results using reasonable values of κ (i.e., $0.04 \leq \kappa \leq 0.0475$), the compliance is always a bit worse than the compliance of the benchmark. However, the grey area is always much better: only one third of the benchmark. Taking into account that the compliance and grey area are competing functions, meaning one decreases when the other increases, this result is as expected. Such a large decrease in grey area would not be possible without a (small) increase in compliance.

Table 8.3: Overview of the results of the explicit penalisation at convergence.

κ	compliance	grey area	iterations
0.03	0.1772	0.00538	100
0.04	0.1792	0.00481	80
0.0425	0.1784	0.00575	67
0.045	0.1811	0.00386	73
0.0475	0.1794	0.00560	56
0.05	0.1687	0.02434	37
benchmark	0.1757	0.0157	67

Combining the different results, it can be concluded that implicit and explicit penalisation give comparable results. It cannot be said one is clearly better than

the other since the two objectives, compliance and grey area, are competing objectives, and are never improving at the same time. However, since using explicit penalisation with the right relaxation factor, a black-and-white result can be guaranteed, this is the preferred penalisation method. Therefore only explicit penalisation will be used in the second example.

The result of the combined LP and topology optimisation in terms of the lamination parameters is shown in Figure 8.3, where only V_1 and V_3 are shown since the laminate is balanced and symmetric. When performing first topology optimisation, using a quasi-isotropic material, followed by LP optimisation of the found topology, the same result is found. This was expected since the topology found using the combined optimisation is exactly the same as the well-known optimal topology for this problem for an isotropic material. To have a good idea of the lay-out of the final structure, the post-processing steps are performed. The contour can be seen in Figure 8.4. The fibre paths, with two balanced layers on the same figure, can be seen in Figure 8.5.

(a) V_1. (b) V_3.
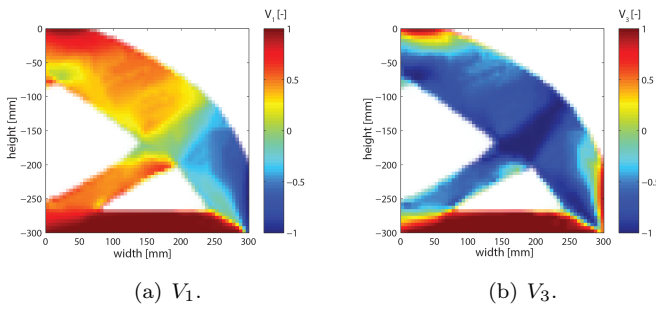
Figure 8.3: Optimal V_1 and V_3 distribution.
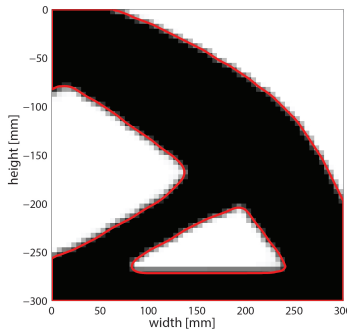
Figure 8.4: Contour derived from the optimal topology.

(a) Layer 1 and 2, outer layers.

(b) Layer 3 and 4.

(c) Layer 5 and 6.

(d) Layer 7 and 8, at symmetry plane.
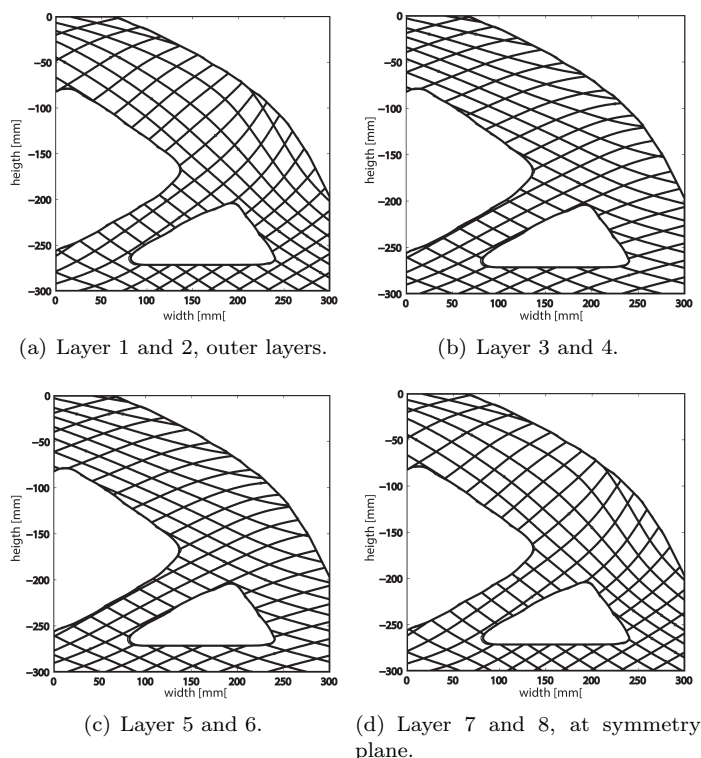
Figure 8.5: Fibre path distribution.

The topology found for this example is well-known to be correct, hence both implicit and explicit penalisation give a good result, certainly in terms of topology optimisation. This result can be compared to the work of Sørensen and Stolpe [136], who have optimised the topology and fibre angle distribution of a single layer using a similar method to the DMO method, discussed in chapter 2. The result is shown in Figure 8.6. Observing this result, it can be seen that the topology is similar, but not the same due to the very coarse mesh, and the fibre angles are comparable. Due to the steering constraint, no exact 0° angle can be obtained along the bottom edge, nor the 90° at the right edge. The 45° fibres are not exactly obtained, but are close when looking at the result obtained using our code in Figure 8.5. It can be concluded that the optimisation gives a good result for the current problem.

As a second example a more slender plate of 200 by 75 mm is optimised. The left side is clamped, the force is upwards on the right on two nodes: one node is exactly in the middle, the other is 2.5 mm above it, as shown in Figure 8.7. The
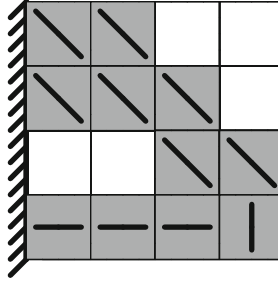
Figure 8.6: Result obtained when optimising the distribution one 1 layer by Sørensen and Stolpe[136].

mesh is 80 by 30 elements. The material properties are: $E_1 = 177$ GPa, $E_2 = 6.8$ GPa, $G_{12} = 2.6$ GPa, $\nu_{12} = 0.27$, and $t_{ply} = 0.45$ mm, which is slightly different than in the previous example. The laminate is only assumed to be symmetric, not balanced. The total thickness is 8 layers. The maximum volume fraction η is set to 0.52. Analogue to the previous example, this problem is solved in two ways: once the topology and LP optimisation are combined, the other time first topology optimisation is performed followed by LP optimisation.
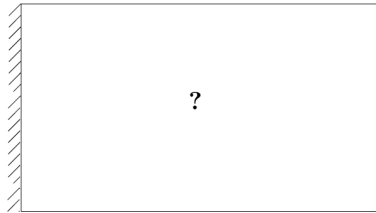
Figure 8.7: Cantilever with load and boundary condition indicated for second example.

A different topology is found for the different optimization methods, as can be seen in Figure 8.8. The loading is not symmetric, but due to the anisotropy of the material, the optimal topology for the anisotropic material is almost symmetric, while for the isotropic material, the topology is not symmetric at all. Besides the topology being different, the compliance is 4.8% better when using the combined optimisation compared to first topology optimisation, followed by LP optimisation. Hence, combing the optimisations can have a significant influence on the optimised topology and compliance.

The lamination parameter distribution can be seen in Figure 8.9. The post-processing steps are done and the resulting fibre paths can be seen in Figure 8.10, where only one set of fibre paths per figure is shown since the laminate is not balanced. Only steering constraints were applied.

(a) Using an isotropic material.

(b) Optimising the lamination parameters.
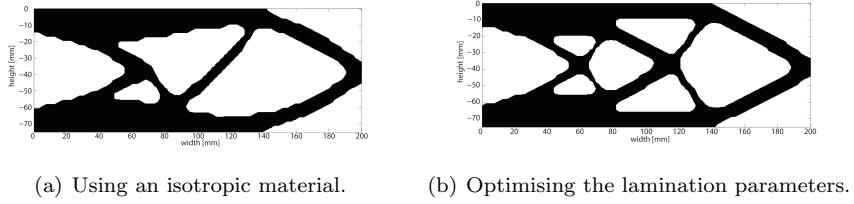
Figure 8.8: Optimal topology.

(a) V_1.

(b) V_2.

(c) V_3.

(d) V_4.
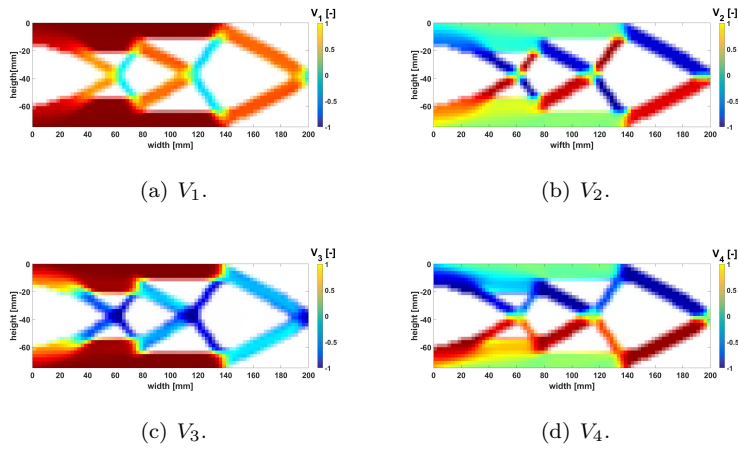
Figure 8.9: Lamination parameter distribution.

(a) Layer 1.

(b) Layer 2.

(c) Layer 3.

(d) Layer 4.
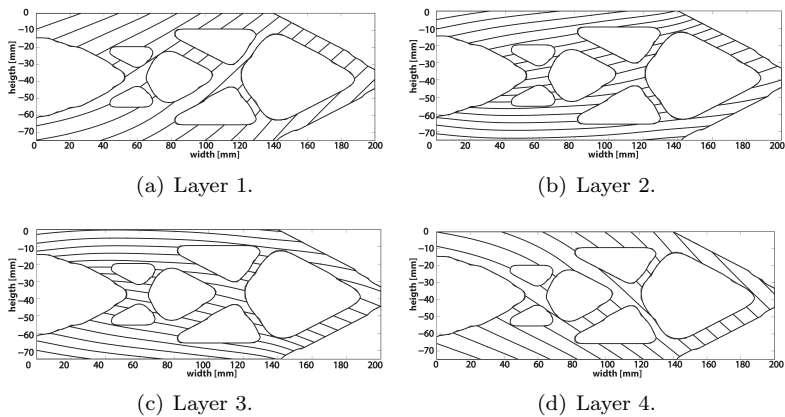
Figure 8.10: Fibre path distribution.

9

VARIABLE THICKNESS LAMINATES

Classical topology optimisation is concerned with deciding whether material is present or not at any given location in the structure. For isotropic materials this is a logical choice: a material is either present or not, something in between is not possible. Composite materials on the other hand, are built up from different layers, which means that, the material can be partially present by only having some of the plies. Hence, density values away from zero or one can be interpreted as only some of the plies being present. Variable thickness laminates are obtained by varying the number of plies from one point to another. The fibre angle distribution needs to be optimised concurrently since the stiffness properties of each ply depend on its (local) fibre angle orientation. When the fibre angle is constant throughout a layer, variable thickness laminates are obtained, when the fibre angle is allowed to change, variable stiffness, variable thickness laminates are obtained.

To optimise variable thickness laminates, it is proposed to split up step two is in two sub-steps, 2.1 and 2.2, similar to the explicit penalisation approach discussed in the previous chapter. In step 2.1, the fibre angle distribution and one fictitious density per node are optimised. The density value is interpreted as scaling the total thickness of the laminate and does not need to be close to zero or one. The

---

This chapter is based on the journal papers 'Optimisation of Ply Drop Order in Variable Stiffness Laminates'[66], and 'Optimisation of Ply Drop Locations in Variable Thickness Composites'[117].

density per node needs to be transformed into a description of the number of layers to obtain physically meaningful laminates. This is done in step 2.2, where each ply is assigned an unknown density distribution. This density distribution is driven to either zero or one. The boundaries where the density changes from near zero to near one determine the ply drop locations. The fibre angle distribution is optimised concurrently during step one and two. To ensure manufacturability, the plies need to be continuous, a requirement usually referred to as *blending*. In this work, blending is enforced by defining the order in which the plies are dropped. Hence, three variables describe variable thickness, variable stiffness laminates: ply drop location, ply drop order, and fibre angle distribution.

In section 9.1, the two-step optimisation (i.e., step 2.1 and 2.2) to determine the ply drop location and fibre angle distribution is discussed, with a pre-defined drop order. This optimisation is performed using the method of successive approximations. To optimise the ply drop order, the method of successive approximations cannot be used since it is an inherently combinatorial problem. Instead, the stacking sequence tables (SST) method, originally proposed by Irisarri et al. [65], is used. This method is used since it has been proven to work well in the past, and is compatible with the formulation that is used in the current work. By combining the SST, a genetic algorithm, with the method of section 9.1, all variables describing the variable stiffness, variable thickness laminates are optimised. This is described in section 9.2. All other optimisations in this work are done using gradient-based algorithms, but an evolutionary algorithm is used to determine the best ply drop order since the variables describing the ply drop order are not continuous. An example problem to assess the influence of the ply drop order and the performance of the algorithm is discussed in section 9.3.

9.1 Ply drop location optimisation

The ply drop location and fibre angle distribution are determined using the method of successive approximations. The ply drop order is fixed in this section, it will be optimised in the next section. The ply drop order is given by a vector $\mathbf{d}$ that gives the order in which the plies are dropped. For example, $\mathbf{d} = [4\ 2\ 3\ 1]$ means that ply 4 is dropped first, followed by ply $2, 3$, and finally ply 1, at the outside. There are no restrictions on the order: inner and outer blending [168] are possible, and any other dropping order is possible.

The general problem is formulated as

$$
\begin{aligned}
\min_{\boldsymbol{\rho},\boldsymbol{\theta}} \quad & \max(f_1, f_2, ..., f_n) \\
s.t. \quad & f_{n+1}, ..., f_m \leq 0 \\
& V \leq \eta \cdot V_0 \\
& \boldsymbol{\rho}, \boldsymbol{\theta} \in \mathcal{D}_i,
\end{aligned} \tag{9.1}
$$

where the design variables for the densities $\boldsymbol{\rho}$ describe the density distribution of each ply at each node. The fibre angle distribution is updated during both steps using the same algorithm as described in chapter 4, while the manufacturing constraints, explained in section 6.1, are satisfied.

Each density variable still needs to satisfy the bounds on density to be in the feasible region $\mathcal{D}_i$ of each node:

$$\rho_\ell \leq \rho_j \leq 1. \tag{9.2}$$

To adhere to the ply drop order, the following constraints are added:

$$\rho_{d_1} \leq \rho_{d_2} \leq \cdots \leq \rho_{d_L}, \tag{9.3}$$

where L is the total number of design layers.

9.1.1 FORMULATION OF PLY DROP LOCATION OPTIMISATION

Based on the results in section 8.4, explicit penalisation is chosen to drive the densities of each layer to either zero or one. Implicit penalisation has been tried but was not successful in driving the individual layer densities to a black-and-white design. Hence, a two-step optimisation is used. In step one all densities at a node are equal to each other, leading effectively to a thickness optimisation at a relatively low computational cost. In step two the grey area is minimised and the actual ply drop locations are determined by 'forcing' all densities of the different layers to either zero or one. The ply drop locations are found at the places where the density of a ply goes from near zero to near one.

In practical problems a lower bound on thickness is often prescribed, for example to enforce a minimum gauge thickness or surface coverage. This implies certain layers will always be present, and have a density of one. These layers/plies will be referred to as full layers/plies. Often the outer layer is chosen to be full to reduce the chance of delaminations occurring. The lower bound on density ρ_ℓ can be set to zero when certain layers are full, since there is no chance of a singular stiffness matrix occurring. The full plies have a density of one during both step 2.1 and 2.2 of the optimisation.

The problem solved during step 2.1 in terms of the densities is formulated as

$$\begin{aligned}
\min_{\boldsymbol{\rho}} \quad & \max(f_1, f_2, ..., f_n) \\
s.t. \quad & f_{n+1}, ..., f_m \leq 0 \\
& V \leq \eta \cdot V_0 \\
& \rho_\ell \leq \rho_i \leq 1 \qquad i = 1, ..., N,
\end{aligned} \tag{9.4}$$

where N represents the number of nodes. The lower bound ρ_ℓ can be set to zero if certain plies are full, otherwise a value of 10^{-3} is chosen. The design variables $\boldsymbol{\rho}$ are described by a vector of length N. The outcome of this step describes the thickness distribution of the structure, but does not give exact ply boundaries.

Similar to the explicit penalisation formulation explained in section 8.2.2, the grey area is minimised during step 2.2, while the objective is allowed to gradually deteriorate:

$$\min_{\boldsymbol{\rho}} \quad g$$
$$\text{s.t.} \quad f_1^{(k+1)}, f_2^{(k+1)}, ..., f_n^{(k+1)} \leq f^U$$
$$f_{n+1}, ..., f_m \leq 0 \tag{9.5}$$
$$V \leq \eta \cdot V_0$$
$$\rho_\ell \leq \rho_{i,j} \leq 1 \qquad\qquad i = 1, ..., N; j = 1, ..., L$$
$$\rho_{i,\mathbf{d}(j)} \leq \rho_{i,\mathbf{d}(j+1)} \qquad i = 1, ..., N; j = 1, ..., L-1,$$

where the superscript $k+1$ denotes the outcome of this iteration. The definition of the grey area is given in eq. (8.15). The design variables $\boldsymbol{\rho}$ are described by a matrix of number of nodes N by the number of design layers L. Initially, all variables at a node are equal to the value found during step one, afterwards they are forced to either zero or one. Similarly to eq. (8.19), the upper bound on the objective f^U is given by

$$f^U = \max(f_1^{(k)}, f_2^{(k)}, ..., f_n^{(k)}) + \kappa \cdot \frac{g}{\sum_{l=1}^n \lambda_l}, \tag{9.6}$$

where k denotes the outcome of the kth iteration, when this is iteration $k+1$.

The optimisations formulated in eqs. (9.4) and (9.5) are solved using the method explained in chapter 4. The formulation of the level two approximations in terms of the density distribution is discussed in section 3.3. The damping function used to render the complete approximation conservative is given in eq. (4.28).

9.1.2 COMBINING FIBRE ANGLE AND PLY DROP LOCATION OPTIM- ISATION

The fibre angle and density optimisation are not performed at the same time, but are combined. The way to combine optimisation with different design variables is explained in section 4.5. The definition of the improvement was not discussed since it depends on the optimisations that are combined. During step one of the optimisation the definition of the improvement is clear: the improvement in objective function. To reduce the number of FEAs, this is calculated using the level one approximation. The convergence criterion during step one is the change in objective function: if this is less than a certain threshold, for example $5 \cdot 10^{-3}$ if the response is properly normalised, the optimisation is considered to be converged.

During step two the definition of the improvement is less clear: the two optimisations have different objectives. The improvement for the fibre angle optimisation is still the improvement in objective function:

$$i_\theta = \max_i \left(f_i^{(k)} \right) - \max_i \left({}^I f_i^{(k+1)} \right). \tag{9.7}$$

The improvement in grey area, and the possible improvement in performance are both taken into account during the optimisation of the density distribution:

$$i_\rho = g^{(k)} - g^{(k+1)} + \max_i \left(f_i^{\,(k)} \right) + \kappa \cdot \frac{g^{(k)}}{\sum_{j=1}^n \lambda_j} - \max_i \left({}^I f_i^{\,(k+1)} \right). \qquad (9.8)$$

The values used for the grey area are the exact values, while the values for the structural responses are calculated using the level one approximation. The convergence criterion during step two is based on the grey area: analogous to the stopping criterion in section 8.2.2, if the grey area is under a certain threshold, or the volume constraint is no longer active, the density distribution has converged. It is assumed that the fibre angle distribution is already converged at this point, since it is optimised during step one. Furthermore, a maximum of three consecutive updates of the same set of design variables is allowed, hence the fibre angle distribution is also updated during step two of the optimisation.

The outcome of this two-step optimisation are a fibre angle and density distribution, hence post-processing is necessary to find a laminate that can be manufactured. The boundaries of the plies are found in the same way as explained in section 8.3. The fibre angle distribution is 'translated' to fibre paths using the method described in section 2.2.

9.2 PLY DROP ORDER OPTIMISATION

In addition to fibre angle distribution and ply drop location, optimised in the previous section, the third variable describing variable stiffness, variable thickness laminates is the ply drop order. To optimise the ply drop order in variable thickness laminates, a genetic algorithm is often used[8,125,131]. Recently, the method of stacking sequence tables (SST) was proposed by Irisarri et al.[65]. The method implements the laminate design guidelines most widely used in aerospace industry. The SST method is adapted in this work to include the possibility of variable stiffness, variable thickness laminates.

9.2.1 STACKING SEQUENCE TABLES

The method of SST is used to optimise variable thickness laminates, hence the fibres are straight, not steered. A structure is optimised by splitting it up in different panels, or patches. To ensure manufacturability, all laminates are derived from a 'guide laminate' by dropping plies in a certain order. The guide laminate is the thickest laminate that can appear throughout the structure. Since the plies are dropped in a certain order, a laminate is uniquely described by the guide laminate and the number of plies.

To optimise the laminate, a GA is used which optimises three 'chromosomes': SST_{lam}, that describes the stacking sequence of the guide laminate, SST_{ins} that describes the order of insertion, and N_{str} that represents the number of plies in the different panels. A difference with the previous section is that the order of insertion is defined, as opposed to the drop order. They are in a way each others' inverse: the ply that is inserted last, is dropped first, and the ply that is inserted first, is dropped last. A ply that is prescribed to be present has an insertion rank 0, while in the ply drop order it is the last one to be dropped; if multiple plies are prescribed, their order in the ply drop order is not important, as long as they are placed at the end. An example of a variable thickness laminate can be seen in Figure 9.1.
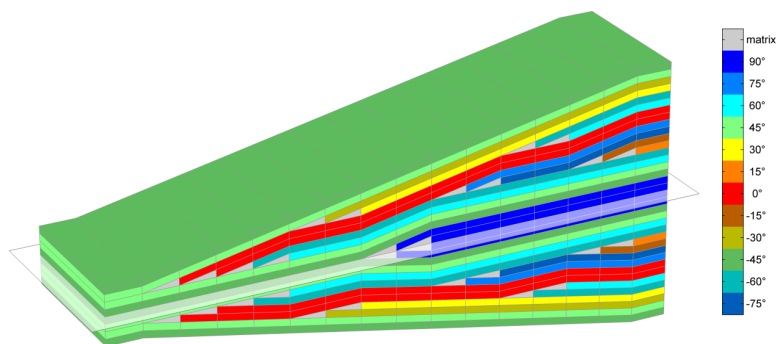
Figure 9.1: Schematic representation of a symmetric thickness transition of a variable thickness laminate.

During the optimisation, design guidelines are taken into account. Not all design guidelines that are implemented are repeated here, some already have been discussed in chapter 7. For a full list of design guidelines taken into account during SST optimisation, the interested reader is referred to the original paper by Irisarri et al. [65]. A guideline that was already mentioned is that the outer layers should be full to avoid delaminations. Another example is the continuity rule, which states that for every three consecutively dropped plies, a continuous ply should be kept. This rule aims at guaranteeing that the loads can be transferred throughout the structure. Another set of rules aims at reducing the stress concentrations caused by ply drops. For example, the taper angle should not exceed 7°. Another example is the rule that, as much as possible, the ply drops should alternately be close and far from the mid-plane. Furthermore, no more than two plies should be stopped at the same point, and a lower bound on the distance between ply drops needs to be adhered to. All these rules aim at dispersing the ply drops to avoid large resin rich areas close to each other.

9

9.2.2 COMBINING STACKING SEQUENCE TABLES AND PLY DROP LOCATION OPTIMISATION

The two-step optimisation approach introduced in the previous section is adapted to combine the principle of SSTs with ply drop location optimisation. The two steps are referred to as step 2.1 and 2.2 to clearly make the distinction with the general three-step optimisation approach of IJsselmuiden. In step 2.1, a stiffness matching is done using the 'standard' SST: a guide laminate and the drop order are optimised. The thickness is not changed compared to the outcome of step one. The best candidates are then used as initial guess for step 2.1 described in section 9.1: the thickness and fibre angle distribution is optimised. During step 2.2 the evolutionary algorithm is used to find the best ply drop order, with the outcome of the gradient-based step two of section 9.1 as fitness function. This is graphically shown in Figure 9.2. The left of this graph is the SST-related part, using an evolutionary algorithm, the right part is performed using a gradient-based optimisation.
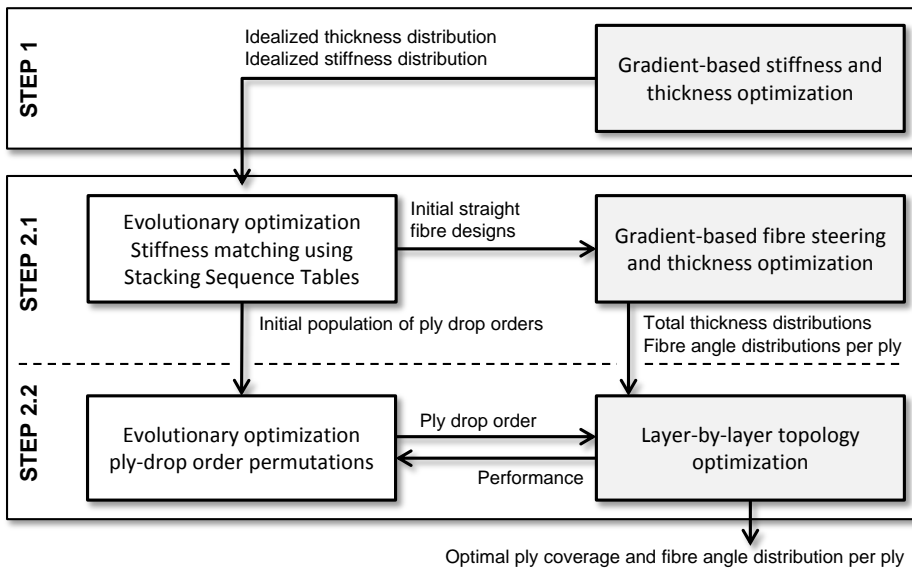
Figure 9.2: Overview of the optimisation strategy.

Stiffness matching using SSTs is performed by minimising the distance between the stiffness matrix found and the wanted stiffness matrix, for both the in- and out-of-plane stiffness matrix. The distance between two matrices is defined as

$$d(\mathbf{C}_1, \mathbf{C}_2) = \left(\mathbf{C}_1^{-1} - \mathbf{C}_2^{-1}\right) : \left(\mathbf{C}_2 - \mathbf{C}_1\right). \tag{9.9}$$

Since the stiffness matching in fibre angles will not match both in- and out-of-

plane stiffness matrices exactly, the Pareto front is generated with the distance to the in-plane stiffness matrix and the distance to the out-of-plane stiffness matrix as the two competing objectives. The non-dominated designs on this Pareto front are used as input for the gradient-based fibre steering and thickness optimisation.

More results need to be generated when a lower bound on thickness is prescribed that cannot be fulfilled by only having full outer plies. Since the optimisation in step 2.1 takes the full plies into account and satisfies all structural constraints, an initial guess for all possible combinations of full plies is necessary for both the gradient-based part of step 2.1 and step 2.2. For example, if a laminate is symmetric and balanced of 32 layers in total and a minimum of 8 layers is prescribed, this means that 2 out of 8 design layers are to be full. The outer layer is full, this is fixed. One more layer needs to be full, which can be any design layer, hence 7 options are generated such that a valid initial guess is available for every possible ply drop order.

An evolutionary algorithm is used to determine the ply drop order during step 2.2. The fibre angle distribution and ply drop location are determined using the method described in the previous section. The outcome of the optimisation is used as the fitness function for the evolutionary algorithm. Hence, compared to the original SST optimisation, only the SST_{ins} is optimised. The permutation used in the original work [65] is re-used in this work. The cross-over operator is inspired by the ordered cross-over operator [46]:

1. Let SST_{ins}^{01} and SST_{ins}^{02} be two insertion rank vectors.

2. A random subset of ranks strictly superior to $rank_{min}$ is selected.

3. In the proposed example $rank_{min} = 1$, and the selected ranks are underlined: $SST_{ins}^{01} = [0\ 2\ \underline{3}\ \underline{5}\ 1\ \underline{6}\ 7\ 0\ 4]$ and $SST_{ins}^{02} = [0\ \underline{6}\ 7\ 1\ 4\ \underline{5}\ 2\ 0\ \underline{3}]$.

4. To create the offspring vector SST_{ins}^{11}, vector SST_{ins}^{01} is copied and the selected subset is reordered according to SST_{ins}^{02}. Vector SST_{ins}^{12} similarly is a copy of SST_{ins}^{02} with the ordering of SST_{ins}^{01} for the selected subset.

5. $SST_{ins}^{11} = [0\ 2\ \underline{6}\ \underline{5}\ 1\ \underline{3}\ 7\ 0\ 4]$ and $SST_{ins}^{12} = [0\ \underline{3}\ 7\ 1\ 4\ \underline{5}\ 2\ 0\ \underline{6}]$.

The continuity of plies is not changed by this cross-over operator since it does not operate on ranks lower than $rank_{min}$, .

Since the ply drop location is no longer determined by the evolutionary algorithm, some guidelines that the original SST adhered to are no longer enforced. The lower bound on distance between ply drops, upper bound on taper angle, and dropping maximum two plies at the same time are no longer satisfied. However, this can be done during post-processing: by slightly changing the boundaries of the found plies, these guidelines can be adhered to. For manufacturing reasons, a

9

lower bound on tow length has to be adhered to, which is also not implemented in the optimisation algorithm. Hence, post-processing of the optimised design is necessary. The reason these constraints are not implemented is that they contradict the grey area reduction. By implementing the upper bound on taper angle, or lower bound on distance between ply drops, some grey area will necessarily appear in the design preventing the convergence of step 2.2.

9.3 RESULTS

The proposed method is applied to the buckling load maximisation of a simply supported square plate under uni-axial compression. The first two buckling modes are considered in the optimisation to avoid mode jumping. The side length of the plate is 500 mm. A graphical representation of this problem can be seen in Figure 9.3. The plate is meshed using 16 elements in both x- and y-direction, which is sufficient to capture the effect of the stiffness change on the buckling load. The base ply properties are the following: $E_{11} = 154$ GPa, $E_{22} = 10.8$ GPa, $G_{12} = 4.02$ GPa, $\nu_{12} = 0.317$, and $t_{ply} = 0.4$ mm. The number of plies can locally vary from 8 to 36 plies, hence 2 design layers are full: the outer layer and one more. A global steering constraint is enforced that corresponds to a lower bound on steering radius of 333 mm. The upper bound on volume corresponds to a 24-ply constant thickness laminate. The results shown are normalised with respect to the performance of a 24-ply constant thickness, quasi-isotropic laminate. In line with the previous chapters, quasi-isotropic is defined as all lamination parameters equal to zero. This problem is solved twice: once with and once without the constraint that the stiffness has to be at least as much as the QI stiffness.
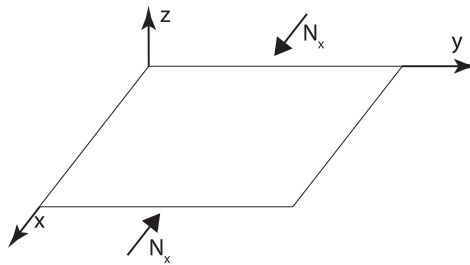
Figure 9.3: Load case and boundary conditions.

To assess the effectiveness of changing the thickness, the performance of constant stiffness, variable stiffness (VS) and variable thickness (VT) laminates of the same weight are compared. Furthermore, the loss in performance of the variables stiffness, variable thickness (VSVT) laminates in going from optimal lamination parameters to fibre angle and density distribution is assessed. Finally, the influ-

ence of the ply drop order is investigated. To assess the influence of the drop order an 'intuitive' reference drop order is selected as $\mathbf{d}_i = [7\ 2\ 8\ 3\ 6\ 4\ 5\ 9\ 1]$. A graphical representation of the dropping order can be seen in Figure 9.4. Furthermore, during the optimisation, the lowest buckling load found during step 2.2 is recorded. Hence, a set of optimised laminates will be created for both problems.

Figure 9.4: Visualisation of the drop order.

9.3.1 BUCKLING OPTIMISATION

The results of the different optimisations are shown in Table 9.1. The optimisation setting used is indicated in the first column. If the laminate has a constant thickness, it consists of 24 layers, hence all laminates have the same weight. The first two normalised buckling loads are shown in the second and third column. The difference relative to a variable stiffness laminate optimised using the current optimiser is shown in the last column. The variable stiffness, variable thickness laminate is shown after both step 2.1 and 2.2. The optimal constant stiffness laminate is all $\pm 45°$.

Table 9.1: Overview of the results of the different optimisations.

optimisation	normalised buckling load 1 [-]	normalised buckling load 2 [-]	difference w.r.t. variable stiffness
CS	1.247	1.663	-52.5 %
VS	2.620	2.645	0 %
LP with constant thickness	3.122	3.186	+ 19.2 %
LP with variable thickness	6.298	6.667	+ 140.4 %
VT	3.084	3.139	+ 17.7 %
VSVT with $\mathbf{d}_i$ (step 2.1)	4.301	4.316	+ 64.2 %
VSVT (step 2.1)	4.314	4.314	+ 64.7 %
VSVT with $\mathbf{d}_i$ (step 2.2)	4.868	4.869	+ 85.8 %
Best VSVT (step 2.2)	5.161	5.173	+ 97.0 %
Worst VSVT (step 2.2)	4.523	4.526	+ 72.6 %

Observing the results in Table 9.1, it can be seen that both variable stiffness and variable thickness lead to significant improvements in buckling load. These results suggest that variable thickness outperform variable stiffness laminates, but this is

9

not necessarily conclusive. Manufacturing constraints are implemented for variable stiffness laminates, which causes a reduction in performance by limiting the load redistribution capability. For variable thickness laminates no manufacturing constraints such as a lower bound on the distance between consecutive ply drops are implemented. This means that the stiffness change from one point to another can be very large since many plies can be dropped at once. Some reduction in performance is expected when the manufacturing constraints are implemented.

Another, at first sight surprising, result is that the performance increases during step 2.2 compared to the outcome of step 2.1. This can be explained by the larger design space: during step 2.1 only one density per node can be changed, while in step 2.2 the density of each layer can be changed per node. This implies the stiffness changes from one point to another can be larger: dropping a ply completely has more influence than purely steering and changing the density (i.e., the effective thickness) of all layers. The difference in buckling load after step 2.1 using the optimised drop order or the prescribed drop order is very small, while after step 2.2 the difference is significant. The optimal drop order is found to be [9 7 5 2 3 6 4 1 8], hence the continuous plies are 1, and 8, while plies 1 and 9 were continuous in the prescribed drop order. The other part of the drop order has no influence during step 2.1 since all densities are equal. Hence, the difference increases during step 2.2. The drop order clearly has a significant influence: the difference between the best and worst buckling load found is more than 60% of the buckling load of a QI laminate. In this case, the intuitive drop order is somewhere in the middle, showing that one will not always be able to find a good drop order based on intuition.

Finally, the loss in performance compared to the optimised LP distribution is discussed. When the thickness is constant almost 16% performance is lost by the translation from LP to optimised fibre angle design. When using variable stiffness, variable thickness laminates this loss is 18%. This is a relatively small difference when one takes into account that the thickness is a continuous variable during the LP optimisation while it has to be a multiple of the ply thickness in the fibre angle and density distribution optimisation. The lack of manufacturing constraints plays a role as well: the thickness can change rapidly, meaning the thickness distribution can be matched accurately, even in places with a steep thickness change. A steep change in stiffness distribution cannot be matched due to the steering constraint.

The fibre paths found for this case can be seen in Figure 9.5. Ply 1 is the outer ply, ply 9 is the ply at the symmetry plane. The layer and its balanced counterpart is always shown in the same figure, the solid blue means there is a void. Observing this figure, it can be seen that most of the time, stiffener-like reinforcements are placed at the edges, for example in plies 2, 3, 5, 7, and 9. Plies 4 and 6 seem to show some extra reinforcement against the buckling mode with two half waves. Plies 1 and 8 are continuous. In the middle of the plate, the lay-up goes towards

$\pm 45°$ in each layer, which is optimal for buckling. At the edges of the plate, most plies are going towards $0°$ to redistribute the load towards the supported edges and lead it into the supports. Only ply 8 goes towards $90°$, which is also advantageous for buckling.

9
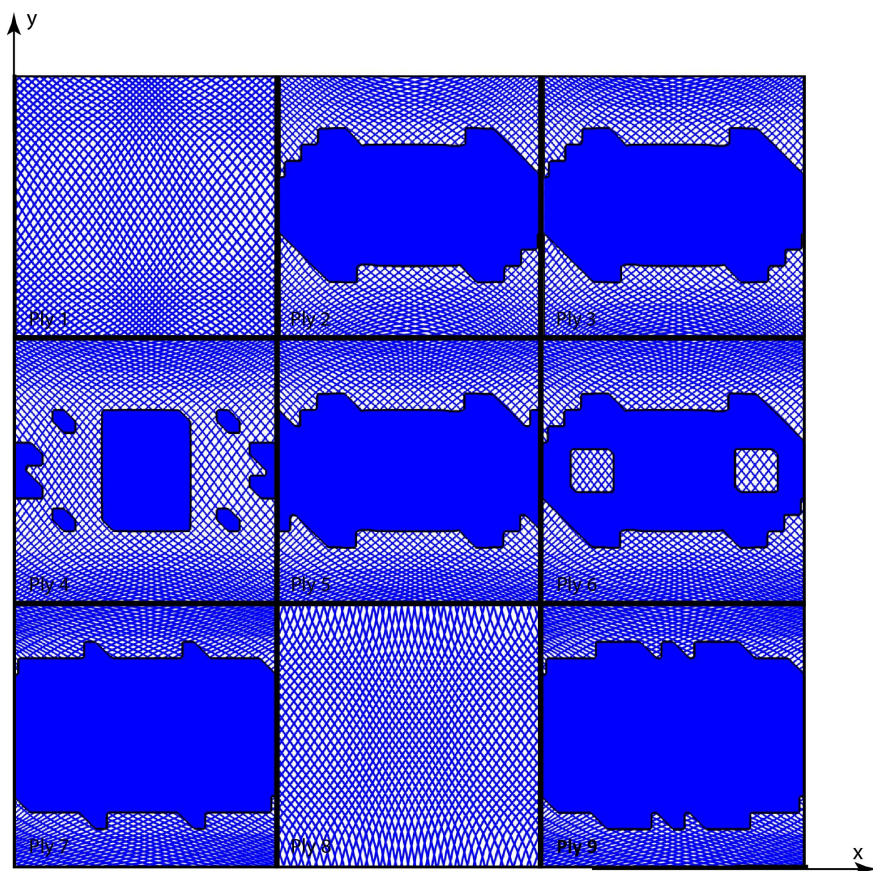
Figure 9.5: The best VSVT laminate after step 2.2.

The thickness distribution is comparable to the thickness obtained by Joshi and Biggers[74] for buckling optimisation of uni-axially loaded plates. The fibre paths cannot be compared since their work was on thickness optimisation, not on fibre angle optimisation. However, the fact that the same stiffener-like reinforcements on the side are found suggests that the thickness distribution found is correct.

9.3.2 BUCKLING OPTIMISATION WITH STIFFNESS CONSTRAINT

The previous problem is re-optimised with a stiffness constraint added. The results are shown in Table 9.2. This table has the same lay-out as the one in the previous subsection, one column in which the stiffness is shown is added. The optimal constant stiffness laminate is not easy to find this time. Using optimisation, it is found to be $[\pm 41 \pm 41 \pm 40 \pm 35 \pm 19 \pm 6]_s$, where the small angles close to the symmetry plane are due to the stiffness constraint. The intuitive drop order is not changed.

Table 9.2: Overview of the results of the different optimisations.

optimisation	normalised buckling load 1 [-]	normalised buckling load 2 [-]	normalised stiffness [-]	difference w.r.t. variable stiffness
CS	1.223	1.840	1.000	-40.0%
VS	2.042	2.473	1.000	0 %
LP, constant thickness	2.109	3.151	1.000	+ 3.3 %
LP, variable thickness	6.236	6.344	1.000	+205.4 %
VT	2.688	2.692	1.002	+ 31.6 %
VSVT with $\mathbf{d}_i$ (step 2.1)	3.798	3.799	1.011	+ 86.5 %
VSVT (step 2.1)	4.021	4.026	1.000	+ 96.9 %
VSVT with $\mathbf{d}_i$ (step 2.2)	4.229	4.233	1.000	+ 107.1 %
Best VSVT (step 2.2)	5.117	5.128	1.000	+ 150.6 %
Worst VSVT (step 2.2)	4.449	4.452	1.000	+ 117.8 %

Observing the results in Table 9.2, it is noticed that the stiffness constraint is always satisfied and always active. Furthermore, the difference between the result with and without stiffness constraint are generally small: the constant stiffness and variable stiffness variable thickness are hardly changing. The variable stiffness on the other hand does change considerably: even the optimum in terms of the LPs is decreased significantly. This can be due to the reduced capability to redistribute the load while satisfying the stiffness constraint. Using a constant stiffness laminate, the inner layers can be changed to cope with the stiffness constraint while the buckling load only slightly decreases. When the same idea is applied to variable stiffness laminates, the load redistribution capacity is decreased. Both the fibre angle and the thickness can be changed for variable stiffness, variable thickness laminates: by adding some stiffener-like reinforcements near the edges the stiffness constraint can be satisfied with a small influence on the buckling load. As usual, it is advantageous to redistribute the load to the supported edges.

Another remarkable result is that the variable stiffness laminate is almost as good as the optimised LP distribution. This is probably due to the limited load redistribution possible while satisfying the stiffness constraint, which indicates that

9

the steering constraint has a limited effect on the performance. As a final remark, it is noticed that the intuitive drop order is really bad: it is worse than the worst drop order checked during optimisation. The best drop order is [9 6 4 2 3 7 5 1 8], where ply 9, which is full in the intuitive drop order is dropped first. This shows that optimising the ply drop order is necessary: the difference in buckling load between the best and worst ply drop order is almost 90% of the buckling load of a QI laminate.

The fibre paths for the best buckling behaviour can be seen in Figure 9.6. The fibre angle distribution has hardly changed compared to the optimum without stiffness constraint: the middle of the plate is still going towards ±45°, almost all sides towards 0°, and ply 8 towards 90° at the sides. The topology on the other hand changes: all the partial plies have the stiffener-like topology. The size of the stiffeners changes, which is advantageous for manufacturing. It is clear that the change in topology is driven by the stiffness constraint, although it only has a limited effect on the buckling load as could be seen in Table 9.2.

This optimisation can be compared to an optimisation performed by Groh and Weaver[47]. They optimised a plate for minimum mass under buckling and static failure constraints. The manufacturing method in mind during the optimisation was the continuous tow shearing technique. This means that the fibre angle and thickness distribution are coupled, which was taken into account during the optimisation. Due to the other objective (mass minimisation versus buckling load maximisation), and different manufacturing technique, the results can only be compared in a qualitative sense. The thickness distribution is similar: the thickness builds up towards the side of the panel, just as in our result, but it is more gradually. Hence, similar results have been obtained using a completely different optimisation technique, indicating that the optimisation finds a feasible optimum.

When observing the lay-out of the different layers in Figures 9.5 and 9.6, it is clear that some post-processing is necessary. The edges are quite ragged which is most likely due to the optimiser wanting to use all volume allowed, and having to pick one full element, it cannot use half elements since the density has to go to zero or one. This could be solved by using a finer mesh, at the expense of increasing computational time, or one could perform a manual post-processing step in cooperation with manufacturing experts to remove the ragged edges and size the integrated stiffeners such that the lower bound on ply drop distance is adhered to. It is also observed that the fibre angle distribution of the parts of the plies that are void seem to have an influence: it is expected that stiffeners of 0° are the most efficient, but it seems that the fibres are going towards ±45° in the void part, and hence are also curved in the stiffener. However, this could also be in order to facilitate the load introduction into the stiffeners.
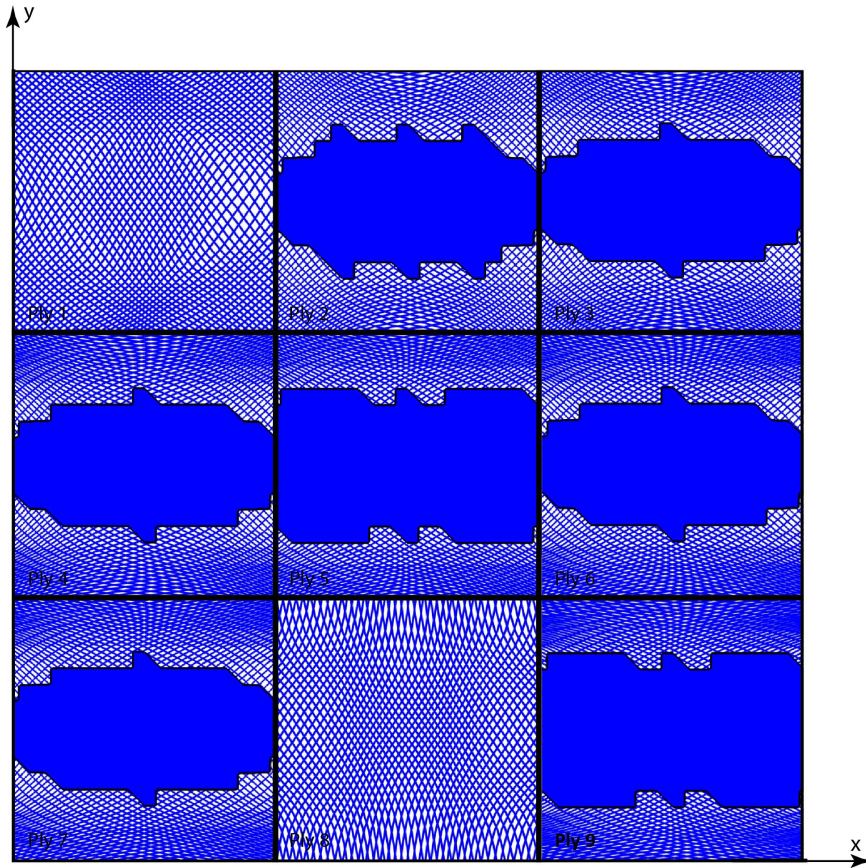
Figure 9.6: The best VSVT laminate after step 2.2.

9

Je schrijft geen boek als je er geen goesting in hebt.
You don't write a book when you don't feel like writing one.
Herman Brusselmans, Belgian writer

10

CONCLUSIONS AND RECOMMENDATIONS

10.1 CONCLUSION

In this thesis, an efficient optimisation algorithm for variable stiffness, variable thickness composite laminates has been developed. The number of finite element analyses necessary to find an optimised design is low. As a basis, the three-step optimisation approach of IJsselmuiden has been used. Step one, the optimisation of the stiffness distribution in terms of the lamination parameters, has been extended in this work to include the possibility to optimise the topology concurrently. Step two, fibre angle retrieval, has been transformed into an efficient fibre angle optimisation in the current work. Step three, fibre path retrieval, has not been extended in this work.

The optimisation is performed using the method of successive approximations. The basis of this algorithm are conservative, convex, separable approximations. A convex approximation of any structural response can be built in terms of the stiffness matrices by extending the idea of linear-reciprocal approximations. Using the principle of force approximations, the approximation in terms of the stiffness matrices can be used to build approximations in terms of the lamination parameters, fibre angle, and density distribution of either the complete laminate or of each ply. By adding an extra function, the so-called damping function, conser-

vativeness is guaranteed, ensuring the optimisation is globally convergent.

The option to concurrently optimise the topology of the structure and the stiffness distribution is introduced during the lamination parameter optimisation. Two methods to obtain a clear topology description were implemented and compared: implicit and explicit penalisation. The final design and computational cost of the two methods were comparable for the problem considered. In the end, explicit penalisation was determined to be the better option since it guarantees a clear topology description.

The majority of the work in this thesis focused on step two, where the fibre angle distribution is found. While in the original three-step optimisation approach this was just a retrieval step, it is turned into a full optimisation step in this thesis. The combination of retrieval and optimisation was shown to be computationally more efficient than pure fibre angle optimisation, which shows the validity of the idea behind the three-step approach. The current work, in this sense, is a direct extension of the original approach. Furthermore, it was shown that the structural performance after retrieval-optimisation is considerably better than after pure retrieval. Hence, the retrieval-optimisation approach combines a high computational efficiency with good structural performance at the optimum.

A steering constraint has been introduced during step two in this work to ensure the optimised design is manufacturable. The steering constraint has to be satisfied locally to avoid the fibre from wrinkling during manufacturing. To limit the number of gaps and overlaps, the average, or global, steering is limited as well. Since a lower steering radius also implies extra manufacturing time, and thus cost, the structural performance as a function of the lower steering bound was investigated. This showed that, if the lower bound on steering radius is small enough, the performance of the optimised design approaches the theoretical optimum found during step one of the three-step optimisation approach. This implies that although the optimiser finds a local optimum, the global optimum is at least satisfactorily approached.

A manufacturable outcome is a good start, but to increase the chance of industrial acceptance, the design should be feasible as well. This is taken into account in the current work by interpreting the design guidelines for non-conventional laminates, meaning laminates with fibre angles other than $0°$, $90°$, and $\pm 45°$. By interpreting the design guidelines and posing them as constraints, a lot of industrial experience, which cannot be quantified, is taken into account in the optimisation. One of the design guidelines interpreted is the ply-count percentage rule, which states that a certain percentage of the plies has to be in $0°$, $90°$, and $\pm 45°$ direction. It was shown that for a buckling optimisation, almost half of the improvement that could be achieved without the ply-count percentage rule was lost when the 'traditional' 10% rule was used. Still, a 28% improvement in buckling load was found compared to a reference conventional laminate. Hence, by sacrificing part of the performance improvement, the industrial feasibility of the optimised design

10

is increased.

The possibility to drop individual plies was included as a final addition to step two of the three-step optimisation approach. This leads to variable thickness laminates. It is possible to combine fibre steering and ply dropping to generate variable stiffness, variable thickness laminates. The fibre angle is always optimised concurrently with the ply drop location, independent of whether the fibre angle is steered or not. A topology-like optimisation of each ply is done with extra constraints to ensure continuity to optimise the ply drop location. The ply drop order is optimised based on the principle of stacking sequence tables, using an evolutionary optimisation algorithm. Promising results were obtained for a buckling optimisation problem employing this method.

Concluding, the optimisation of variable stiffness laminates leads to manufacturable designs, and additional constraints can be formulated to have industrially-feasible designs. This is seen as a first step towards certification of non-conventional laminates. When varying the thickness, the optimisation gives an optimised design, but some manual adjustments are necessary in order to find a manufacturable design. For example, the exact ply drop locations need to be slightly altered to adhere to the minimum distance between ply drops. These are usually small changes, hence the outcome of the optimisation is still useful.

10.2 OVERVIEW OF THE CONTRIBUTIONS OF THIS THESIS

The most important contributions of this thesis, and their possible use in other applications, can be summarised as follows:

- Efficient implementation of local steering constraint for variable stiffness laminates, in the form of a gradient constraint.

- Formulation of design guidelines for non-conventional laminates. The basic idea of the design guidelines is adhered to using this formulation, while they are more convenient to pose as constraints during optimisation.

- Implementation of design guidelines in a gradient-based composite optimisation. By taking the design guidelines into account during optimisation, the feasibility of the optimised design is improved. This could be a first (small) step towards certification. Probably, certification of non-conventional constant stiffness laminates is a first step, followed by variable thickness laminates with non-conventional fibre angles, while variable stiffness laminates will take the longest to find their way to industry.

- Combination of topology and stiffness optimisation. This gives the possibility to concurrently optimise the material properties and the location of the material is used.

10

- Gradient-based topology optimisation for variable thickness laminates, with constraints on the manufacturability and continuity of each ply. This leads to variable thickness laminates with non-conventional fibre angles, and smaller parts with the same thickness, which are more likely to be accepted by industry than variable stiffness laminates since there are no gaps and overlaps present. Since the stiffness changes over the structure, it may be a first step towards certification of non-conventional laminates with varying mechanical properties over the structure.

10.3 RECOMMENDATIONS

Even though the optimisation of variable stiffness laminates leads to manufacturable, feasible designs, some additional capabilities could be implemented. For example the balanced layers: currently a $-\theta$ layer is always next to the $+\theta$ layer. This could be easily extended to allow balanced layers to be non-adjacent. As long as symmetry is preserved, the location of the balanced layer is not important, and could lead to a (slightly) improved structural performance. The requirement that the laminate has to be symmetric is possibly the largest limitation of the code: it is not possible to take advantage of any extension-bending coupling using the current code. Overcoming this would require taking the B-matrix into account in approximating structural responses, which requires expanding the level one approximation. The level two approximations would not change.

The dispersion of plies is another possible improvement: one could not only define a lower bound on the difference between adjacent plies, but define it between multiple layers, to be sure the plies are better dispersed. By defining this lower bound between multiple layers, the plies would be guaranteed to be spread over a wider angle range. It was noticed in the numerical tests throughout this thesis that most of the time, the dispersion of the angles was low if no constraint was posed on it. By having a lower bound between consecutive layers, it was noted that two angles were sometimes repeated, which can be avoided by having a lower bound between multiple layers. A possible disadvantage of this idea is that the optimiser is more likely to get stuck in a local optimum.

The development of the variable thickness optimisation is not yet as advanced as the variable stiffness optimisation, hence more opportunities for future development can be identified. One, the ply drop locations should be automatically optimised such that a minimum distance between ply drops is adhered to. Currently, this is assumed to be a manual post-processing step. Implementing it in the optimisation would reduce the time spent between optimisation and manufacturing. Two, when using AFP, a minimum length needs to be laid down. This should be implemented in the optimisation since now small regions of some layers have to be either removed, or made larger to make them manufacturable. Im-

10

plementation is not as straightforward as it may seem at first sight: the distance laid down is a function of both the shape that is laid down, and the fibre angle. One possibility would be to chose the shape such that a minimum distance is laid down for any fibre angle.

Some limitations in terms of ply drop orders can be found as well. One, the dropping order is currently the same all over the structure, it may be possible to define different dropping orders in different regions of the structure, as long as continuity is maintained. For example, if a certain region of the structure thickens locally, one may consider to have different fibre angles on both sides, as is shown in Figure 10.1, however, this is not possible with the current code. Two, one may consider the possibility to define different fibre angles for the parts of the 'same' layer that are not connected, and thus have to be manufactured separately anyway. This means that when a ply is dropped and later added again, the fibre angle can be changed completely, since these are different parts in the structure. From a manufacturing point-of-view this is easy, from an optimisation point-of-view this is quite challenging since the present formulation does not keep track of the connectivity of layers.

Figure 10.1: Ply drop pattern not possible with the current optimisation strategy.

Finally, step three of the three-step optimisation approach should be worked out in more detail to automatically generate the fibre paths and cut positions, hence the tow-by-tow description of the structure for the AFP machine. Some manual post-processing will be necessary before manufacturing the part, but if the tow-by-tow description is defined automatically, the amount of manual work will be reduced considerably. When the exact tow-by-tow description is being defined, other considerations such as location of gaps and/or overlaps can be optimised. This would require more investigation into the effect of these 'defects' on the structural performance. Once this is available, step three may also be turned into a fibre path optimisation rather than the current fibre path retrieval. With these improvements the three-step optimisation approach can reach its full potential, generating manufacturable, feasible designs that could lead to a reduced structural weight.

10

$\mathbf{A}$
DETERMINING THE INITIAL DAMPING FACTOR

For the stiffness approximation, a move limit in terms of stiffness matrices is used[59]. This leads to

$$\overset{I}{\zeta}^2 = \frac{w_i}{2} \cdot \left(\left(||\boldsymbol{\phi}_m : \mathbf{A}^{-1} - \boldsymbol{\psi}_m : \mathbf{A}|| \right)^2 + \left(||\boldsymbol{\phi}_b : \mathbf{D}^{-1} - \boldsymbol{\psi}_b : \mathbf{D}|| \right)^2 \right). \qquad \text{(A.1)}$$

This is not guaranteed to give a non-zero value, hence the inequality

$$||\mathbf{A} - \mathbf{B}|| \leq ||\mathbf{A}|| + ||\mathbf{B}|| \qquad \text{(A.2)}$$

is used to ensure a non-zero value of the damping factor, leading to

$$\overset{I}{\zeta}^2 = \frac{w_i}{2} \cdot \left(\left(||\boldsymbol{\phi}_m : \mathbf{A}^{-1}|| + ||\boldsymbol{\psi}_m : \mathbf{A}|| \right)^2 + \left(||\boldsymbol{\phi}_b : \mathbf{D}^{-1}|| + ||\boldsymbol{\psi}_b : \mathbf{D}|| \right)^2 \right). \quad \text{(A.3)}$$

To determine the initial $\overset{II}{\zeta}_\theta$, consider the general approximation:

$$\overset{II}{f}(\theta) = \overset{I}{f}_0 + \mathbf{g} \cdot \Delta\boldsymbol{\theta} + \Delta\boldsymbol{\theta}^T \left(\mathbf{H} + \overset{II}{\zeta}_\theta \mathbf{H}_d \right) \Delta\boldsymbol{\theta}, \qquad \text{(A.4)}$$

where $\mathbf{H}_d$ denotes regularisation matrix. The optimality criterion is

$$-\mathbf{g} = \left(\mathbf{H} + \overset{II}{\zeta}_\theta \mathbf{H}_d \right) \Delta\boldsymbol{\theta}. \qquad \text{(A.5)}$$

$\Delta\boldsymbol{\theta}$ can be found to be

$$\Delta\boldsymbol{\theta} = -\left(\mathbf{H} + \overset{II}{\zeta}_{\theta}\mathbf{H}_d\right)^{-1}\mathbf{g}. \tag{A.6}$$

Assuming that the damping function has a value of 1 at the new iterate,

$$\frac{1}{2}\Delta\boldsymbol{\theta}^T\mathbf{H}_d\Delta\boldsymbol{\theta} = 1, \tag{A.7}$$

and the Hessian of the approximation $\mathbf{H}$ is zero, combining eqs. (A.6) and (A.7), the initial damping factor is found to be

$$\overset{II}{\zeta}{}_{\theta}^2 = \frac{1}{2}\cdot\left(\mathbf{g}^T\cdot\mathbf{H}_d^{-1}\cdot\mathbf{g}\right). \tag{A.8}$$

B

SOLUTION PROCEDURE OF THE OPTIMISATION PROBLEM WITH DESIGN GUIDELINES

Starting from the Lagrangian, eq. (7.20), the matrices of the positive semi-definite constraint are rewritten. Instead of the 2-dimensional arrays $\mathbf{X}_i$, one can also define a 3-dimensional array $\boldsymbol{\mathcal{X}}$, such that $\boldsymbol{\mathcal{X}}_{abi} = \mathbf{X}_i$. Defining two operators:

$$\boldsymbol{\mathcal{X}}^T \cdot \mathbf{Y} = \sum_{i=1}^{L} \boldsymbol{\mathcal{X}}_{abi} \cdot \mathbf{Y}_{ab} \tag{B.1}$$

$$\boldsymbol{\mathcal{X}} \cdot \mathbf{x} = \sum_{i=1}^{L} \boldsymbol{\mathcal{X}}_{abi} \cdot \mathbf{x}_i. \tag{B.2}$$

The optimality conditions are found to be

$$
\begin{aligned}
-r_{x_j} &= \mathbf{g} + \zeta_1 \cdot \mathbf{g}^{(1)} - \boldsymbol{\mathcal{X}}^T \cdot \mathbf{Y} + \zeta_2 \left(\mathbf{Y} : \mathbf{I}\right) \mathbf{g}^{(2)} + \\
&\quad \sum_k \lambda_k \cdot \left(\frac{\partial \hat{g}}{\partial x_j} + \zeta_3 \cdot \frac{\partial d_{3k}}{\partial x_j} \right) + \sum_k \gamma_k \cdot \left(\frac{\partial \hat{h}}{\partial x_j} + \zeta_4 \cdot \frac{\partial d_{4k}}{\partial x_j} \right) \\
-r_{\lambda_k} &= \hat{g} + \zeta_3 \cdot d_{(3k)}(x) + s_{g_k} \\
-r_{\gamma_k} &= \hat{h} + \zeta_4 \cdot d_{(4k)}(x) + s_{h_k} \\
-r_{s_{g_k}} &= \lambda_k \cdot s_{g_k} - \mu \\
-r_{s_{h_k}} &= \gamma_k \cdot s_{h_k} - \mu \\
-r_{\mathbf{Y}} &= -\mathbf{X}_0 - \boldsymbol{\mathcal{X}}^T \cdot \mathbf{x} + \alpha \cdot \mathbf{I} + \zeta_2 d_2(x) \cdot \mathbf{I} + \mathbf{Z} \\
-r_{\mathbf{Z}} &= \mathbf{Z} \cdot \mathbf{Y} - \mu \cdot \mathbf{I},
\end{aligned}
\tag{B.3}
$$

where the criteria of the slack variables have been multiplied with the slacks to avoid numerical problems.[172] Linearising these equations leads to

$$
\begin{aligned}
r_{x_j} &= \mathbf{H} \cdot \mathbf{dx} + \zeta_1 \mathbf{H}^{(1)} \cdot \mathbf{dx} + \zeta_2 \left(\mathbf{Y} : \mathbf{I}\right) \cdot \mathbf{H}^{(2)} \cdot \mathbf{dx} - \boldsymbol{\mathcal{X}}^T \cdot \mathbf{dY} + \zeta_2 \left(\mathbf{dY} : \mathbf{I}\right) \cdot \mathbf{g}^{(2)} + \\
&\quad \left(\frac{\partial \hat{g}}{\partial x_j} + \zeta_3 \cdot \frac{\partial d_{3k}}{\partial x_j} \right) d\lambda_k + \left(\frac{\partial \hat{h}}{\partial x_j} + \zeta_4 \cdot \frac{\partial d_{4k}}{\partial x_j} \right) d\gamma_k \\
r_{\gamma_k} &= \sum_j \frac{\partial \hat{h}}{\partial \theta_j} dx_j + \zeta_4 \sum_j \frac{\partial d_{4j}}{\partial \theta_j} dx_j + ds_{h_k} \\
r_{\lambda_k} &= \sum_j \frac{\partial \hat{g}}{\partial \theta_j} dx_j + \zeta_3 \sum_j \frac{\partial d_{3j}}{\partial \theta_j} dx_j + ds_{g_k} \\
r_{s_g} &= d\lambda_k \cdot s_{g_k} + \lambda \cdot ds_{g_k} \\
r_{s_h} &= d\gamma_k \cdot s_{h_k} + \lambda \cdot ds_{h_k} \\
r_{\mathbf{Y}} &= -\boldsymbol{\mathcal{X}} \cdot \mathbf{dx} + \zeta_2 \left(\mathbf{g}^{(2)T} \cdot \mathbf{dx} \right) \cdot \mathbf{I} + \mathbf{dZ} \\
r_{\mathbf{Z}} &= \mathbf{dZ} \cdot \mathbf{Y} + \mathbf{Z} \cdot \mathbf{dY}.
\end{aligned}
\tag{B.4}
$$

Defining $\boldsymbol{\lambda}$, $\boldsymbol{\gamma}$, $\mathbf{S_g}$ and $\mathbf{S_h}$ as the diagonal matrices containing λ_k, γ_k, s_{g_k} and s_{h_k} on their diagonal, the linearisation can be rewritten as

$$
\begin{aligned}
r_x &= \mathbf{H_i} \cdot \mathbf{dx} - \boldsymbol{\mathcal{X}}^T \cdot \mathbf{dY} + \zeta_2 \left(\mathbf{dY} : \mathbf{I}\right) \cdot \mathbf{g}^{(2)} + \hat{\mathbf{G}}^T \mathbf{d\lambda} + \hat{\mathbf{H}}^T \mathbf{d\gamma} \\
r_\lambda &= \hat{\mathbf{G}} \cdot \mathbf{dx} + \mathbf{dS_g} \\
r_\gamma &= \hat{\mathbf{H}} \cdot \mathbf{dx} + \mathbf{dS_h} \\
r_{S_g} &= \mathbf{d\lambda} \cdot \mathbf{S_g} + \boldsymbol{\lambda} \cdot \mathbf{dS_g} \\
r_{S_h} &= \mathbf{d\gamma} \cdot \mathbf{S_h} + \boldsymbol{\gamma} \cdot \mathbf{dS_h},
\end{aligned}
\tag{B.5}
$$

where the rows k of $\hat{\mathbf{G}}$ and $\hat{\mathbf{H}}$ are constructed according to

$$
\hat{\mathbf{G}}_k = \frac{\partial \hat{g}_k}{\partial x_j} + \zeta_3 \cdot \frac{\partial d_{3k}}{\partial x_j}
\tag{B.6}
$$

$$
\hat{\mathbf{H}}_k = \frac{\partial \hat{h}_k}{\partial x_j} + \zeta_4 \cdot \frac{\partial d_{4k}}{\partial x_j}.
\tag{B.7}
$$

$d\mathbf{S_g}$, $d\mathbf{S_h}$, $d\boldsymbol{\lambda}$, $d\boldsymbol{\gamma}$, $d\mathbf{Z}$, and $d\mathbf{Y}$ can be found to be

$$
\begin{aligned}
d\boldsymbol{\lambda} &= \mathbf{S_g}^{-1} \cdot \left(\mathbf{r_{s_g}} - \boldsymbol{\lambda} d\mathbf{S_g}\right) \\
d\boldsymbol{\gamma} &= \mathbf{S_h}^{-1} \cdot \left(\mathbf{r_{s_h}} - \boldsymbol{\gamma} d\mathbf{S_h}\right) \\
d\mathbf{S_g} &= \mathbf{r_\lambda} - \hat{\mathbf{G}} d\mathbf{x} \\
d\mathbf{S_h} &= \mathbf{r_\gamma} - \hat{\mathbf{H}} d\mathbf{x} \\
d\mathbf{Z} &= r_{\mathbf{Y}} + \boldsymbol{\mathcal{X}} \cdot d\mathbf{x} - \zeta_2 \left(\mathbf{g}^{(2)T} \cdot d\mathbf{x}\right) \cdot \mathbf{I} \\
d\mathbf{Y} &= \mathbf{Z}^{-1} \cdot r_{\mathbf{z}} - \mathbf{Z}^{-1} \cdot d\mathbf{Z} \cdot \mathbf{Y}.
\end{aligned}
\tag{B.8}
$$

Filling this into the equation for r_x leads to

$$
\begin{aligned}
r_x &= \mathbf{H_i} \cdot d\mathbf{x} + \\
&\quad \zeta_2 \left(\left(\mathbf{Z}^{-1}\mathbf{r_z} - \mathbf{Z}^{-1}\left(\mathbf{r_y} + (\boldsymbol{\mathcal{X}} \cdot d\mathbf{x}) - \zeta_2\left(\mathbf{g}^{(2)T}d\mathbf{x}\right)\mathbf{I}\right)\mathbf{Y}\right) : \mathbf{I}\right)\mathbf{g}^{(2)} - \\
&\quad \boldsymbol{\mathcal{X}}^T \cdot \left(\mathbf{Z}^{-1}\mathbf{r_z} - \mathbf{Z}^{-1}\left(\mathbf{r_y} + \boldsymbol{\mathcal{X}} \cdot d\mathbf{x} - \zeta_2\left(\mathbf{g}^{(2)T}d\mathbf{x}\right)\mathbf{I}\right)\mathbf{Y}\right) + \\
&\quad \hat{\mathbf{G}}^T \cdot \mathbf{S_g}^{-1} \cdot \left(\mathbf{r_{s_g}} - \boldsymbol{\lambda}\left(\mathbf{r_\lambda} - \hat{\mathbf{G}} d\mathbf{x}\right)\right) + \\
&\quad \hat{\mathbf{H}}^T \cdot \mathbf{S_h}^{-1} \cdot \left(\mathbf{r_{s_h}} - \boldsymbol{\gamma}\left(\mathbf{r_\gamma} - \hat{\mathbf{H}} d\mathbf{x}\right)\right).
\end{aligned}
\tag{B.9}
$$

Rewriting leads to

$$
\begin{aligned}
r_x - \zeta_2 &\left(\left(\mathbf{Z}^{-1}\mathbf{r_z} - \mathbf{Z}^{-1}\mathbf{r_y}\mathbf{Y}\right) : \mathbf{I}\right)\mathbf{g}^{(2)} + \\
&\qquad\qquad \boldsymbol{\mathcal{X}}^T \cdot \left(\mathbf{Z}^{-1}\mathbf{r_z} - \mathbf{Z}^{-1}\mathbf{r_y}\mathbf{Y}\right) \\
-\hat{\mathbf{G}}^T \cdot \mathbf{S_g}^{-1} &\cdot \mathbf{r_{s_g}} + \hat{\mathbf{G}}^T \cdot \mathbf{S_g}^{-1} \cdot \boldsymbol{\lambda} \cdot \mathbf{r_\lambda} - \\
\hat{\mathbf{H}}^T \cdot \mathbf{S_h}^{-1} &\cdot \mathbf{r_{s_h}} + \hat{\mathbf{H}}^T \cdot \mathbf{S_h}^{-1} \cdot \boldsymbol{\gamma} \cdot \mathbf{r_\gamma} = \\
\mathbf{H_i} \cdot d\mathbf{x} - \zeta_2 &\left(\left(\mathbf{Z}^{-1}\left(\boldsymbol{\mathcal{X}} \cdot d\mathbf{x}\right)\mathbf{Y}\right) : \mathbf{I}\right)\mathbf{g}^{(2)} + \\
\zeta_2^2 &\left(\mathbf{Z}^{-1}\left(\mathbf{g}^{(2)T}\right)d\mathbf{x}\mathbf{I}\mathbf{Y} : \mathbf{I}\right)\mathbf{g}^{(2)} + \\
\boldsymbol{\mathcal{X}}^T\mathbf{Z}^{-1}\left(\boldsymbol{\mathcal{X}} \cdot d\mathbf{x}\right)\mathbf{Y} &- \zeta_2\boldsymbol{\mathcal{X}}^T\mathbf{Z}^{-1}\left(\mathbf{g}^{(2)T}d\mathbf{x}\right)\mathbf{I}\mathbf{Y} + \\
\left(\hat{\mathbf{G}}^T \cdot \mathbf{S_g}^{-1} \cdot \boldsymbol{\lambda} \cdot \hat{\mathbf{G}}\right) &\cdot d\mathbf{x} + \left(\hat{\mathbf{H}}^T \cdot \mathbf{S_h}^{-1} \cdot \boldsymbol{\gamma} \cdot \hat{\mathbf{H}}\right) \cdot d\mathbf{x}.
\end{aligned}
\tag{B.10}
$$

The part related to the positive semi-definite constraint, line three and four in eq. (B.10), needs to be rewritten in the form $\mathbf{V} \cdot d\mathbf{x}$. Most parts can be written

B

as (sum of) 2-dimensional arrays:

$$
\begin{aligned}
\boldsymbol{\mathcal{X}}^T \mathbf{Z}^{-1} \left(\mathbf{g}^{(2)T} \mathbf{dx} \right) \mathbf{IY} &= \boldsymbol{\mathcal{X}}^T \mathbf{Z}^{-1} \mathbf{Y} \cdot \mathbf{g}^{(2)T} \mathbf{dx} \\
&= \sum_i \mathbf{X_i}^T \mathbf{Z}^{-1} \mathbf{Y} \cdot \mathbf{g}^{(2)T} dx_i \\
&= \mathbf{b}^{(2)} \mathbf{g}^{(2)} \mathbf{dx} \\
\left(\mathbf{Z}^{-1} \left(\boldsymbol{\mathcal{X}} \cdot \mathbf{dx} \right) \mathbf{Y} : \mathbf{I} \right) \mathbf{g}^{(2)} &= tr \left(\mathbf{Z}^{-1} \left(\boldsymbol{\mathcal{X}} \cdot \mathbf{dx} \right) \mathbf{Y} \right) \mathbf{g}^{(2)} \\
&= \sum_i tr \left(\mathbf{Z}^{-1} \mathbf{X_i} \mathbf{Y} \right) \mathbf{g}^{(2)} dx_i \\
&= \mathbf{b}^{(1)} \mathbf{g}^{(2)} \mathbf{dx} \\
\left(\mathbf{Z}^{-1} \left(\mathbf{g}^{(2)T} \mathbf{dx} \right) \mathbf{IY} : \mathbf{I} \right) \mathbf{g}^{(2)} &= tr \left(\mathbf{Z}^{-1} \left(\mathbf{g}^{(2)T} \mathbf{dx} \right) \mathbf{IY} \right) \mathbf{g}^{(2)} \\
&= tr \left(\mathbf{Z}^{-1} \mathbf{Y} \right) \mathbf{g}^{(2)} \mathbf{g}^{(2)T} \mathbf{dx} \\
&= \mathbf{H}^{(7)} \mathbf{dx},
\end{aligned}
\tag{B.11}
$$

with

$$
\begin{aligned}
\mathbf{b} &= tr \left(\mathbf{Z}^{-1} \mathbf{X_i} \mathbf{Y} \right) \\
\mathbf{H}^{(7)} &= tr \left(\mathbf{Z}^{-1} \mathbf{Y} \right) \mathbf{g}^{(2)} \mathbf{g}^{(2)T}.
\end{aligned}
\tag{B.12}
$$

For the first part of the fourth line this cannot be done. Hence, it is rewritten as

$$
\boldsymbol{\mathcal{X}}^T \mathbf{Z}^{-1} \left(\boldsymbol{\mathcal{X}} \cdot \mathbf{dx} \right) \mathbf{Y} = \boldsymbol{\mathcal{X}}^T \mathbf{Z}^{-1} \boldsymbol{\mathcal{X}}^T \cdot \mathbf{Y} \cdot \mathbf{dx} = \mathbf{H}^{(6)} \cdot \mathbf{dx}.
\tag{B.13}
$$

Since the 3-dimensional arrays are not defined in a matrix-environment, one has to use

$$
\mathbf{H}^{(6)}{}_{ij} = \left[\boldsymbol{\mathcal{X}}^T \mathbf{Z}^{-1} \boldsymbol{\mathcal{X}}^T \cdot \mathbf{Y} \right]_{ij} = \left(\mathbf{X_i} \cdot \mathbf{Z}^{-1} \cdot \mathbf{X_j} \right) : \mathbf{Y}.
\tag{B.14}
$$

To determine the primal step size, the slack $\mathbf{Z}$ should stay positive semi-definite; to determine the dual step size, the dual variable $\mathbf{Y}$ should stay positive semi-definite. Using

$$
\left(\mathbf{Z} + \eta \mathbf{dZ} \right) \mathbf{a} = \mathbf{0},
\tag{B.15}
$$

the maximum step size is the smallest negative eigenvalue.

Observing the equations in this appendix, it is noticed that only the expression for r_x and the Hessian are influenced by the additional constraints. Hence, posing multiple constraints in the same optimisation problem only influences these expressions, the size of the problem that is solved is not influenced.

BIBLIOGRAPHY

[1] A350xwb technology. `http://www.airbus.com/aircraftfamilies/passengeraircraft/a350xwbfamily/technology-and-innovation`. Accessed: 10 November 2015.

[2] Boeing 787 from the gound up. `http://www.boeing.com/commercial/aeromagazine/articles/qtr_4_06/AERO_Q406_article4.pdf`. Accessed: 10 November 2015.

[3] Hexcel presentation. `https://www.sec.gov/Archives/edgar/data/717605/000110465908025101/a08-11139_1defa14a.htm`. Accessed: 26 August 2016.

[4] NLR report: AUTOW. `http://reports.nlr.nl:8080/xmlui/bitstream/handle/10921/967/TP-2008-789.pdf?sequence=1`. Accessed: 26 August 2016.

[5] T. Abatzoglou and B. O'Donnell. Minimization by coordinate descent. *Journal of optimization theory and applications*, 36: 163 – 174, 1982.

[6] M. M. Abdalla, C. Kassapoglou, and Z. Gürdal. Formulation of composite laminate robustness constraint in lamination parameters space. In *50th AIAA/ASME/ASCE/AHS/ASC Structures, Structural Dynamics and Materials Conference*. American Institute of Aeronautics and Astronautics, 2009.

[7] M.M. Abdalla, S. Setoodeh, and Z. Gürdal. Design of variable stiffness composite panels for maximum fundamental frequency using lamination parameters. *Composite Structures*, 81(2):283 – 291, 2007.

[8] D.B. Adams, L.T. Watson, Z. Gürdal, and C. M. Anderson-Cook. Genetic algorithm optimization and blending of composite laminates by locally reducing laminate thickness. *Advances in Engineering Software*, 35(1):35 – 43, 2004.

[9] J.A. Bailie, R.P. Ley, and A. Pasricha. A summary and review of composite laminate design guidelines. *Langley RC, Hampton*, 1997.

[10] S.W. Beckwith. Designing with composites: Suggested best practices rules. *SAMPE journal*, 45:36 – 37, 2009.

[11] M.P. Bendsøe. Optimal shape design as a material distribution problem. *Structural optimization*, 1(4):193–202, 1989.

[12] M.P. Bendsøe and N. Kikuchi. Generating optimal topologies in structural design using a homogenization method. *Computer Methods in applied mechanics and engineering*, 71:197 – 224, 1988.

[13] M.P. Bendsøe and O. Sigmund. *Topology Optimization: Theory, Methods and Applications*. Springer, 1995.

[14] A.W. Blom. *Strucural Performance of Fibre-Placed Variable-Stiffness Composite Conical and Cylindrical Shells*. Ph.D. thesis, Delft University of Technology, 2010.

[15] A.W. Blom, M.M. Abdalla, and Z. Gürdal. Optimization of course locations in fiber-placed panels for general fiber angle distributions. *Composites Science and Technology*, 70(4):564 – 570, 2010.

[16] A.W. Blom, C.S. Lopes, P.J. Kromwijk, Z. Gürdal, and P.P. Camanho. A theoretical model to study the influence of tow-drop areas on the stiffness and strength of variable-stiffness laminates. *Journal of Composite Materials*, 43(5):403–425, 2009.

[17] A.W. Blom, S. Setoodeh, J.M.A.M. Hol, and Z. Gürdal. Design of variable-stiffness conical shells for maximum fundamental eigenfrequency. *Computers and Structures*, 86(9):870 – 878, 2008.

[18] A.W. Blom, P.B. Stickler, and Z. Gürdal. Optimization of a composite cylinder under bending by tailoring stiffness properties in circumferential direction. *Composites Part B: Engineering*, 41(2):157 – 165, 2010.

[19] A.W. Blom, B.F. Tatting, J.M.A.M. Hol, and Z. Gürdal. Fiber path definitions for elastically tailored conical shells. *Composites Part B: Engineering*, 40(1):77 – 84, 2009.

[20] M.W. Bloomfield, C.G. Diaconu, and P.M. Weaver. On feasible regions of lamination parameters for lay-up optimization of laminated composites. *Proceedings of the Royal Society of London A: Mathematical, Physical and Engineering Sciences*, 465(2104):1123–1143, 2009.

[21] L.B. Booker, D.E. Goldberg, and J.H. Holland. Classifier systems and genetic algorithms. *Artificial intelligence*, 40(1):235–282, 1989.

[22] S. Boyd and L. Vandenberghe. *Convex optimisation*. Cambridge university press, 2004.

[23] C.J. Brampton, C.K. Wu, and A.H. Kim. New optimization method for steered fiber composites using the level set method. *Structural and Multidisciplinary Optimization*, 52(3):493–505, 2015.

[24] T.R. Brooks, G. Kennedy, and J. Martins. High-fidelity aerostructural optimization of a high aspect ratio tow-steered wing. In *Proceedings of the 57th AIAA/ASCE/AHS/ASC Structures, Structural Dynamics, and Materials Conference*, 2016.

[25] M. Bruyneel. SFP–a new parameterization based on shape functions for optimal material selection: application to conventional composite plies. *Structural and Multidisciplinary Optimization*, 43(1):17–27, 2011.

[26] M. Bruyneel, P. Duysinx, and C. Fleury. A family of mma approximations for structural optimization. *Structural and Multidisciplinary Optimization*, 24(4):263–276, 2002.

[27] M. Bruyneel, P. Duysinx, C. Fleury, and T. Gao. Extensions of the shape functions with penalization parameterization for composite-ply optimization. *AIAA Journal*, 49(10):2325–2329, 2016/05/12 2011.

[28] S. Buchanan. Development of a wingbox rib for a passenger jet aircraft using design optimization and constrained to traditional design and manufacture requirements. In *Proceedings of CAE Technology Conference*, volume 2007, 2007.

[29] L.-W. Chang, S.-S. Yau, and T.-W. Chou. Notched strength of woven fabric composites with moulded-in holes. *Composites*, 18(3):233 – 241, 1987.

[30] F.L. Chernousko and A.A. Lyubushin. Method of successive approximations for solution of optimal control problems. *Optimal Control Applications and Methods*, 3(2):101–114, 1982.

[31] B.H. Coburn, Z. Wu, and P.M. Weaver. Buckling analysis and optimization of blade stiffened variable stiffness panels. In *Proceedings of the 56th AIAA/ASCE/AHS/ASC Structures, Structural Dynamics, and Materials Conference*, 2015.

[32] The Boeing Company. Curved fiber paths for composite laminates, 2011. US Patent 8,756,037.

[33] K. Croft, L. Lessard, D. Pasini, M. Hojjati, J. Chen, and A. Yousefpour. Experimental study of the effect of automated fiber placement induced defects on performance of composite laminates. *Composites Part A: Applied Science and Manufacturing*, 42(5):484 – 491, 2011.

[34] P.J. Crothers, K. Drechsler, D. Feltin, I. Herszberg, and T. Kruckenberg. Tailored fibre placement to minimise stress concentrations. *Composites Part A: Applied Science and Manufacturing*, 28(7):619 – 625, 1997.

[35] G. Delgado. *Optimization of composite structures: A shape and topology sensitivity analysis.* Phd thesis, Ecole Polytechnique X, June 2014.

[36] C.L. Dym and I.H. Shames. Nonlinear elasticity. In *Solid Mechanics*, pages 449–492. Springer New York, 2013.

[37] D.O. Evans. Fiber placement. In S.T. Peters, editor, *Handbook of Composites*, pages 476–487. Springer US, 1998.

[38] K. Fayazbakhsh, M.A. Nik, D. Pasini, and L. Lessard. Defect layer method to capture effect of gaps and overlaps in variable stiffness laminates made by automated fiber placement. *Composite Structures*, 97:245 – 251, 2013.

[39] C.A. Felippa. *Introduction to finite element methods.* University of Colorado, Boulder, 2001.

[40] C. Fleury. Conlin: An efficient dual optimizer based on convex approximation concepts. *Structural optimization*, 1(2):81–89, 1989.

[41] C. Fleury and V. Braibant. Structural optimization: A new dual method using mixed variables. *International Journal for Numerical Methods in Engineering*, 23(3):409–428, 1986.

[42] J. Foldager, J.S. Hansen, and N. Olhoff. A general approach forcing convexity of ply angle optimization in composite laminates. *Structural optimization*, 16(2-3):201–211, 1998.

[43] T. Gao, W. Zhang, and P. Duysinx. A bi-value coding parameterization scheme for the discrete optimal orientation design of the composite laminate. *International Journal for Numerical Methods in Engineering*, 91(1):98–114, 2012.

[44] T. Gao, W.H. Zhang, and P. Duysinx. Simultaneous design of structural layout and discrete fiber orientation using bi-value coding parameterization and volume constraint. *Structural and Multidisciplinary Optimization*, 48(6):1075–1088, 2013.

[45] H. Ghiasi, D. Pasini, and L. Lessard. Optimum stacking sequence design of composite materials part i: Constant stiffness design. *Composite Structures*, 90(1):1 – 11, 2009.

[46] D.E. Goldberg. *Genetic algorithms in search, optimization, and machine learning.* Addison-Wesley Pub. Co, Reading, Mass, 1989.

[47] R.M.J. Groh and P.M. Weaver. Mass optimization of variable angle tow, variable thickness panels with static failure and buckling constraints. In *56th AIAA/ASME/ASCE/AHS/ASC Structures, Structural Dynamics and Materials Conference*, January 2015.

160

[48] L.K. Grunenfelder, N. Suksangpanya, C. Salinas, G. Milliron, N. Yaraghi, S. Herrera, K. Evans-Lutterodt, S.R. Nutt, P. Zavattieri, and D. Kisailus. Bio-inspired impact-resistant composites. *Acta Biomaterialia*, 10(9):3997 – 4008, 2014. Biomineralization.

[49] Z. Gürdal and R. Olmedo. In-plane response of laminates with spatially varying fiber orientations - variable stiffness concept. *AIAA Journal*, 31(4):751–758, 2014/11/30 1993.

[50] Z. Gürdal, B. Tatting, and C.K. Wu. Tow-placement technology and fabrication issues for laminated composite structures. In *46th AIAA/ASME/ASCE/AHS/ASC Structures, Structural Dynamics and Materials Conference*. American Institute of Aeronautics and Astronautics, 2014/11/30 2005.

[51] Z. Gürdal, B.F. Tatting, and C.K. Wu. Variable stiffness composite panels: effects of stiffness variation on the in-plane and buckling response. *Composites Part A: Applied Science and Manufacturing*, 39(5):911–922, 2008.

[52] R.T. Haftka and Z. Gürdal. *Elements of Structural Optimization*. Contributions to Phenomenology. Springer Netherlands, 1992.

[53] V.B. Hammer, M.P. Bendsøe, R. Lipton, and P. Pedersen. Parametrization in laminate design for optimal compliance. *International Journal of Solids and Structures*, 34(4):415 – 434, 1997.

[54] C.T. Herakovich. On the relationship between engineering properties and delamination of composite materials. *Journal of Composite Materials*, 15:336–348, 1981.

[55] J.H. Holland and J.S. Reitman. Cognitive systems based on adaptive algorithms. *SIGART Bull.*, (63):49–49, June 1977.

[56] S. Honda, Y. Narita, and K. Sasaki. Discrete optimization for vibration design of composite plates by using lamination parameters. *Advanced Composite Materials*, 18(4):297–314, 2009.

[57] M. Wand Hyer, R.J. Rust, and W.A. Waters Jr. Innovative design of composite structures: design. manufacturing and testing of plates utilizing curvilinear fiber trajectories. In *NASA Contractor Report 197045*, 1994.

[58] M.W. Hyer and H.H. Lee. The use of curvilinear fiber format to improve buckling resistance of composite plates with central circular holes. *Composite Structures*, 18(3):239 – 261, 1991.

[59] S.T. IJsselmuiden. *Optimal design of variable stffness composite structures using lamination parameters*. Ph.D. thesis, Delft University of Technology, 2011.

[60] S.T. Ijsselmuiden, M.M. Abdalla, and Z. Gürdal. Implementation of strength-based failure criteria in the lamination parameter design space. *AIAA Journal*, 46(7):1826–1834, 2015/04/15 2008.

[61] S.T. Ijsselmuiden, M.M. Abdalla, and Z. Gürdal. Optimization of variable-stiffness panels for maximum buckling load using lamination parameters. *AIAA Journal*, 48(1):134–143, 2010.

[62] S.T. IJsselmuiden, M.M. Abdalla, O. Seresta, and Z. Gürdal. Multi-step blended stacking sequence design of panel assemblies with buckling constraints. *Composites Part B: Engineering*, 40(4):329 – 336, 2009.

[63] I.N. Imam. The schur complement and the inverse m-matrix problem. *Linear Algebra and its Applications*, 62:235 – 240, 1984.

[64] F.-X. Irisarri, M.M. Abdalla, and Z. Gürdal. Improved shepard's method for the optimization of composite structures. *AIAA Journal*, 49(12):2726–2736, 2016/05/23 2011.

[65] F.-X. Irisarri, A. Lasseigne, F.-H. Leroy, and R. Le Riche. Optimal design of laminated composite structures with ply drops using stacking sequence tables. *Composite Structures*, 107(0):559 – 569, 2014.

[66] F.-X. Irisarri, D.M.J. Peeters, and M.M. Abdalla. Optimisation of ply drop order in variable stiffness laminates. *Composite Structures*, pages –, 2016.

[67] J.C. Jaeger. *Elementary theory of elastic plates.* Pergamon press, 1964.

[68] D.C. Jegley, B.F. Tatting, and Z. Gürdal. Optimization of elastically tailored tow-placed plates with holes. In *Proceedings of the AIAA/ASME/ASCE/AHS/ASC 44th Structures, Structural Dynamics and Materials Conference, Norfolk, VA*, pages 2003–1420, 2003.

[69] D.C. Jegley, B.F. Tatting, and Z. Gürdal. Tow-steered panels with holes subjected to compression or shear loading. In *Proceedings of the AIAA/ASME/ASCE/AHS/ASC 46th structures, structural dynamics and materials (SDM) conference, Austin, TX*, pages 2005–2017, 2005.

[70] M. Jeliazkov, P.S.A. Mouri, C.S. Lopes, M.M. Abdalla, and D.M.J. Peeters. Buckling and first-ply failure optimisation of stiffened variable angle tow panels. In *20th international conference on composite materials, Copenhagen*, 2015.

[71] Z. Jing, X. Fan, and Q. Sun. Global shared-layer blending method for stacking sequence optimization design and blending of composite structures. *Composites Part B: Engineering*, 69:181 – 190, 2015.

[72] R.M. Jones. *Mechanics Of Composite Materials*. Materials Science and Engineering Series. Taylor & Francis, 1998.

[73] S.E Jones and M.J Platts. Practical matching of principal stress field geometries in composite components. *Composites Part A: Applied Science and Manufacturing*, 29(7):821 – 828, 1998.

[74] M. G. Joshi and S. B. Biggers Jr. Thickness optimization for maximum buckling loads in composite laminated plates. *Composites Part B: Engineering*, 27(2):105 – 114, 1996.

[75] C. Kassapoglou. *Design and analysis of composite structures*. John Wiley and Sons, Ltd, 2010.

[76] D.W. Kelly and M. Elsley. A procedure for determining load paths in elastic continua. *Engineering Computations*, 12(5):415–424, 1995.

[77] D.W. Kelly and M.W. Tosh. Interpreting load paths and stress trajectories in elasticity. *Engineering Computations*, 17(2):117–135, 2000.

[78] A. Khani, S.T. IJsselmuiden, M.M. Abdalla, and Z. Gürdal. Design of variable stiffness panels for maximum strength using lamination parameters. *Composites Part B: Engineering*, 42(3):546 – 552, 2011.

[79] B.C. Kim, K. Hazra, P.M. Weaver, and K. Potter. Limitations of fibre placement techniques for variable angle tow composites and their process-induced defects. In *18th international conference on composite materials*, 2011.

[80] B.C. Kim, K.D. Potter, and P.M. Weaver. Continuous tow shearing for manufacturing variable angle tow composites. *Composites, Part A: Applied Science and Manufacturing*, 43(8):1347–1356, 2012.

[81] B.C. Kim, K.D. Potter, and P.M. Weaver. Multi-tow shearing mechanism for high-speed manufacturing of variable angle tow composites. In *15th European Conference on Composite Materials (ECCM15), Venice, IT*, 2012.

[82] B.C. Kim, P.M. Weaver, and K. Potter. Manufacturing characteristics of the continuous tow shearing method for manufacturing of variable angle tow composites. *Composites Part A: Applied Science and Manufacturing*, 61:141 – 151, 2014.

[83] B.C. Kim, P.M. Weaver, and K. Potter. Computer aided modelling of variable angle tow composites manufactured by continuous tow shearing. *Composite Structures*, 129:256 – 267, 2015.

[84] J.-S. Kim, C.-G. Kim, and C.-S. Hong. Optimum design of composite structures with ply drop using genetic algorithm and expert system shell. *Composite Structures*, 46(2):171 – 187, 1999.

[85] S. Kodiyalam and G.N. Vanderplaats. Shape optimization of three-dimensional continuum structures via force approximation techniques. *AIAA Journal*, 27(9):1256–1263, 2016/04/04 1989.

[86] L. Krog, A. Tucker, M. Kemp, and R. Boyd. Topology optimization of aircraft wing box ribs. In *10th AIAA/ISSMO multidisciplinary analysis and optimization conference*, pages 1–11, 2004.

[87] L. Krog, A. Tucker, and G. Rollema. Application of topology, sizing and shape optimization methods to optimal design of aircraft components. In *Proc. 3rd Altair UK HyperWorks Users Conference*, 2002.

[88] E. Lemaire, S. Zein, and M. Bruyneel. Optimization of composite structures with curved fiber trajectories. *Composite Structures*, 131:895 – 904, 2015.

[89] D. Liu, V.V. Toporov, O.M. Querin, and D.C. Barton. Bilevel optimization of blended composite wing panels. *Journal of Aircraft*, 48(1):107–118, 2015/07/01 2011.

[90] S. Liu, Y. Hou, X. Sun, and Y. Zhang. A two-step optimization scheme for maximum stiffness design of laminated plates based on lamination parameters. *Composite Structures*, 94(12):3529 – 3537, 2012.

[91] C.S. Lopes, P.P. Camanho, Z. Gürdal, P. Maim, and E.V. Gonzlez. Low-velocity impact damage on dispersed stacking sequence laminates. part ii: Numerical simulations. *Composites Science and Technology*, 69(78):937 – 947, 2009.

[92] C.S. Lopes, Z. Gürdal, and P.P. Camanho. Variable-stiffness composite panels: Buckling and first-ply failure improvements over straight-fibre laminates. *Computers and Structures*, 86(9):897 – 907, 2008.

[93] C.S. Lopes, Z. Gürdal, and P.P. Camanho. Tailoring for strength of composite steered-fibre panels with cutouts. *Composites Part A: Applied Science and Manufacturing*, 41(12):1760 – 1767, 2010.

[94] C.S. Lopes, O. Seresta, M.M. Abdalla, Z. Gürdal, B. Thuis, and P.P. Camanho. *Stacking Sequence Dispersion and Tow-Placement for Improved Damage Tolerance*. American Institute of Aeronautics and Astronautics, 2015/05/26 2008.

[95] D. H.-J.A. Lukaszewicz, C. Ward, and K. D. Potter. The engineering aspects of automated prepreg layup: History, present and future. *Composites Part B: Engineering*, 43(3):997 – 1009, 2012.

[96] E. Lund. Buckling topology optimization of laminated multi-material composite shell structures. *Composite Structures*, 91(2):158 – 167, 2009.

[97] T. Macquart, M.T. Bordogna, P. Lancelot, and R. De Breuker. Derivation and application of blending constraints in lamination parameter space for composite optimisation. *Composite Structures*, 135:224 – 235, 2016.

[98] T. Macquart, N. Werter, and R. De Breuker. Aeroelastic tailoring of blended composite structures using lamination parameters. In *57th AIAA/ASCE/AHS/ASC Structures, Structural Dynamics, and Materials Conference*, page 1966, 2016.

[99] A. Marouene, R. Boukhili, J. Chen, and A. Yousefpour. Buckling behavior of variable-stiffness composite laminates manufactured by the tow-drop method. *Composite Structures*, 139:243 – 253, 2016.

[100] A. Marouene, R. Boukhili, J. Chen, and A. Yousefpour. Effects of gaps and overlaps on the buckling behavior of an optimally designed variable-stiffness composite laminates a numerical and experimental study. *Composite Structures*, 140:556 – 566, 2016.

[101] G. Marsh. Automating aerospace composites production with fibre placement. *Reinforced Plastics*, 55(3):32 – 37, 2011.

[102] P. Mattheij, K. Gliesche, and D. Feltin. Tailored fiber placement-mechanical properties and applications. *Journal of Reinforced Plastics and Composites*, 17(9):774–786, 1998.

[103] A.G.M. Michell M.C.E. Lviii. the limits of economy of material in frame-structures. *Philosophical Magazine Series 6*, 8(47):589–597, 1904.

[104] Y.M. Meddaikar, F.-X. Irisarri, and M.M. Abdalla. Laminate optimization of blended composite structures using a modified shepard's method and stacking sequence tables. *Structural and Multidisciplinary Optimization*, pages 1–12, 2016.

[105] M.H. Nagelsmit, C. Kassapoglou, and Z. Gürdal. AP-PLY: A new fibre placement architecture for fabric replacement. *SAMPE Journal*, 47(2):36 – 45, 2011.

[106] S. Nagendra, S. Kodiyalam, J. E. Davis, and V. N. Parthasarathy. Optimization of tow fiber paths for composite design. In *36th AIAA/American Society of Mechanical Engineers/American Society of Civil Engineers/American Helicopter Society/ Society for Composites Structures, Structural Dynamics, and Materials Conference*, 1995.

[107] A. Nagy, M.M. Abdalla, and Z. Gürdal. Design of anisotropic composite shells using an isogeometric approach. In *Proceedings of the 13th AIAA/ISSMO Multidisciplinary Analysis Optimization Conference*, 2010.

[108] Y. Narita. Layerwise optimization for the maximum fundamental frequency of laminated composite plates. *Journal of Sound and Vibration*, 263(5):1005 – 1016, 2003. Arthur W. Leissa 70th Birthday Issue.

[109] M.A. Nik, K. Fayazbakhsh, D. Pasini, and L. Lessard. Surrogate-based multi-objective optimization of a composite laminate with curvilinear fibers. *Composite Structures*, 94(8):2306 – 2313, 2012.

[110] M.A. Nik, K. Fayazbakhsh, D. Pasini, and L. Lessard. A comparative study of metamodeling methods for the design optimization of variable stiffness composites. *Composite Structures*, 107:494 – 501, 2014.

[111] M.A. Nik, K. Fayazbakhsh, D. Pasini, and L. Lessard. Optimization of variable stiffness composites with embedded defects induced by automated fiber placement. *Composite Structures*, 107:160 – 166, 2014.

[112] B. Niu, N. Olhoff, E. Lund, and G. Cheng. Discrete material optimization of vibrating laminated composite plates for minimum sound radiation. *International Journal of Solids and Structures*, 47(16):2097 – 2114, 2010.

[113] P. Pedersen. Examples of density, orientation, and shape-optimal 2d-design for stiffness and/or strength with orthotropic materials. *Structural and Multidisciplinary Optimization*, 26(1):37–49, 2004.

[114] D.M.J. Peeters and M.M. Abdalla. Effect of steering constraints on the performance of variable stiffness laminates. In *20th international conference on composite materials, Copenhagen*, 2015.

[115] D.M.J. Peeters and M.M. Abdalla. Structural approximations for composite optimisation. In *World conference on structural and multidisciplinary optimisation 11, Sydney*, 2015.

[116] D.M.J. Peeters and M.M. Abdalla. Design guidelines in nonconventional composite laminate optimization. *Journal of Aircraft*, pages 1–11, available online 2016.

[117] D.M.J. Peeters and M.M. Abdalla. Optimization of ply drop locations in variable-stiffness composites. *AIAA Journal*, pages 1–9, 2016/04/01 2016.

[118] D.M.J. Peeters, S. Hesse, and M.M. Abdalla. Stacking sequence optimisation of variable stiffness laminates with manufacturing constraints. *Composite Structures*, 125:596 – 604, 2015.

[119] D.M.J. Peeters, D. van Baalen, and M.M. Abdalla. Combining topology and lamination parameter optimisation. *Structural and Multidisciplinary Optimization*, pages 1–16, 2015.

[120] T. Rahman, S.T. Ijsselmuiden, M.M. Abdalla, and E.L. Jansen. Postbuckling analysis of variable stifness composite plates using a finite element-based perturbation method. *International Journal of Structural Stability and Dynamics*, 11(04):735–753, 2011.

[121] G. Raju, S. White, Z. Wu, and P.M. Weaver. Optimal postbuckling design of variable angle tow composites using lamination parameters. In *56th AIAA/ASCE/AHS/ASC Structures, Structural Dynamics, and Materials Conference*, page 0451, 2015.

[122] E. Richter, K. Uhlig, A. Spickenheuer, L. Bittrich, E. Maäder, and G. Heinrich. Thermoplastic composite parts based on online spun commingled hybrid yarns with continuous curvilinear fibre patterns. In *16th European Conference on Composite Materials*, June 2014.

[123] L.A. Schmit and C. Fleury. Structural synthesis by combining approximation concepts and dual methods. *AIAA Journal*, 18(10):1252–1260, 2016/03/10 1980.

[124] T.A. Sebaey, E.V. Gonzlez, C.S. Lopes, N. Blanco, and J. Costa. Damage resistance and damage tolerance of dispersed {CFRP} laminates: Design and optimization. *Composite Structures*, 95(0):569 – 576, 2013.

[125] O. Seresta, Z. Gürdal, D.B. Adams, and L.T. Watson. Optimal design of composite wing structures with blended laminates. *Composites Part B: Engineering*, 38(4):469 – 480, 2007.

[126] S. Setoodeh, M.M. Abdalla, and Z. Gürdal. Approximate feasible regions for lamination parameters. In *11th AIAA/ISSMO Multidisciplinary Analysis and Optimization Conference*, volume 2, pages 814–822. Portsmouth, 2006.

[127] S. Setoodeh, M.M. Abdalla, S.T. IJsselmuiden, and Z. Gürdal. Design of variable-stiffness composite panels for maximum buckling load. *Composite Structures*, 87(1):109 – 117, 2009.

[128] A.P. Seyranian, E. Lund, and N. Olhoff. Multiple eigenvalues in structural optimization problems. *Structural optimization*, 8(4):207–227, 1994.

[129] B. Shirinzadeh, G. Alici, C.W. Foong, and G. Cassidy. Fabrication process of open surfaces by robotic fibre placement. *Robotics and Computer-Integrated Manufacturing*, 20(1):17 – 28, 2004.

[130] O. Sigmund and J. Petersson. Numerical instabilities in topology optimization: A survey on procedures dealing with checkerboards, mesh-dependencies and local minima. *Structural optimization*, 16(1):68–75, 1998.

[131] G. Soremekun, Z. Gürdal, C. Kassapoglou, and D. Toni. Stacking sequence blending of multiple composite laminates using genetic algorithms. *Composite Structures*, 56(1):53 – 62, 2002.

[132] R. Sørensen and E. Lund. In-plane material filters for the discrete material optimization method. *Structural and Multidisciplinary Optimization*, 52(4):645–661, 2015.

[133] R. Sørensen and E. Lund. Thickness filters for gradient based multi-material and thickness optimization of laminated composite structures. *Structural and Multidisciplinary Optimization*, pages 1–24, 2015.

[134] S.N. Sørensen and E. Lund. Topology and thickness optimization of laminated composites including manufacturing constraints. *Structural and Multidisciplinary Optimization*, 48(2):249–265, 2013.

[135] S.N. Sørensen, R. Sørensen, and E. Lund. Dmto a method for discrete material and thickness optimization of laminated composite structures. *Structural and Multidisciplinary Optimization*, 50(1):25–47, 2014.

[136] S.N. Sørensen and M. Stolpe. Global blending optimization of laminated composites with discrete material candidate selection and thickness variation. *Structural and Multidisciplinary Optimization*, pages 1–19, 2015.

[137] A. Spickenheuer, M. Schulz, K. Gliesche, and G. Heinrich. Using tailored fibre placement technology for stress adapted design of composite structures. *Plastics, Rubber and Composites*, 37(5):227–232, 2008.

[138] J. Stegmann and E. Lund. Discrete material optimization of general composite shell structures. *International Journal for Numerical Methods in Engineering*, 62(14):2009–2027, 2005.

[139] A.B. Strong. *Fundamentals of Composites Manufacturing, Second Edition: Materials, Methods and Applications*. Society of Manufacturing Engineers, 2008.

[140] K. Svanberg. The method of moving asymptotesa new method for structural optimization. *International Journal for Numerical Methods in Engineering*, 24(2):359–373, 1987.

[141] K. Svanberg. a class of globally convergent optimization methods based on conservative convex separable approximations. *Siam J. optim*, 2:555–573, 2002.

[142] H. Temmen, R. Degenhardt, and T. Raible. Tailored Fibre Placement Optimization Tool. In *25th International Congress of The Aeronautical Sciences*, 2006.

[143] G.A.A. Thuwis, R. Breuker, M.M. Abdalla, and Z. Gürdal. Aeroelastic tailoring using lamination parameters. *Structural and Multidisciplinary Optimization*, 41(4):637–646, 2009.

[144] M.W. Tosh and D.W. Kelly. On the design, manufacture and testing of trajectorial fibre steering for carbon fibre composite laminates. *Composites Part A: Applied Science and Manufacturing*, 31(10):1047 – 1060, 2000.

[145] S. W. Tsai and H.T. Hahn. *Introduction to composite materials*. Technomic, Westport, 1989.

[146] S.W. Tsai. Mechanics of composite materials part i. Technical Report AFML-TR-66-149, Part I, Air force materials laboratory research and technology disivion, Wright-Patterson Air force base, Ohio, June 1966.

[147] S.W. Tsai. Mechanics of composite materials part ii. Technical Report AFML-TR-66-149, Part II, Air force materials laboratory research and technology disivion, Wright-Patterson Air force base, Ohio, November 1966.

[148] S.W. Tsai and J.D.D. Melo. An invariant-based theory of composites. *Composites Science and Technology*, 100(0):237 – 243, 2014.

[149] T. Ungwattanapanit and H. Baier. Postbuckling analysis and optimization of stiffened fuselage panels utilizing variable-stiffness laminates. In *Congress of the International Council of the Aeronautical Sciences, ICAS [29., 2014, St. Petersburg]*, 2014.

[150] J. van Campen, O. Seresta, M.M. Abdalla, and Z. Gürdal. General blending definitions for stacking sequence design of composite laminate structures. In *Proceedings of the 49th AIAA/ASME/ASCE/AHS/ASC Structures, Structural Dynamics, and Materials Conference, 16th AIAA/ASME/AHS Adaptive Structures Conference,10th AIAA Non-Deterministic Approaches Conference, 9th AIAA Gossamer Spacecraft Forum, 4th AIAA Multidisciplinary Design Optimization Specialists Conference*, 2008.

[151] J.M.J.F. van Campen, C. Kassapoglou, and Z. Gürdal. Generating realistic laminate fiber angle distributions for optimal variable stiffness laminates. *Composites Part B: Engineering*, 43(2):354 – 360, 2012.

[152] W.M. van den Brink, W.J. Vankan, and R. Maas. Buckling optimized variable stiffness laminates for a composite fuselage window section. In *28th international congress of the aeronautical sciences*, 2012.

[153] N. P. van Dijk, K. Maute, M. Langelaar, and F. van Keulen. Level-set methods for structural topology optimization: a review. *Structural and Multidisciplinary Optimization*, 48(3):437–472, 2013.

[154] G.N. Vanderplaats and S.H. Han. Arch shape optimization using force approximation methods. *Structural Optimization*, 2(4):193–201, 1990.

[155] G.N. Vanderplaats and H.L. Thomas. An improved approximation for stress constraints in plate structures. *Structural Optimization*, 6(1):1–6, 1993.

[156] G.N. Vanderplats and S. Kodiyalam. Two-level approximation method for stress constraints in structural optimization. *AIAA Journal*, 28(5):948–951, 2016/04/04 1990.

[157] S. Venkataraman and R.T. Haftka. *Optimization of composite panelsa review*, pages 479 – 488. 14th Annual Technical Conference of the American Society of Composites, Dayton, OH (1999), 1999.

[158] J.R. Vinson and R.L. Sierakowski. *The behavior of structures composed of composite materials*. Mechanics of Structural Systems. Springer Netherlands, 2012.

[159] C.K. Wu. Design and analysis of tow-steered composite shells using fiber placement. In *Proceedings of the ASC 23rd Annual Technical Conference, Memphis, Tennessee, September 9-11, 2008, paper no. 125.*, 2008.

[160] C.K. Wu, B. Farrokh, B. Stanford, and P.M. Weaver. Imperfection insensitivity analyses of advanced composite tow-steered shells. In *Proceedings of the 57th AIAA/ASME/ASCE/AHS/ASC Structures, Structural Dynamics, and Materials Conference*, 2016.

[161] C.K. Wu, B.K. Stanford, G.A. Hrinda, Z. Wang, R.A. Martin, and H.A. Kim. Structural assessment of advanced tow-steered shells. In *Proceedings of the 54th AIAA/ASME/ASCE/AHS/ASC Structures, Structural Dynamics, and Materials Conference*, 2013.

[162] C.K. Wu, B.K. Stanford, J.D. Turpin, and R.A. Martin. Structural performance of advanced composite tow-steered shells with cutouts. In *Proceedings of the 55th AIAA/ASME/ASCE/AHS/ASC Structures, Structural Dynamics, and Materials Conference*, 2014.

[163] C.K. Wu, B. Tatting, B. Smith, R. Stevens, G. Occhipinti, J. Swift, D.Achary, and R. Thornburgh. Design and manufacturing of tow-steered composite shells using fiber placement. In *Proceedings of the 50th AIAA/ASME/ASCE/AHS/ASC Structures, Structural Dynamics, and Materials Conference*, 2009.

[164] C.K. Wu, J.D. Turpin, N.W. Gardner, B. Stanford, and R.A. Martin. Structural characterization of advanced composite tow-steered shells with large cutouts. In *Proceedings of the 56th AIAA/ASME/ASCE/AHS/ASC Structures, Structural Dynamics, and Materials Conference*, 2015.

[165] Z. Wu, G. Raju, S. White, and P.M. Weaver. Optimal design of postbuckling behaviour of laminated composite plates using lamination parameters. In *55th AIAA/ASMe/ASCE/AHS/SC Structures, Structural Dynamics, and Materials Conference*, page 1376, 2014.

[166] Z. Wu, P.M. Weaver, G. Raju, and B.C. Kim. Buckling analysis and optimisation of variable angle tow composite plates. *Thin-Walled Structures*, 60(0):163 – 172, 2012.

[167] K. Wurpel. *Modeling manufacturable tow paths*. M.Sc. thesis, Delft University of Technology, 2015.

[168] Z. Xiaoping and J. Peng. Structural optimization of composite wing based on different blending models using genetic algorithm. *Applied Mechanics and Materials*, 401-403:886–890, 2013.

[169] D. Goldfarb Z. Wen and K. Scheinberg. Block coordinate descent methods for semidefinite programming. in Miguel F. Anjos and Jean B. Laserre, editors, handbook on semidefinite, cone and polynomial optimization: theory, algorithms, software and applications, Springer, ISBN: 978-1-4614-0768-3, October 2012.

[170] S. Zein and M. Bruyneel. A bilevel integer programming method for blended composite structures. *Advances in Engineering Software*, 79:1 – 12, 2015.

[171] S. Zein, B. Colson, and S. Grihon. A primal-dual backtracking optimization method for blended composite structures. *Structural and Multidisciplinary Optimization*, 45(5):669–680, 2012.

[172] C. Zillober. A combined convex approximationinterior point approach for large scale nonlinear programming. *Optimization and Engineering*, 2(1):51–73, 2001.

[173] E. Zympleoudis, K. Potter, P.M. Weaver, and B.C. Kim. Automated high volume production of complex composites parts: Cmts (continuous multi-tow shearing). In *20th International Conference on Composite Materials (ICCM20), Copenhagen, Denmark*, 2015.

LIST OF PUBLICATIONS

JOURNAL PUBLICATIONS

1. D.M.J. Peeters, Z. Hong, M.M. Abdalla, Structural Approximations for composite optimisation, *to be submitted*

2. D.M.J. Peeters, G. Gonzalez Lozano, M.M. Abdalla, Effect of Steering Limit Constraints on the Performance of Variable Stiffness Laminates, *submitted*

3. D.M.J. Peeters, M.M. Abdalla, Design Guidelines in Nonconventional Composite Laminate Optimization, *Journal of Aircraft*, published online, 2016

4. F.-X. Irisarri, D.M.J. Peeters, M.M. Abdalla, Optimisation of Ply Drop Order in Variable Stiffness Laminates, *Composite Structures*, Vol. 152, September 2016, Pages 791-799

5. D.M.J. Peeters, M.M. Abdalla, Optimisation of Ply Drop Locations in Variable Thickness Composites, *AIAA Journal*, Vol. 54, No. 5 (2016), pp. 1760-1768

6. D.M.J. Peeters, S.H. Hesse, M.M. Abdalla, Stacking Sequence Optimisation of Variable Stiffness Laminates with Manufacturing Constraints, *Composite Structures*, Vol. 125, July 2015, Pages 596-604

7. D.M.J. Peeters, D. van Baalen, M.M. Abdalla, Combining Topology and Lamination Parameter Optimisation, *Structural and Multidisciplinary Optimization*, Vol. 52, July 2015, Pages 105-120

CONFERENCE PUBLICATIONS

1. D.M.J. Peeters, F.-X. Irisarri, M.M. Abdalla, Optimising the ply dropping order in variable stiffness, variable thickness laminates using stacking sequence tables, *17th European Conference on Composite Materials, 26-30 June 2016, Munich, Germany*

2. D.M.J. Peeters, M.M. Abdalla, Stacking Sequence Constraints in Non-conventional Composite Laminate Optimisation, *56th AIAA/ASCE/AHS/ASC Structures, Structural Dynamics, and Materials Conference, AIAA SciTech, 4-8 January 2016, San Diego, California, USA*

3. D.M.J. Peeters (on behalf of the CANAL project), Creating Non-conventional Laminates, *AeroDays 2015, 20-23 October 2015, London, UK*

4. D.M.J. Peeters, M.M. Abdalla, Effect of Steering Constraints on the Performance of Variable Stiffness Laminates, *20th International Conference on Composite Materials, 19-24 July 2015, Copenhagen, Denmark*

5. D.M.J. Peeters, M.M. Abdalla, Structural Approximations for Composite Optimisation, *11th World Conference on Structural and Multi-disciplinary Optimisation, 7-12 June 2015, Sydney, Australia*

6. D.M.J. Peeters, M.M. Abdalla, Optimisation of Variable Stiffness Composites with Ply Drops, *55th AIAA/ASCE/AHS/ASC Structures, Structural Dynamics, and Materials Conference, AIAA SciTech, 5-9 January 2015, Kissimmee, Florida, USA*

7. D.M.J. Peeters, S.H. Hesse, M.M. Abdalla, Multi-objective and Multi-constraint Optimisation of Variable Stiffness Composite Laminates, *16th European Conference on Composite Materials, 22-26 June 2014, Seville, Spain*

8. D.M.J. Peeters, D. van Baalen, M.M. Abdalla, Combining Topology and Lamination Parameter Optimisation, *54th AIAA/ASCE/AHS/ASC Structures, Structural Dynamics, and Materials Conference, AIAA SciTech, 13-17 January 2014, National Harbor, Maryland, USA*

CURRICULUM VITAE

Daniël Maria Jozef Peeters was born on 2 November 1989 in Turnhout, Belgium. While he lived in the small town of Gierle, during primary school, he drove every day together with his mother to Arendonk. During the secondary school, from 2001 to 2007, he biked every day to the Sint-Jozefcollege in Turnhout, following Latin-Mathematics. In 2007, he decided to leave Belgium, and go study in Delft, the Netherlands, at the faculty of Aerospace Engineering. In September 2011 he went to Zürich for half a year during his MSc studies as part of his honour's track. Afterwards, he stayed three more months in Switzerland, doing his internship at Stadler in Altenrhein working on the design of train wheels.

On his return to Delft in June 2012, he started his master thesis on the subject of the optimisation of variable stiffness laminates. He found the subject so interesting that, after obtaining his MSc in Delft with distinction in December 2012, he continued working on this subject as a PhD student from February 2013 in the chair of Aerospace Structures and Computational Mechanics at Delft University of Technology. While his PhD ends, he is still eager to continue working in an academic environment on (the optimisation of) composite materials.